# REPORT DOCUMENTATION PAGE

Form Approved OMB No. 0704-0188



| 1. REPORT DATE *(DD-MM-YYYY)* | 2. REPORT TYPE | 3. DATES COVERED *(From – To)* |
|---|---|---|
| 12-11-2009 | Final Report | 1 Sep 09 - 02-Feb-10 |

**4. TITLE AND SUBTITLE**

Detailed and Simplified Chemical Kinetics of Aviation Fuels and Surrogates

**5a. CONTRACT NUMBER**
FA8655-06-1-3052

**5b. GRANT NUMBER**

**5c. PROGRAM ELEMENT NUMBER**

**6. AUTHOR(S)**

Professor Peter R Lindstedt

**5d. PROJECT NUMBER**

**5d. TASK NUMBER**

**5e. WORK UNIT NUMBER**

**7. PERFORMING ORGANIZATION NAME(S) AND ADDRESS(ES)**

Imperial College London
Exhibition Road
London SW7 2AZ
United Kingdom

**8. PERFORMING ORGANIZATION REPORT NUMBER**

N/A

**9. SPONSORING/MONITORING AGENCY NAME(S) AND ADDRESS(ES)**

EOARD
Unit 4515 BOX 14
APO AE 09421

**10. SPONSOR/MONITOR'S ACRONYM(S)**

**11. SPONSOR/MONITOR'S REPORT NUMBER(S)**
Grant 06-3052

**12. DISTRIBUTION/AVAILABILITY STATEMENT**

Approved for public release; distribution is unlimited.

**13. SUPPLEMENTARY NOTES**

**14. ABSTRACT**

This report results from a contract tasking Imperial College London as follows: 1.0 Introduction and Overview

Current fuel quality regulations for aviation kerosene provide significant scope for large regional and source differences. The chemistry of high-performance fuels aimed at specific applications and devices show less variation but their chemistries remain complex. There is now arguably a well-established need to incorporate accurate chemical mechanisms into calculation procedures [1]. Flow timescales associated with high performance propulsion devices also increasingly lead to difficulties associated with the burning characteristics of the current generation of propulsion fuels. In particular, chemical time-scale restrictions pose a particular challenge in terms of combustion initiation and/or flame stability. The current development of alternative combustor designs based premixed or partially premixed lean burn technologies further emphasises the need to consider finite rate chemistry effects. Critical steps in the derivation of realistic chemical mechanisms include the definition of a surrogate (or model) fuel and validation of the performance of the surrogate against practical fuel samples. The required practical parameter space typically leads to a need to determine heat release characteristics, burning velocities, effects of strain, ignition delay times, the dynamics of the fuel breakdown process and quantification of key intermediate species. The latter is often essential in understanding the propensity of a device to form pollutants, such as soot, that may affect signatures and combustor life. Furthermore, current indications suggest that fuel sources will become significantly more diverse in the future and may, for example, encompass Fischer-Tropsch and/or bio-derived components. The current proposal outlines a route towards surrogate fuel mechanisms of sufficient accuracy and generality to support the development of practical devices.

The combination of advanced, laser based diagnostic techniques and detailed kinetic modelling has made invaluable contributions to the understanding of the chemistry of fuel conversion [2]. Such research efforts rely upon the continued development and application of innovative diagnostic techniques and advances in the understanding of fundamental chemical reaction sequences. Much effort has been devoted to the combustion of natural gas based fuel mixtures and past key differences [3-5] affecting the C1-C2 chemistry are now significantly reduced [6,7]. Progress has to a large extent been based on identification of critical reaction paths and the availability of increasingly accurate determination of key rate constants combined with high-quality validation data. Progress for complex aviation fuel mixtures has been slower due to uncertainties in major reaction pathways, particularly for aromatic species, limited chemical kinetic and thermochemical data and sparse data sets of limited suitability for detailed validation. However, the only approach that has the potential to achieve the objective of ensuring a priori knowledge of combustion properties of a particular fuel blend is through the application of detailed kinetic modelling following the independent validation of the chemistry of each fuel component present in the surrogate mixture.

Early efforts aimed at producing surrogate fuel models for endothermic and aviation fuels were pursued by Lindstedt and Maurice [8-10] who primarily considered n-heptane [8], toluene [9], n-decane [10] and mixtures thereof [9,10]. The work resulted a set of first generation models that identified some key issues in the aromatic and PAH chemistry subsequently pursed further by Lindstedt et al. [11] and Lindstedt and Rizos [12]. The latter work resulted in a reassessment of principal reaction paths leading to second ring formation. More recent efforts in the European Community have resulted in surrogate fuel models based on two-component mixtures of n-decane and n-propyl-benzene [13]. The number of fuel components was intentionally limited due to the constraints imposed by the practical application of such models. The removal of the limitations of high Damköhler number based closures for the chemical reaction rate source term are essential in the context of a wide range of practical applications where strong direct kinetic effects are present. Promising approaches that are not based on a presumed flame structure include hybrid transported probability density function/finite volume and Large Eddy Simulation (LES) based approaches. For example, Kuan and Lindstedt [14] computed transient turbulent flames with a large scalar space featuring 20 independent scalars and Sheiki [15] has highlighted the progress made in the application of LES with finite rate chemistry. The introduction of thermochemistry into such computations requires the application of rigorous simplification procedures to reduce the number of independent scalars.

The group at Imperial College [16-18] have further developed a reaction class based approach to model the oxidation of naphthalene, 1-methyl naphthalene and n-propyl benzene. For example, reaction classes for higher aromatics, such as naphthalene and indene, were defined based on similarities with the oxidation of cyclopentadiene and benzene [11,12]. The application of the approach to n-propyl benzene was shown to lead to encouraging agreement. The application of a surrogate fuel model based on n-decane and n-propyl benzene to model the combustion of a practical Jet-A sample (collected at a major European airport) provided a further indication that comparatively simple surrogate fuel models can reproduce key oxidation features of practical fuels. Further information is available elsewhere [16].

The work proposed will serve to provide consistent reaction mechanisms for surrogate aviation fuels and their components. To this effect, collaboration with USC (Egolfopoulos, Wang), AFRL (Edwards, Williams) and the wider surrogate fuels working group and collaborators at Stanford University (Hanson, Davidson).

References

[1] Tishkoff, J.M., Drummond, J.P., Edwards, T. and Nejad, A.S., Future Direction of Supersonic Combustion Research: Air Force/NASA Workshop on Supersonic Combustion, Paper AIAA 97-1017 (1997).

[2] Lindstedt, R.P. 'Modelling of the Chemical Complexities of Flames', Invited Plenary Lecture, Proc. Combust Inst. 27:269-285 (1998).

[3] Berg, P.A., Smith, G.P., Jeffries. J.B. and Crosley. D.R., Nitric Oxide Formation and Reburn in Low-Pressure Methane Flames, Proc. Combust. Inst. 27:1377-1384 (1998).

[4] Juchmann, W., Latzel, H., Shin, D.I., Peiter, G., Dreier, T., Wolfrum, J., Leung, K.M. and Lindstedt, R.P., 'Absolute Radical Concentration Measurements and Modelling of Low Pressure CH4/O2/NO Flames', Proc. Combust. Inst. 27:469-476 (1998).

[5] Sick, V., Hildenbrand, F. and Lindstedt, R.P. 'Quantitative Laser-Based Measurements and Detailed Kinetic Modelling of Nitric Oxide Concentrations in Methane/Air Counterflow Diffusion Flames', Proc. Combust. Inst. 27:1401-1409 (1998).

[6] Gibaud C., Snyder, J.A., Sick, V. and Lindstedt, R.P. Laser induced fluorescence measurements and modelling of absolute CH Concentrations in strained laminar methane/air diffusion flames, Proc. Combust. Inst. 30: 455-463 (2005).

[7] Driscoll, J.J., Sick, V., Farrow, R.L., Schrader, P.E., Rizos, K.-A. and Lindstedt, R.P. NO Reburn and Formation Chemistry in Methane Diffusion Flames, Z. Phys. Chem. 219:679-698 (2005).

[8] Lindstedt, R.P. and Maurice, L.Q., 'Detailed Kinetic Modeling of n-Heptane Combustion', Combustion, Science and Technology, 107, pp.317-353, (1995).

[9] Lindstedt, R.P. and Maurice, L.Q., 'Detailed Kinetic Modeling of Toluene Combustion', Combustion, Science and Technology, 120, pp. 119-167, (1996).

[10] Lindstedt, R.P. and Maurice, L.Q., 'Detailed Kinetic Models for Aviation Fuels', AIAA Journal of Propulsion and Power, 16(2), pp. 187-195 (2000).

[11] Lindstedt, R.P., Maurice, L.Q. and Meyer, M. Thermodynamic and kinetic issues in the formation and oxidation of aromatic species, The Royal Society of Chemistry, Faraday Discussion, 119, 409-432 (2001).

[12] Lindstedt, R.P. and Rizos, K.-A. The Formation and Oxidation of Aromatics in Cyclopentene and Methyl-Cyclopentadiene Mixtures, Proc. Comb. Inst. 29:2291-2298 (2002).

[13] Final Report, Computational Fluid Dynamics for Combustion (CFD4C), CEC Project No: GRD1-1999-10325 (2003).

[14] Kuan, T.S. and Lindstedt, R.P. Transient Transported PDF Modeling of Bluff Body Stabilized Flames, Proc. Combust. Inst., 30:767-774 (2005) and Time-resolved transported PDF modelling of a bluff body stabilized turbulent flame, US Joint Meeting of the Combustion Institute, March 2005.

[15] Sheikhi, M.R.H., Drozda, T.G., Givi, P., Jaberi, F.A. and Pope, S.B. Large Eddy Simulation of a Turbulent Non-premixed piloted Jet Flame (Sandia Flame D), Proc. Combust. Inst. 30:549-556 (2005).

[16] Potter, M. L. Detailed Chemical Kinetic Modelling of Propulsion Fuels, PhD Thesis, Imperial College London, September (2003).

[17] Lindstedt, R P, High Temperature Pathways to Poly-aromatic Hydrocarbons. Zel'dovich Memorial Conference on Combustion and Detonation, Moscow, Russia, August 30 – Sept 3, 2004, pp. 20-21, ISBN No: 5-94588-027-2.

[18] Lindstedt, R.P. and Potter, M.L. Detailed Chemical Kinetic Modeling of Diesel Fuel Compounds, In Preparation.

[19] Dagaut, P. CFD4C EU Progress Report, Private Communication, March 2003.

2.0 Expected Results

1. A JAVA tool for the generation of chemical mechanisms based on reaction classes relevant to surrogate fuel components.

2. Defined "target" parameters for the evaluation of the fidelity of derived reaction mechanisms. Task performed with project partners.

3. Definitions of what constitutes acceptable agreement for detailed and reduced reaction mechanisms in the context of "target"

parameters. Task performed with project partners.

4. Detailed reaction mechanisms derived for alkyl-substituted aromatics such as toluene, m-xylene, 1-methyl naphthalene and n-propyl benzene. Revision may be required with respect to selected target molecules in light of findings obtained during the project.

5. Detailed reaction mechanisms derived for selected n-alkane, cyclo-paraffin and iso-paraffin components.

6. Detailed reaction mechanisms for surrogate fuels evaluated against "target" data. At least two fuel components to be considered in the smallest mechanism.

3.0 Scope of Activities

All tasks to be performed by Imperial College. Collaboration predominantly with AFRL, University of Southern California (USC) and with the Surrogate Fuels Working Group. The tasks outlined below are sequential and describe quarterly targets beginning 3 months after the commencement of the project. Deliverables are in terms of brief progress reports, contributions to EOARD/AFOSR sponsored meetings and publications as appropriate. In addition, reporting will be performed in accordance with EOARD and AFOSR requirements.

Task 1. Extend existing JAVA tool for the generation of reaction mechanisms to incorporate preliminary reaction classes for alkyl-substituted aromatics.

Task 2. Evaluation of derived reaction mechanisms via comparisons with experimental data from the literature and "target" data as obtained by project partners (USC and others).

Task 3. Extend the JAVA based tool to incorporate alkane components including simplified low temperature chemistry.

Task 4. Evaluation of the derived reaction mechanism for a pure n-alkane component as well as for a preliminary two-component surrogate. Comparisons with agreed "target" parameters and test cases (AFRL, Surrogate Fuels Working Group).

Task 5. Refinement of reaction classes for alkyl-substituted aromatics based on joint work with project partners (USC).

Task 6. Refinement of reaction classes for n-alkane components to incorporate a simplified low temperature mechanism based on characteristic reaction steps.

Task 7. Extend existing JAVA tool to incorporate preliminary reaction classes for cyclo-alkanes derived in collaboration with project partners (USC).

Task 8. Evaluation of the derived reaction mechanism for a selected cyclo-alkane via comparisons with experimental data from the literature and "target" data as obtained by project partners (AFRL, USC and others).

Task 9. Extend existing JAVA based tool to incorporate preliminary reaction classes for iso-alkanes derived in collaboration with project partners (USC).

Task 10. Evaluation of the derived reaction mechanism for a selected iso-alkane via comparisons with experimental data from the literature and as obtained by project partners (USC and others).

Task 11. Formulation and evaluation of surrogate fuel mechanisms based on derived and validated component mechanisms. Decision on desired dimensionality of the surrogate fuel mechanism (AFRL, USC and the Surrogate Fuels Working Party).

Task 12. Final Report

4.0 Technical Approach and Methodology

The current technical approach is based on the further development of reaction classes for surrogate fuel components. In addition to the examples mentioned in the introduction, the technique has been shown to produce encouraging results for aromatic molecules such as naphthalene and 1-methyl naphthalene [16-18]. The latter is a key surrogate fuel component for Diesel fuel mixtures and a potential target fuel component identified by the Surrogate Fuels working group. A further benefit with the approach is that improved chemical kinetic data can directly impact related fuel compounds. To support the rapid evaluation of mechanisms in light of improved chemical kinetic and validation data, a JAVA based reaction class tool has been developed and applied to heterogeneous reaction systems. The simplification to encompass gas phase reactions is procedural. An important advantage is that the approach can readily be applied to identify key sensitivities that merit detailed computational chemistry and/or experimental investigations. Emerging combustion technologies place greater emphasis on the low to intermediate temperature oxidation window and the inclusion of appropriate reaction classes has a tendency to result in excessive mechanism sizes. It is therefore argued that the approach be constrained to selected characteristic adducts representative of wider reaction classes. A task-by-task outline of the current computational project is given below.

Tasks 1, 3, 7 and 9. A JAVA based tool has been created for the automatic generation of heterogeneous reaction mechanisms, which will be modified to consider homogeneous gas phase reaction classes of direct relevance to surrogate fuel mechanisms. The initial reaction classes and rate data will be based on work performed at Imperial College. Refinements will take into account work performed by project partners. The generated mechanisms will be constrained with respect to size by the selection of preferred fuel components and oxidation routes. Further reductions in size will result from path and sensitivity analyses performed as part of other tasks.

Tasks 2, 4, 8, 10 and 11. Evaluation of derived reaction mechanisms via comparisons with experimental data from the literature and "target" data as obtained by project partners. The reaction mechanisms will also be subjected to path and sensitivity analyses with a view to reducing the dimensionality of the system.

Tasks 5 and 6. Refinement of reaction classes will take place based on collaboration with project partners as appropriate.

**15. SUBJECT TERMS**
EOARD, Fuels, Combustion

| 16. SECURITY CLASSIFICATION OF: | | | 17. LIMITATION OF ABSTRACT | 18, NUMBER OF PAGES | 19a. NAME OF RESPONSIBLE PERSON |
|---|---|---|---|---|---|
| a. REPORT | b. ABSTRACT | c. THIS PAGE | UL | | SURYA SURAMPUDI |

| | | | | | |
|---|---|---|---|---|---|
| UNCLAS | UNCLAS | UNCLAS | | 85 | **19b. TELEPHONE NUMBER** *(Include area code)*<br>+44 (0)1895 616021 |

Imperial College London

# Detailed and Simplified Chemical Kinetics of Aviation Fuels and Surrogates

## Final Report on Grant FA8655-06-1-3052

**R.P. Lindstedt and V. Markaki**

Department of Mechanical Engineering, Imperial College London, Exhibition Road, London, SW7 2AZ, UK

**Principal Investigator R. P. Lindstedt**

**Submitted to the European Office of Aerospace Research and Development, 86 Blenheim Crescent, Ruislip HA4 7HB, UK.**

**September 2009**

## Summary

The chemistries of aviation fuels are invariably complex due to the constituent large hydrocarbon molecules. There are also large compositional variations for a given fuel type. Furthermore, flow timescales encountered in high-performance propulsion devices lead to difficulties associated with kinetically controlled or influenced phenomena such as flame stability, extinction and re-light. Indications are that fuel sources will become significantly more diverse in the future and may encompass Fischer-Tropsch and/or bio-derived components. The combustion properties of such fuels can vary significantly from those in current use and this work outlines a route towards surrogate fuel mechanisms of sufficient accuracy and generality to support the development of practical devices.

A reaction class based route to the derivation of detailed chemical kinetic mechanisms for alkyl-substituted aromatics is outlined and applied to the cyclopentadiene/indene, benzene/naphthalene, toluene/1-methyl naphthalene systems. Work has also been extended to the n-propyl benzene system. Important reaction channels were identified for all systems and for selected pathways potential energy surfaces were determined via density functional theory (DFT) and composite quantum mechanical computations. Both the Rice-Ramsperger-Kassel-Marcus/master equation (RRKM/ME) and variable transition state theory (VTST) approaches were used to derive estimates of the rate constants. Improved thermodynamic data for a wide range of intermediate species was also determined at the G3MP2B3 level in combination with DFT analysis for internal rotations. The use of 1-methyl naphthalene as a surrogate fuel component has been identified in the context of modulating the sooting tendencies of aviation surrogates and significant progress with respect to the identification of oxidation and formation channels is reported.

Results obtained from chemical kinetic modelling of cyclopentadiene, toluene, n-propyl benzene, naphthalene and 1-methyl naphthalene oxidation in shock tubes, jet-stirred and plug-flow reactors at various sets of representative stoichiometries and temperatures suggest that the developed reaction mechanims exhibit significantly improved generality.

## Acknowledgements

The authors wish to express their gratitude to the Air Force Office of Scientific Research (AFOSR) and the European Office of Aerospace Research and Development (EOARD) for providing the financial support for this work. We would also like to express our gratitude to Dr. J. Tishkoff and Dr. S. Surampudi. The contributions of Dr. R. K. Robinson, who provided much of the thermochemical and reaction rate data as part of a complementary effort, are also gratefully acknowledged.

## 1.0 Background

The increase in global fuel consumption over the last century has resulted in major socioeconomic and environmental challenges. Transportation and, to an increasing extent, aviation, is one of the major fuel consumption sectors. This has led to the need for engines with operating envelopes that can comply with environmental and energy saving directives. New aircraft engines are expected to perform with maximum combustion efficiency as well as providing stability and low emissions. Furthermore, it can be expected that new fuel types will become necessary and a sound understanding of current products forms an essential starting point.

Aromatic hydrocarbons and, to a much lesser extent, polycyclic aromatic hydrocarbons (PAH) are key components of current aviation fuels. It is well known that aromatic compounds, apart from being responsible for pollutant emissions, also have carcinogenic and mutagenic properties [1-3]. They also contribute to the detection of aircraft due to the associated infrared signals produced. The aromatic components of aviation fuels can also reduce the life cycle of the combustor as the associated particulate formation increases the radiative heat transfer to the combustor walls [4] and also influences maintenance requirements. Hence, the optimisation of combustor behaviour requires a good knowledge of the chemistry of aromatic fuel components as well as calculation methods for turbulent flows that are capable of exploiting such advances.

A typical aviation fuel consists of various classes of hydrocarbon compounds and exhibit different behaviours due to refining processes and crude oil feedstocks [5]. In general, the characteristics of an aviation fuel is determined by operational needs. Fuels are typically developed to have good combustion characteristics combined with good physical properties such as low temperature fluidity. The blends also need to consist of storable hydrocarbon compounds. In the 1940's, the U.S. Air Force used 'wide-cut' fuel, which was available in large quantities at that time. Wide-cut fuels were highly volatile and were replaced by kerosene fuels in the 1970's (Jet A, Jet A-1 and JP-8) for safety reasons [6].

The complexities of jet fuels are such that the direct simulation of their combustion behaviour is not possible due to the thousands of chemical compounds present. However, recent scientific advances in the modelling of combustion systems have provided important insight that is complementary to experimental studies. Such detailed modelling can be expected to provide essential understanding of the overall behaviour of a combustion system provided that the chemistry of the fuel and the formation of pollutants are sufficiently well understood. Due to the complexities of practical fuels it is necessary to

represent actual fuel mixtures with functionally similar blends featuring a more limited number of representative compounds. Such surrogate mixtures can be characterized accurately and makes it feasible to study combustion processes in detail using computational methods following the application of rigorous systematic reduction methods.

A surrogate aviation fuel can be chosen to reproduce physical and chemical properties of an aviation fuel such as heat capacity, enthalpy, viscosity, rates of reaction or specific ignition and oxidation behaviours. Surrogate mixtures can be used both computationally and experimentally. A physical surrogate is a mixture that can reproduce physical properties such as density, heat capacity, volatility and a chemical surrogate is a mixture with a chemical class composition that matches the real jet fuel and can reproduce chemical properties such as reaction rates, ignition and sooting behaviour. A surrogate mixture that has the same chemical and physical properties as the real fuel is characterized as a comprehensive surrogate and can be expected to match diverse aspects of the real fuel behaviour such the evaporation process and the sooting tendency [7].

The current work evaluates the use of a reaction class based concept for the generation of chemical mechanisms for surrogate fuel compounds. Reaction classes for higher aromatics, such as naphthalene and indene are defined based on similarities with the oxidation of cyclopentadiene and benzene and subsequently applied to model the oxidation of toluene, n-propyl benzene, naphthalene and 1-methyl naphthalene. The current work extends past efforts related to the aforementioned systems. The selected compounds have been identified as important in the context of a range of surrogate fuel compositions from gasoline to aviation fuels. Specifically, methyl groups on aromatic rings (e.g. xylenes and tri-methyl benzenes), or alkyl branches in general, have been identified as important in the context of ignition properties and 1-methyl naphthalene may also be used to modulate sooting tendencies in aviation and Diesel surrogates. These systems therefore constitute a natural starting point for the evaluation of the current approach. The composition of an aviation fuel may be determined via UV spectrophotometric analysis of the concentration of individual compounds and a chromatographic analysis of the total aromatic content. An example of a chromatograph of a fuel sample is shown in Figure 1.1.

The construction of a chemical mechanism is a complex task that can be simplified with the identification of principal reaction pathways and reaction classes combined with major intermediate species that are formed through oxidation or pyrolysis of higher hydrocarbon molecules. Some reactions have been studied experimentally under combustion conditions and determined rates can often be implemented directly in the relevant mechanism following a critical appraisal. Such reactions can also be utilised as template reaction steps

for the estimation of relevant routes and reaction rates of higher hydrocarbons by making adjustments based on molecular properties. When suitable experimental data is not available, other ways of determining new steps and reaction rates are through the application of collision theory [11], quantum mechanical methods [12] and semi-empirical methods [13].

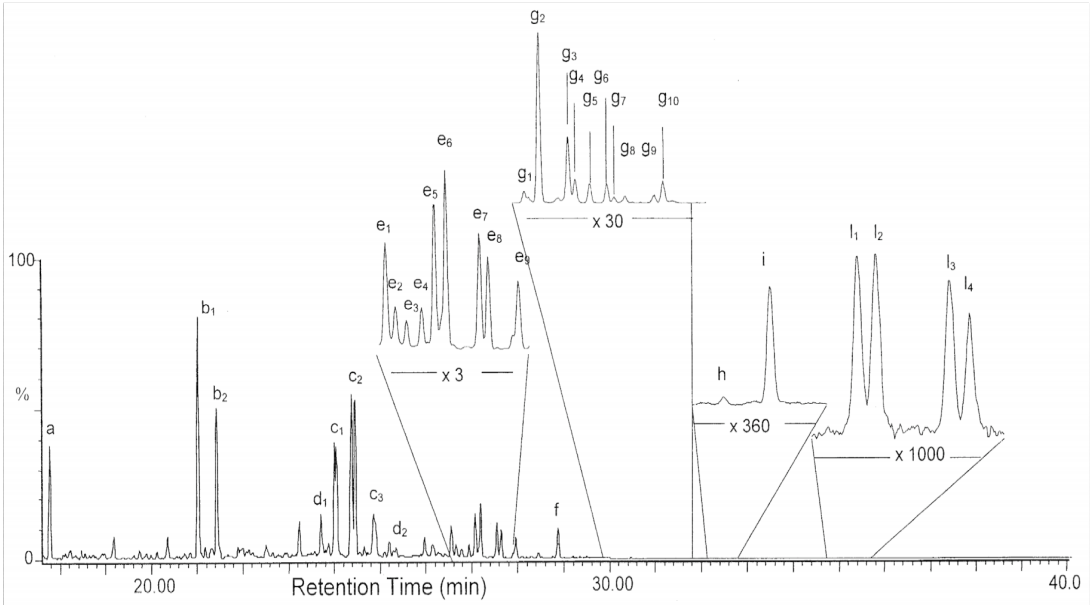


Figure 1.1. Chromatogram of a fuel sample. a) naphthalene, b) methyl naphthalene, c) ethyl naphthalenes, d) $C_3$-naphthalenes, e) diphenylamine, f) $C_4$-naphthalenes, g) phenanthrene, h) anthracene, i) methyl anthracene [9]

Reaction rates that have been determined with all of the aforementioned methods are utilised in the present work and details are provided for each specific system in the following sections. Important reaction channels were identified for all systems and for selected pathways potential energy surfaces (PES) were determined via density functional theory (DFT) and composite quantum mechanical computations [15]. Both the Rice-Ramsperger-Kassel-Marcus/master equation (RRKM/ME) and variable transition state theory (VTST) approaches were used to derive estimates of the rate constants. Improved thermodynamic data for a wide range of intermediate species was also determined at the G3MP2B3 level in combination with DFT analysis for internal rotations [15]. Data has also been obtained from Burcat and Ruscic [14] where appropriate. The parts of the detailed chemical mechanisms discussed in the current report can be found in Appendix A.

## 2.0 The Cyclopentadiene System

The study of the chemical kinetics of aromatic hydrocarbons in combustion processes has become a main focus of combustion research. Apart from the environmental impact caused by soot formation, polyaromatic compounds have a biological impact on human health. However, detailed chemical models are often tentative. There is a limited amount of elementary reaction rate data in the literature, which is mostly focussed on single ring molecules such as benzene and toluene. Benzene oxidizes to the phenoxy radical which decomposes to the cyclopentadienyl radical and carbon monoxide. The cyclopentadienyl radical is subject to ring opening and forms a transition point between aromatic and aliphatic compounds [24]. Cyclopentadiene is also an important intermediate species in the combustion of other single ring aromatics. The potential importance of the cyclopentadienyl radical in PAH growth has also been noted in various studies [25-31]. Hence, an adequate knowledge of the cyclopentadienyl combustion chemistry is essential for the accurate modelling of the aromatic components of the aviation fuels.

The pyrolysis of cyclopentadiene has been extensively studied behind reflected shock waves [24, 32-36], but there is only one detailed oxidation study, performed by Butler and Glassman [24] using a plug flow reactor. It is generally agreed that the cyclopentadiene consumption under pyrolytic conditions begins with CH fission leading to the formation of the cyclopentadienyl radical plus a hydrogen atom (13).

$$C_5H_6 = C_5H_5 + H \qquad (13)$$

There are significant differences in reaction rates obtained in the different studies. Roy *et al.* [34] studied the pyrolysis of cyclopentadiene in argon mixtures over a pressure range of 0.7 to 5.6 bar and obtained a rate constant of $k_{13}= 4.0 \times 10^{14} \exp(-38760/T)\ s^{-1}$ for which they concluded that there was no pressure dependence. Kern *et al.* [36] studied cyclopentadiene pyrolysis at reduced pressures in the range 100-450 Torr and proposed a barrier of 368 kJ/mol for the CH fission when combined with a non-Arrhenius fit. Colket *et al.* [35] proposed a rate constant of $k_{13}= 2 \times 10^{15} \exp(-339\ \text{kJ mol}^{-1}/RT)\ s^{-1}$ for a range of slightly higher pressures than the study of Roy *et al.* [34]. Zhong and Bozzelli [37] suggested a rate of $k_{13}= 5.96 \times 10^{14} \exp(-314\ \text{kJ mol}^{-1}/RT)\ s^{-1}$, which was calculated using the Quantum Rice-Ramsperger Kassel (QRRK) approach at atmospheric pressure and a temperature range of 900 - 1300 K.

Roy *et al.* [33] studied the reverse reaction, which involves the cyclopentadienyl recombination with a hydrogen atom (-13), behind reflected shock waves and a rate

constant of $k_{-13}$=2.6 x $10^{11}$ $m^3$ $kmol^{-1}$ $s^{-1}$ was obtained at a pressure of 2 bar. Hence, in combination with the previous study by the same group, an equilibrium constant for reaction (13) was calculated. Moreover, data for the enthalpy of formation of the $C_5H_5$ were obtained. Zhong and Bozzelli [37] also proposed a high-pressure limit rate constant of $k_{-13}$= 3.2 x $10^{11}$ $m^3$ $kmol^{-1}$ $s^{-1}$ for reaction (-13). The rate proposed was tested against the data of Lovell *et al.* [38] at 1 atm and 1100 K and there were discrepancies of about a factor of 2 between the model and measurements. In the current work the rate determined by Kern *et al.* [36] has been adopted.

The H abstraction leading to the formation of the cyclopentadienyl radical and molecular hydrogen is another important reaction channel for the decomposition of cyclopentadiene.

$$C_5H_6 + H = C_5H_5 + H_2 \qquad (9)$$

Roy *et al.* [34] studied reaction (9) and obtained a rate constant of $k_9$ = 2.8 x $10^{10}$ exp(-1137/T) $m^3$ $kmol^{-1}$ $s^{-1}$. On the other hand Emdee *et al.* [39] proposed a rate constant of $k_9$ = 2.19 x $10^5$ x $T^{1.77}$ exp(-125 kJ $mol^{-1}$/RT) $m^3$ $kmol^{-1}$ $s^{-1}$. Moskaleva and Lin [40] studied the reaction between hydrogen and cyclopentadiene at the modified Gaussian-2 level of theory and provided potential energy surfaces and reaction rates for the channel. The transition state (TST) and Rice-Ramsperger-Kassel-Marcus (RRKM) calculations performed produced a rate constant $k_9$ = 3.03 x $10^5$ $T^{1.71}$ exp(-117 kJ $mol^{-1}$/T) $m^3$ $kmol^{-1}$ $s^{-1}$ valid for a temperature range 1000 K ≤ T ≤ 3000 K. The study showed that the abstraction rate constant does not have any pressure dependency, but a positive temperature dependence. Moskaleva and Lin [40] also showed that, apart from hydrogen abstraction, hydrogen addition to the cyclopentadiene ring should also be included in the modelling of the system.

The CH fission leading to the cyclopentadienyl radical is followed by C-C breakage and the formation of acetylene and the propargyl radical (3). Studies have shown that this reaction is a multi-step process which leads to a stable intermediate and then a ring opening producing open chain radicals followed by the C-C fission for the formation of the final products [41].

$$C_5H_5 = C_3H_3 + C_2H_2 \qquad (3)$$

Roy *et al.* [34] performed computations for reaction channel (3) and optimized the geometries of the cyclopentadienyl radical and of all the intermediates, the transition states and products at the UHF/6-31G* level. According to their study, the cyclic $C_5H_5$ decay is initiated by a 1,2-H transfer followed by a ring opening and isomerization to a number of straight chain radicals that lead to the formation of acetylene and the propargyl radical. However, application of the proposed rate resulted in an over-prediction of acetylene

concentrations by a factor of three. Hence, they reduced the rate constant by a corresponding factor and achieved a good agreement with measurements. In addition to this study, Moskaleva and Lin [40] estimated the barrier heights of the 1,2 hydrogen transfer in the cyclopentadienyl radical (274.9 kJ/mol), ring opening (317.1 kJ/mol) and C-C breakage (317.1 kJ/mol), which are in agreement with values proposed by Roy *et al.* [34] obtained using lower level computations [41]. Kern *et al.* [36] also obtained a rate constant for reaction (3) using RRKM computations. The 1,2-H migration was identified as the rate-limiting step with a barrier of 259.0 kJ/mol. The result is in contrast to Roy *et al.* [34] who proposed the ring opening as the rate limiting step. Kern *et al.* [36] also showed that there is a 10-fold reaction-path-degeneracy that arises from a facile pseudorotation in the molecule.

Cyclopentadiene, apart from the unimolecular decomposition leading to the formation of acetylene and the propargyl radical which contribute to PAH growth, can also recombine with itself or its radical leading to the formation of naphthalene or indene [26, 42]. There are a number of studies that have exploited this potential formation mechanism. Melius *et al.* [26] studied the recombination of two cyclopentadienyl radicals that lead to the formation of naphthalene via a nine step mechanism that goes through the formation of hydrofulvalene and involves a three-membered ring closing and opening of resonance-stabilized radicals. Kislov and Mebel [43] showed that at low temperatures naphthalene was the major product whereas at high temperatures fulvalene was dominant. Lu *et al.* [44] extended the mechanism of PAH growth of naphthalene formation from cyclopentadienyl recombination, as proposed by Melius *et al.* [26], to compounds that contain four six-membered rings.

Lindstedt *et al.* [45] and Lindstedt and Rizos [46] questioned the global reaction rate proposed by Marinov *et al.* [42], as computations [46] showed that naphthalene levels were up 35 times higher than measurements in systems with high cyclopentadienyl concentrations. Moreover, McEnally and Pfefferle [47] performed experimental work with $^{13}C$-labeled aromatic compounds and showed that the labelled cyclopentadienyl moieties did not contribute significantly to second ring formation under their conditions. Hence, an alternative two-step reaction featuring stabilization of $C_5H_5$-$C_5H_4$ with a a barrier of 34 kJ/mol was proposed by Lindstedt *et al.* [45]. The applied barrier thus follows the potential energy surface determined by Melius *et al*. [26].

The potential role of cyclopentadienyl moieties in PAH growth was also studied by Mulholland and co-workers [48] and the results suggest that indene, naphthalene and benzene are major products of cyclopentadiene pyrolysis. Apart from the cyclopentadienyl

radical route to naphthalene, recombination has also been proposed as route to other aromatics. The importance of such reaction for PAH growth was studied by Violi and co-workers [49-51], who proposed a two-step molecule-radical addition mechanism followed by rearrangement. Wang *et al.* [25] applied the molecule radical mechanism in order to produce new pathways for the formation of indene and naphthalene during cyclopentadienyl pyrolysis. Four new reaction pathways for aromatic growth from cyclopentadiene pyrolysis were proposed leading to naphthalene, indene and benzene via intramolecular addition, C-H and C-C scissions. Density functional theory calculations were performed to calculate transition states, energy barriers for isomerizations, β-scissions and dissociation reactions. The study suggested that indene was mainly formed by intramolecular addition of cyclopentadiene to cyclopentadienyl via a resonantly stabilised cyclopentadiene-cyclopentadienyl dimer.

Kislov and Mebel [52] also studied indene formation via the combination of cyclopentadiene and the cyclopentadienyl radical and showed that at temperatures relevant to combustion, indene was the major product (> 50%). The mechanism suggested, combined with their computed tests, was in agreement with experimental data for cyclopentadienyl pyrolysis that showed both naphthalene and indene as major products. Another reaction route that involves the cyclopentadienyl radical features its combination with the methyl radical leading to the formation of fulvene ($C_5H_4CH_2$), which subsequently isomerizes to benzene. Moskaleva *et al.* [53] studied this reaction route and showed that the combination of the two radicals produce an intermediate specie ($C_5H_5CH_3$) that proceeds to the formation of $C_5H_4CH_3$ + H. The hydrogen elimination occurs from the ring since the C-H bond is weaker than that of the methyl group. The second hydrogen atom elimination comes from $C_5H_4CH_3$ leading to the formation of fulvene. The reaction channel was also studied by Melius *et al.* [26] who underlined the importance of hydrogen migration around the cyclopentadienyl moiety in providing resonance-stabilized radicals. The findings are also supported by a more recent study of Lindstedt and Rizos [46] on the oxidation of cyclopentene.

## 2.1 The Current Contribution

The starting point for the current work stems from previous studies related to the chemistry of aromatics [45, 46], the oxidation of fine carbon based particles [54] and an earlier study by Zhong and Bozzelli [37]. The current report is focussed on the oxidation of cyclopentadiene, but pyrolysis cases have also been studied with similar agreement to that shown below.

The developed mechanism was validated under the plug flow reactor conditions used by Butler [55]. Rates were analysed for both fuel lean and rich conditions and for temperatures varying from 1100 to 1200 K. The studies identified possible reaction channels featuring O, OH, $HO_2$ and $O_2$, though estimates of the rates of reaction have proved problematic in the past. In the current work, reaction rates for isomerization reactions and the thermal dissociation of oxygenated $C_5$ species were updated using potential energy surfaces (PES) determined via density functional theory (DFT) and composite quantum mechanical computations [15]. Both the Rice-Ramsperger-Kassel-Marcus/master equation approach (RRKM/ME) and variable transition state theory (VTST) approaches were used to derive estimates of the rate constants [15]. Improved thermodynamic data for a wide range of intermediate species was also determined at the G3MP2B3 level in combination with density functional theory analysis for internal rotations.

The oxidation of cyclopentadiene was studied under plug flow reactor conditions obtained from Butler [55]. The full reaction mechanism applied here consists of 1431 reversible reactions and 269 chemical species. Three oxidation cases were computed for stoichiometric and rich fuel mixtures at atmospheric pressure utilizing nitrogen as the carrier gas. The conditions are presented in Table 2.1.

| Case | Φ | $T_0$ (K) | Initial Fuel (ppm) | Initial Oxygen (ppm) | Modelling Time Shift (ms) | Experimental Time Shift (ms) |
|---|---|---|---|---|---|---|
| 1 | 1.03 | 1198 | 2243 | 14128 | 20 | 36 |
| 2 | 1.03 | 1148 | 1051 | 6618 | 50 | 123 |
| 3 | 1.61 | 1153 | 2070 | 8363 | 20 | 50 |

Table 2.1 Experimental and modelling conditions for cyclopentadiene oxidation in a flow reactor. (The experimental time shifts correspond to the time shift applied in the computations performed by Butler [55]).

A reaction rate analysis was performed for a stoichiometric fuel mixture with Φ = 1.03 at T = 1148 K, P = 1 atm and an initial fuel concentration of 1051 ppm. The fuel is consumed via four major channels that involve hydrogen abstraction via H, O and OH radicals and thermal decomposition.

Major species concentrations are compared to measurements as shown in Figs. 2.1 – 2.6. It can be seen that there is reasonably good agreement. However, surface chemistry interference with the gas phase chemistry was identified as a problem by Butler [55] and some caution is hence required. Moreover, during the experimental studies, measurements showed an initial discontinuous drop in the fuel concentration at the first data point due to

the recirculation zone in the diffuser and surface chemistry near the throat of the reactor [55]. Hence, a time shift is necessary in order to reproduce the species profiles.

Reaction (9) is responsible for 35% of the total fuel consumption and is assigned a rate proposed by Robinson [15]. The channel is of major importance as small perturbations to the reaction rate causes big differences in the fuel consumption profile. Approximately 25% of the fuel decay proceeds via reaction (11) that was assigned a rate proposed by Lindstedt and Rizos [46]. A rate discussed by Leung and Lindstedt [58] was used for reaction (10), which consumes a further 10%. Reaction (13) is responsible for 12% of the total fuel consumption and was assigned a rate proposed by Kern *et al*. [36].

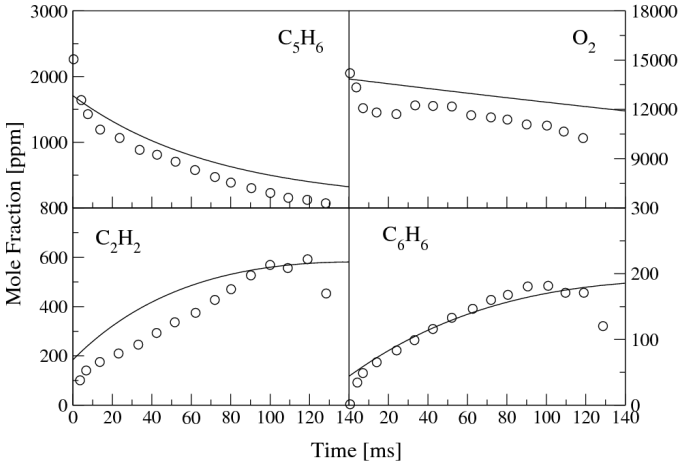


Figure 2.1 Concentration profiles during cyclopentadiene oxidation in a plug flow reactor for Φ = 1.03, P =1 atm, T = 1198 K, initial fuel concentration 2243 ppm (Case 1, Table 2.1). Circles are measurements [55] and the solid line the current simulation.

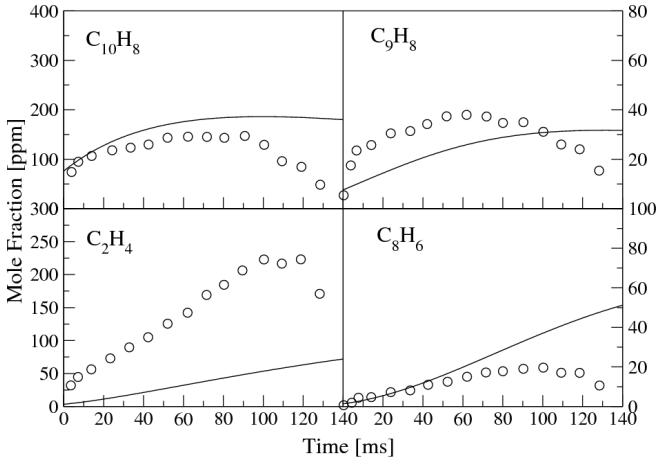


Figure 2.2 Concentration profiles during cyclopentadiene oxidation in a plug flow reactor for Φ = 1.03, P =1 atm, T = 1198 K, initial fuel concentration 2243 ppm (Case 1, Table 2.1). Circles are measurements [55] and the solid line the current simulation.

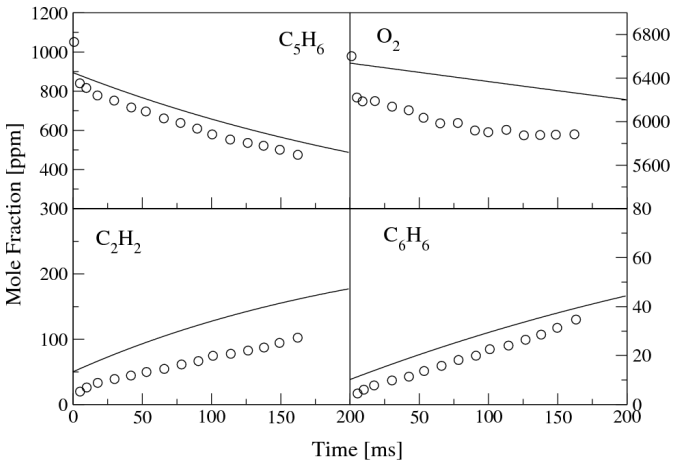


Figure 2.3 Concentration profiles during cyclopentadiene oxidation in a plug flow reactor for Φ = 1.03, P =1 atm, T = 1148 K, initial fuel concentration 1050 ppm (Case 2, Table 2.1). Circles are measurements [55] and the solid line the current simulation.

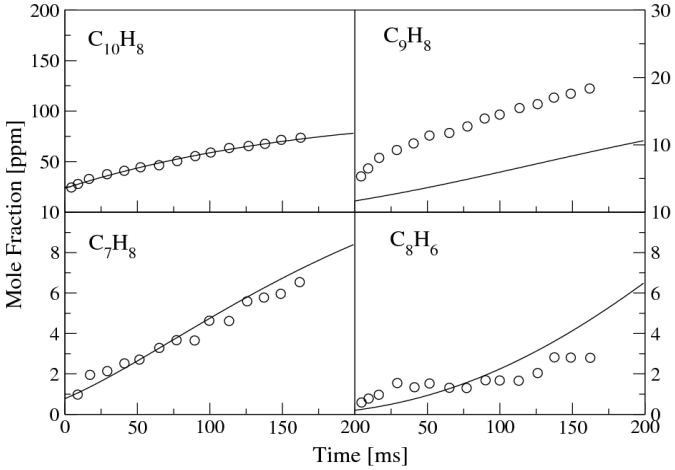


Figure 2.4 Concentration profiles during cyclopentadiene oxidation in a plug flow reactor for Φ = 1.03, P =1 atm, T = 1148 K, initial fuel concentration 1050 ppm (Case 2, Table 2.1). Circles are measurements [55] and the solid line the current simulation.

Around 85% of the fuel consumption leads to the cyclopentadienyl radical. The consumption of $C_5H_5$ follows two major routes. The pathway leading to $C_{10}H_9F$ (6) is responsible for 33% of the consumption and was assigned a rate proposed by Lindstedt *et al.* [45]. The second major consumption channel (33%) occurs via thermal decomposition of the cyclopentadienyl radical via C-C scission leading to acetylene and the propargyl radical (3). The channel is of significant importance and affects the temporal evolution of the acetylene concentration profile. A rate of Kern *et al.* [36] was also evaluated, but found to lead to an overproduction of acetylene by 50%. Hence, an adjustment by a factor of 2 was applied leading to more reasonable acetylene profiles.

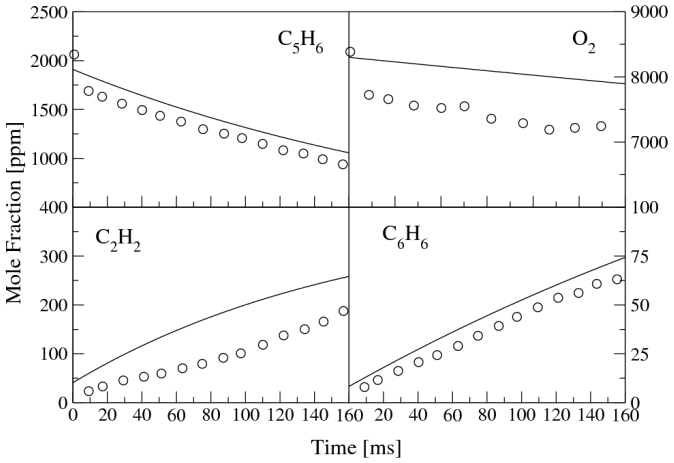


Figure 2.5 Concentration profiles during cyclopentadiene oxidation in a plug flow reactor for Φ = 1.61, P =1 atm, T = 1153 K, initial fuel concentration 2070 ppm (Case 3, Table 2.1). Circles are measurements [55] and the solid line the current simulation.

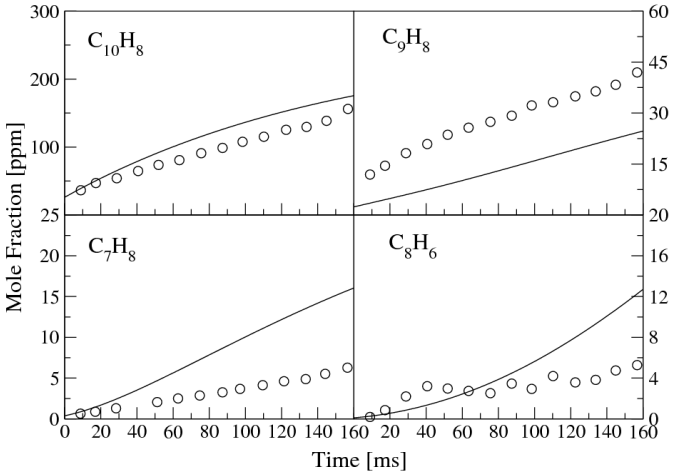


Figure 2.6 Concentration profiles during cyclopentadiene oxidation in a plug flow reactor for Φ = 1.61, P =1 atm, T = 1153 K, initial fuel concentration 2070 ppm (Case 3, Table 2.1). Circles are measurements [55] and the solid line the current simulation.

The oxidation channels featuring $HO_2$ attack leading to the formation of $C_5H_4O$ (7) and $C_5H_5O$ (5) are each responsible for 8% of the $C_5H_5$ consumption.

$$C_5H_5 + C_5H_5 = C_{10}H_9F + H \quad (6)$$

$$C_5H_5 = C_3H_3 + C_2H_2 \quad (3)$$

$$C_5H_5 + HO_2 = C_5H_4O + H_2O \quad (7)$$

$$C_5H_5 + HO_2 = C_5H_5O + OH \quad (5)$$

The $C_{10}H_9F$ moiety is a precursor to naphthalene, which is subsequently formed via thermal dissociation (79). Naphthalene decomposes through two major reaction channels that involve hydrogen abstraction (78) via OH (49%) and oxygen addition (77) forming $C_{10}H_7O$

(39%) that were assigned rates adopted from the kinetics of benzene and adjusted according to molecular weight differences.

$C_{10}H_9F = C_{10}H_8 + H$ (79)

$C_{10}H_8 + OH = C_{10}H_7 + H_2O$ (78)

$C_{10}H_8 + O = C_{10}H_7O + H$ (77)

Indene is formed predominantly (48%) through acetylene recombination with the benzyl radical (34). The rate assigned to this channel was adopted from Colket *et al.* [59]. An additional 44% of the indene formation comes from the recombination of cyclopentadiene and cyclopentadienyl radical (12) with the simultaneous abstraction of a methyl radical. The reaction channel was studied extensively by Wang *et al.* [25], who proposed possible intermediate routes for the naphthalene and indene formation via $C_5H_6$ (CPD) and $C_5H_5$ (CPDyl) recombination. In this study it is assumed that the recombination of the two species does not stabilize to the CPD-CPDyl intermediate, but leads to a bridged intermediate specie with the radical on the bridged atom. The highest energy barrier (177 kJ/mol) that occurs from the conversion of this bridged specie to the final indene molecule through other intermediate routes, as discussed by Wang *et al.* [25], was used as the activation energy of the global step.

$C_7H_7 + C_2H_2 = C_9H_8 + H$ (34)

$C_5H_5 + C_5H_6 = C_9H_8 + CH_3$ (12)

Indene decomposes solely to the indenyl radical via three major reaction routes. Reaction (73) is responsible for 59% of the indene consumption, (65) for 21% and (74) 12% respectively. Reactions rates utilized for these three indenyl consumption routes are adopted from suggestions by Potter [60] based on the kinetics of cyclopentadiene with reaction rates proposed by Lindstedt and Rizos [46] and Rizos [57].

$C_9H_8 + H = C_9H_7 + H_2$ (73)

$C_9H_7 + H = C_9H_8$ (65)

$C_9H_8 + OH = C_9H_7 + H_2O$ (74)

Approximately 63% of the total indenyl radical comes from indene and 23% is produced via CO expulsion from $C_{10}H_7O$, which is one of the major products of naphthalene oxidation. The indenyl radical is the precursor of phenylacetylene via the formation of $C_9H_7O$. The indenyl radical oxidizes to $C_9H_7O$ (83%) via reaction with the $HO_2$ radical. The reaction rate utilized for this channel was obtained by Lindstedt *et al.* [54]. The $C_9H_7O$ molecule decomposes to $C_8H_7$ (100%) via CO expulsion followed by thermal dissociation of $C_8H_7$ leading to the formation of phenylacetylene.

$C_9H_7 + HO_2 = C_9H_7O + OH$ (68)

$C_9H_7O = C_8H_7 + CO$ (75)

$C_8H_7 = C_8H_6 + H$ (58)

Phenylacetylene is consumed via four major reaction pathways that predominantly feature oxygen attack. The displacement of the chain via oxygen atom attack is responsible for 33% of the phenylacetylene consumption (54) and the step features a rate suggested by Lindstedt *et al.* [45]. The second major channel (22%) involves hydrogen abstraction via OH (52). A rate adopted by Frenklach et al. [61] was assigned to this channel. Moreover, reactions (53) and (51) involve hydrogen abstraction/oxygen addition and consume 12% and 11%, respectively. Rates applied to these channels were adopted from Potter [60].

$C_8H_6 + O = C_6H_5 + C_2HO$ (54)

$C_8H_6 + OH = C_8H_5 + H_2O$ (52)

$C_8H_6 + O = C_8H_5O + H$ (53)

$C_8H_6 + O = C_6H_5C_2O + H$ (51)

Toluene is formed from the benzyl radical, with the formation of the benzyl radical controlled (84%) by the recombination of the cyclopentadienyl radical with acetylene. The rate for the channel originally stems from the work of Colket and Seery [62].

$C_5H_5 + C_2H_2 = C_7H_7$ (2)

$C_7H_8 = C_7H_7 + H$ (38)

Approximately 22% of toluene leads to the formation of benzene through a chain displacement reaction via hydrogen. However, benzene is predominantly formed (94%) through isomerisation from fulvene (26). The isomerization of fulvene to benzene is assigned a rate proposed by Marinov *et al.* [63]. Fulvene is mostly produced via isomerization reactions from $C_6H_6$(S) (43%) and $C_6H_6$(B) (26%) and via thermal hydrogen dissociation (26%) from $C_5H_4CH_3$. The methyl cyclopentadienyl radical is formed via recombination of $CH_3$ with $C_5H_5$ (93%) and was assigned a rate adopted from suggestions of Lindstedt *et al.* [45]. Acetylene is predominantly formed (77%) by the thermal decomposition of the cyclopentadienyl radical.

$C_5H_5 = C_2H_2 + C_3H_3$ (3)

A reaction rate analysis was also performed for a fuel rich mixture with $\Phi = 1.61$ at T = 1153 K, P = 1 atm and an initial fuel concentration of 2070 ppm. The fuel consumption follows the same routes as in the stoichiometric case. However, the impact of reaction (9) increases by 4% and the impact of reactions (11) and (14) reduce by 4-5% compared to the stoichiometric case.

$C_5H_6 + H = C_5H_5 + H_2$ (9)

$C_5H_6 + OH = C_5H_5 + H_2O$ (11)

$C_5H_7 = C_5H_6 + H$ (14)

The cyclopentadienyl radical follows two major consumption routes under fuel rich conditions, as was the case for the stoichiometric conditions, and 38% of $C_5H_5$ leads to $C_{10}H_9F$ via recombination and 26% thermally decomposes to acetylene and the propargyl radical. The reactions featuring $HO_2$ attack and leading to formation of $C_5H_5O$ and $C_5H_4O$ perform similarly to the stoichiometric case and found to be responsible for 8% of total cyclopentadienyl consumption.

The naphthalene, indene, styrene, toluene, butadiene and acetylene formation and consumption routes follow the same behaviour as in stoichiometric mixtures with a perturbation of order 4-6% for each of the steps. Apart from the rate analysis performed for a temperature range of 1149 – 1153 K, a test was also performed for a stoichiometric fuel mixture (Case 1 – Table 2.1) at the temperature of T = 1198 K in order to identify important fuel decomposition pathways. Reactions (9) and (11) were found to be dominant and contribute 33% and 27% to the fuel consumption. Moreover, reaction (10) is responsible for 12% at the higher temperature.

$C_5H_6 + H = C_5H_5 + H_2$ (9)

$C_5H_6 + OH = C_5H_5 + H_2O$ (11)

$C_5H_6 + O = C_5H_5 + OH$ (10)

It should be highlighted that once the cyclopentadienyl radical is formed, its consumption is controlled by two dominant reaction channels that are identical to the $C_5H_5$ consumption route for rich mixtures, with the difference that the role of reactions (6) and (3) is somewhat affected. The impact of reaction (3) increases from 32% for stoichiometric and 26% for rich mixtures at T = 1149 K to 34% for stoichiometric mixtures at a temperature of T = 1198 K. Whereas the contribution of the cyclopentadienyl recombination reaction falls from 38% for rich and 33% for stoichiometric mixtures at the lower temperature, to 24% for stoichiometric mixtures at the higher temperature. Accordingly, the more the temperature increases, the more the thermal decomposition of $C_5H_5$ dominates consumption.

$C_5H_5 + C_5H_5 = C_{10}H_9F + H$ (6)

$C_5H_5 = C_3H_3 + C_2H_2$ (3)

Due to the impact of the $C_5H_5$ decomposition channels on the evolution of the cyclopentadienyl radical, the concentration of the naphthalene is increased by about 50% compared to the lower temperature case of about T = 1150 K. Added to this, the fuel at T =

1198 K shows a steep decomposition profile and the acetylene concentration is double compared to the T = 1153 K oxidation case.

The increased impact of the thermal decomposition route of the $C_5H_5$, is responsible for the increased propargyl radical and acetylene concentrations. The propargyl radical pool follows a recombination route that produces benzene. Hence, as expected, the benzene concentration is increased by 60% at the temperature of T = 1198 K as compared to the T = 1150 K cases. Moreover, the concentration of benzene is affected by the increased contribution of reaction (1) leading to $C_5H_4CH_3$, which is the precursor to fulvene.

$$C_5H_5 + CH_3 = C_5H_4CH_3 + H \qquad (1)$$

The formation and consumption routes of the rest of the intermediate species, such as indene, phenylacetylene, toluene follow the same behaviour as at lower temperatures.

## 3.0 The Oxidation of Toluene

Alkylated benzenes are a significant hydrocarbon class in practical fuels, hence a detailed knowledge of their combustion chemistry is necessary. Toluene is the simplest example and its chemistry constitutes the starting point for the development of mechanisms describing other alkylated benzenes. Specifically, in the current work the molecule forms the basis for the further evaluation of the chemistry of n-propyl benzene and 1-methyl naphthalene as described in subsequent sections.

There is a comparatively rich literature on the oxidation of toluene as compared to other aromatic molecules. Emdee *et al.* [39] developed a model for high temperature toluene oxidation utilizing previous benzene and toluene schemes and validated it with flow reactor experiments at temperatures from 1100 to 1200 K at atmospheric pressure. Klotz *et al.* [65] updated the Emdee *et al.* [39] model and validated it against toluene-butane fuel blends. Dagaut *et al.* [66] developed a model that describes toluene oxidation and validated it against jet-stirred reactor data for a temperature range of 1000 – 1375 K and equivalence ratios from 0.5 - 1.5. Lindstedt and Maurice [67] developed a comprehensive toluene mechanism and validated it against experimental data from plug flow reactors, shock tubes, counterflow diffusion flames and premixed flames. Sivaramakrishnan *et al.* [68] developed a detailed chemical model based on an earlier literature model for toluene oxidation and validated it against shock tube experimental data at temperatures in the region 1200 - 1500 K, over a wide pressure range (25 – 610 bar) and for stoichiometries of $\Phi = 1$ and $\Phi = 5$.

A number of experimental studies reported in the literature describe toluene oxidation or thermal decomposition. Ignition delay times in argon mixtures were measured by Burcat *et al.* [69] for toluene concentration of 0.5 to 1.5%, 4.48 to 13.45% oxygen, temperatures in the range of 1339 - 1797 K and with reflected shock pressures from 1.95 to 8.85 atm. More recent studies on toluene oxidation were performed by Vasudevan *et al.* [70] and Davidson and co-workers [71]. Vasudevan *et al.* [70] measured ignition delay times and OH radical concentrations in toluene/$O_2$/Ar mixtures behind reflected shock waves at high temperatures (1400 - 2000 K) and low pressures (1 - 4 atm) for equivalence ratios of 0.5 - 1.875 with toluene concentrations of 0.025 - 0.5%. The measured toluene ignition delay times were compared with the models of Pitz *et al.* [72], Dagaut *et al.* [66] and Lindstedt and Maurice [67]. At low to moderate temperatures, the data agrees with the model of Dagaut *et al.* [66] and Pitz *et al.* [72] whereas at higher temperatures the model by Dagaut *et al.* [66] shows a better agreement with measurements. The measurements of ignition delay times against fuel concentration shows that the ignition time falls as the fuel concentration increases and this trend is also supported by Burcat *et al.* [69]. The Lindstedt and Maurice [67] model captures the trend of the experimental model but with lower ignition delay times. The Pitz *et al.* [72] and Dagaut *et al.* [66] models can predict the ignition delays at low fuel concentrations but show a significant disagreement at high fuel concentrations.

Davidson *et al.* [71] measured OH concentrations and ignition delay times in a shock tube for toluene/air at low temperatures (855 - 1269 K) and high pressures (14 - 59 atm) for equivalence ratios of 0.5 and 1 in synthetic air. The ignition delays were compared against the models of Pitz *et al.* [72] and Dagaut *et al.* [66]. The model of Dagaut *et al.* [66] predicts ten times longer ignition delays than the experiments of Davidson *et al*. [71] and the model of Pitz *et al.* [72] predicts ignition delay times up to two times longer than the measurements. However, for $\Phi = 0.5$ the model of Pitz *et al.* [72] captures the data well.

The toluene initiation reactions have been the target of several studies. Pamidimukkala *et al.* [73] performed shock tube studies with time-of-flight mass spectrometry and laser schlieren densitometry for a temperature range of 1550 - 2000 K and pressures of 0.2 - 0.5 atm. Their study supports the dominance of C-C scission in toluene dissociation leading to the production of methyl and phenyl radicals (39) against the C-H scission leading to the benzyl radical and the hydrogen atom (38).

$$C_7H_8 \xrightarrow{k_{1079}} C_7H_7 + H \qquad (38)$$

$$C_7H_8 \xrightarrow{k_{1080}} C_6H_5 + CH_3 \qquad (39)$$

In addition, it was suggested that the stability of the benzyl radical leads to a partial equilibrium, whereas the less stable phenyl radical makes reaction (39) irreversible and hence a major route in the thermal dissociation of toluene. Colket and Seery [62] performed shock tube studies fortemperature range of 1100 - 2700 K and suggested that (39) always controls the distribution of products from toluene dissociation.

Rao and Skinner [74] monitored the formation of hydrogen atoms under pyrolytic conditions behind shock waves in argon mixtures at a total pressure of 0.4 atm and for a temperature range of 1450 - 1790 K. Rate constants for the two major toluene dissociation channels were proposed and it was concluded that the hydrogen abstraction reaction (38) is the only important initiation step. The study was also supported by Muller-Markgraf and Troe [75], who studied the benzyl radical absorption during its decay behind shock waves. Added to this, Brouwer *et al.* [76], utilising UV spectroscopy to study the toluene thermal decomposition, highlighted the dominance of the hydrogen dissociation channel.

Braun-Unkhoff [77] monitored the formation of the hydrogen atom during thermal decomposition in the temperature range of 1300-1800 K, pressures of 1.5 - 7.8 bar in argon mixtures and highlighted the importance of $CH_3$ formation (39) for the product distribution. The results also suggested that the hydrogen abstraction from toluene leading to the formation of benzyl radical is important.

Rate constants were proposed in the above studies for the two dissociation channels. For the C-H bond scission, Rao and Skinner [74] assigned an energy barrier of 360 kJ/mole, Braun-Unkhoff *et al.* [77] assigned a value of 374 kJ/mole and Brouwer *et al.* [76] a value of 369 kJ/mole. Later shock tube studies by Hippler and Troe [78] revised the C-H bond scission dissociation channel and assigned a new rate with a barrier of 360 kJ/mole over a temperature range of 1200-1500 K and a value of 356 kJ/mole in a flow system over a temperature range of 913-1143 K.

Eng *et al.* [79] investigated the thermal decomposition of toluene at temperatures in the range 1350 - 1900 K and for pressures from 0.1 to 2.0 bar. It was suggested that toluene dissociation proceeds mainly via (38) for which a rate constant was determined based on H-atom detection via calibrated atomic resonance absorption spectroscopy. The reaction showed no pressure dependence at lower temperatures, whereas at the highest temperature a slight pressure dependence was observed. Moreover, Eng *et al.* [79] suggested that the branching ratio $k_{38} / (k_{38} + k_{39})$ for toluene decomposition is affected by temperature and pressure.

A more recent study of the thermal decomposition of toluene was performed by Oehlschlaeger *et al.* [80], who investigated the contribution of the two dissociation channels

in shock wave experiments over a temperature range of 1400 - 1780 K and at a pressure of 1.5 bar. The benzyl radical absorption at 266 nm was monitored during toluene decomposition in argon mixtures and the rates for the two channels were determined. Moreover, it was suggested that the above branching ratio between the two channels varied from 0.8 at 1450 K to 0.6 at 1800 K. The findings were compared to previous studies and it was found that the overall decomposition rate agrees with a deviation of less than 30% from the results of Braun-Unkhoff *et al.* [77] and Eng *et al.* [79] and, hence, is faster than proposed by Pamidimukkala *et al.* [73] and Rao and Skinner [74]. The branching ratio is in good agreement with Eng *et al.* [79], but in disagreement with Pamidimukkala *et al.* [73] and Braun-Unkhoff *et al.* [77].

In the present study, the comprehensively validated detailed mechanism developed by Lindstedt and Maurice [67], with subsequent developments by Potter [60], was used as a starting point for the re-evaluation of the toluene chemistry in light of recent studies. The toluene sub-mechanism features 103 elementary reactions and 23 species. Further analysis was performed and improvements made by considering new reaction channels and rates.

### 3.1 The Current Contribution

The complete mechanism was validated and analysed against data and conditions corresponding to i) shock tube data for toluene pyrolysis [77] and ii) shock tube data for toluene oxidation [69, 70]. The rates of toluene pyrolysis were analysed at conditions corresponding to the shock tube experiments of Braun-Unkhoff *et al.* [77]. Moreover, the toluene sub-mechanism was analysed at conditions corresponding to toluene oxidation in argon mixtures behind reflected shock waves (e.g. Vasudevan *et al.* [70] and Burcat *et al.* [69]). The validation and analysis of the current model was performed in order to analyse the principal reaction paths and to evaluate the new reaction steps and reaction rate updates. All the elementary reaction steps are assumed reversible with the reverse rates computed via chemical equilibrium. The following decomposition pathways were updated using the reaction rates determined by Oehlschlaeger *et al.* [80].

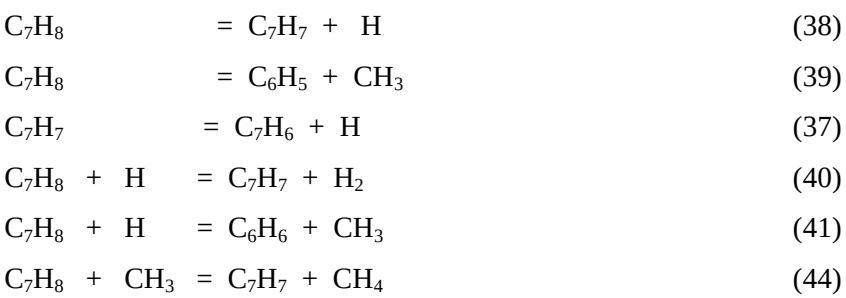

$C_7H_8 = C_7H_7 + H$ (38)

$C_7H_8 = C_6H_5 + CH_3$ (39)

$C_7H_7 = C_7H_6 + H$ (37)

$C_7H_8 + H = C_7H_7 + H_2$ (40)

$C_7H_8 + H = C_6H_6 + CH_3$ (41)

$C_7H_8 + CH_3 = C_7H_7 + CH_4$ (44)

Another addition involves the thermal decomposition of the benzylperoxy radical (50). The reaction rate was adjusted to the reverse rate of the corresponding dissociation reaction of the phenylperoxy radical (31) from DiNaro *et al.* [81].

$C_7H_7OO = C_7H_7O + O$ (50)

$C_6H_5OO = C_6H_5O + O$ (-31)

Reaction (50) was tested under the shock tube conditions of Davidson *et al.* [71] and was found to play a significant role in the evaluation of the OH profile and reduced the ignition delay time by approximately 22% as compared to the starting mechanism. The current model still fails to accurately capture low temperature (< 1269 K) ignition data and the following reaction path was also considered.

$C_7H_7 + O_2 = C_7H_7OO$ (36)

$C_7H_7OO = C_7H_6OOH$ (R1)

$C_7H_6OOH = C_7H_6O + OH$ (R2)

Reaction (R1) was found to be the rate-limiting step of the reaction sequence. Due to lack of accurate pathway information, the global step given by reaction (49) was added to the mechanism with a rate and barrier based on suggestions of Hunter *et al.* [82], with the relative isomerization $C_2H_5OO = C_2H_4OOH$ used as a reference for estimation purposes.

$C_7H_7OO = C_7H_6O + OH$ (49)

The three-step reaction pathway (36, R1, R2) follows the study of Zellner and Ewig [83], Walch [84] and Clothier *et al.* [85] for the arguably related sequence (R3 to R6)

$CH_3 + O_2 = CH_3OO$ (R3)

$CH_3OO = CH_3O + O$ (R4)

$CH_3OO = CH_2OOH$ (R5)

$CH_2OOH = CH_2O + OH$ (R6)

The reaction of methyl with molecular oxygen producing the methylperoxy radical leads either, via decomposition, to the methoxy radical and atomic oxygen (R4) or, via isomerization, to $CH_2OOH$ (R5). The later step is potentially important pathway under radical depleted conditions (e.g. during ignition). The activation energy for the transition state (R4) was found to be 243 kJ/mol whereas the activation energy for the transition state (R5) was only 160 kJ/mol. Hence, it was suggested that the production of $CH_2O$ + OH via (R6) occurs with a smaller activation barrier and dominates at temperatures below 2800 K. The two different channels for the $CH_3OO$ decomposition come from different electronic states. The species can exist either in the X3Σg- ground state (R4), where the closest 2p

orbital of the oxygen is double occupied from the electrons and 1,3-hydrogen migration is not possible, or in the 1Δg state (R5) where the same 2p orbital of the oxygen is singly occupied and hydrogen migration is favourable [84]. A schematic representation of the the ground and excited state of the oxygen atom on the benzylperoxy radical is shown in Fig. 3.1. However, according to Clothier *et al.* [85] the activation energy of reactions (R3-R4) is approximately 121 kJ/mol less that the value estimated by Zellner and Ewig [83].

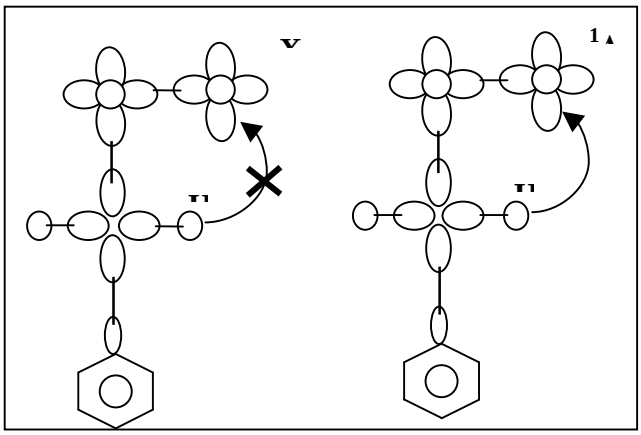

Figure 3.1 Schematic representation of electronic states of the two benzoperoxy radicals.

It is obvious that the above analogy is in need of refinement and that the current rates are subject to uncertainties. However, the pathway increases in significance under lower temperature conditions and the current study shows that further work is desirable. Another reaction step (2) that plays a significant role in both toluene pyrolysis and oxidation processes was added with a rate adopted from Colket and Seery [62].

$$C_5H_5 + C_2H_2 = C_7H_7 \qquad (2)$$

A rate from Muller-Markgraf and Troe [75] was also tested for the reverse reaction and was found to lead to an increase in ignition delays of approximately 20%.

The thermal decomposition of toluene in shock tubes was studied at conditions corresponding to experiments performed by Braun-Unkhoff *et al.* [77] in order to evaluate the branching ratio of the main toluene decomposition reaction channels and to monitor the temporal evolution of the hydrogen radical. Braun-Unkhoff *et al.* [77] studied the thermal decomposition in argon mixtures and measured H profiles at fuel concentrations of 2 - 19.3 ppm, temperatures of 1515 - 1655 K and pressures of 1.89 - 1.93 bar (Table 3.1). An attempt was made to model the experimental profiles using a ten-step reaction scheme to which adjustments had to be made in order to achieve the appropriate fit to the profiles.

The analysis outlined below follows Lindstedt and Maurice [67] and was performed to assess the consistency of the revised principal reaction paths mentioned above.

| | $C_7H_8$ (ppm) | T [K] | P [bar] |
|---|---|---|---|
| 1 | 2.0 | 1515 | 1.85 |
| 2 | 2.8 | 1655 | 1.89 |
| 3 | 3.0 | 1585 | 1.93 |
| 4 | 19.3 | 1555 | 1.92 |

Table 3.1 Experimental and modelling conditions for toluene thermal decomposition

The computed hydrogen profiles for all the experimental conditions are shown in Figs. 3.2 – 3.5. The modelled hydrogen profiles are reasonably well captured and show that the adopted branching ratio and rates determined by Oehlschlaeger *et al.* [80] are satisfactory.

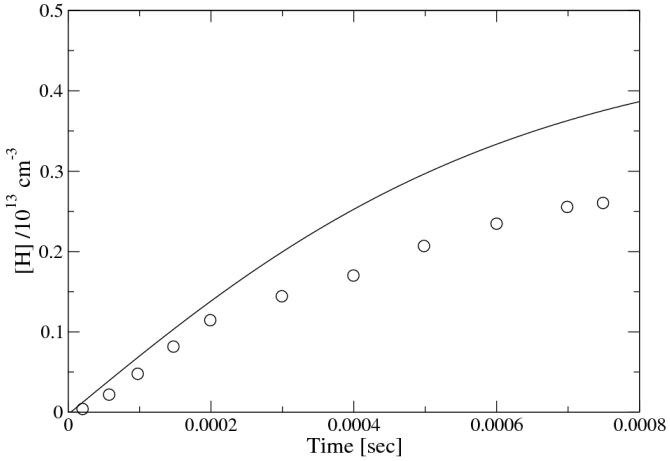


Figure 3.2 Hydrogen radical concentration against time for toluene thermal decomposition with an initial fuel concentration of 2.0 ppm, T = 1515 K and P = 1.85 bar. The solid line indicates the current computations and the circles indicate the experimental data from Braun-Unkhoff *et al.* [77].

The data used to validate the toluene mechanism under oxidation conditions was obtained from Vasudevan *et al.* [70], who monitored the time resolved OH radical concentration profiles in toluene/$O_2$/Ar mixtures in shock tubes. Vasudevan *et al.* [70] measured OH concentration profiles over a wide range of conditions. The study provides unique time-resolved data of a complementary nature to the pyrolysis experiments discussed above. In the present work, computations were performed corresponding to data with a temperature of 1689 K and pressure of 1.79 atm ($\Phi$ = 1, 0.1% $C_7H_8$, 0.9% $O_2$, 99% Ar). The computed profile is shown in Fig. 3.6 along with the experimental data of Vasudevan *et al.* [70].

There is excellent agreement between the measurements and the current toluene model. The OH profile can be divided in three regions; The first shows the rapid increase in the *OH* concentration due to toluene decomposition, the second where OH rises, indicating the presence and impact of the chain branching reactions and the third where the OH production is close to zero [70].

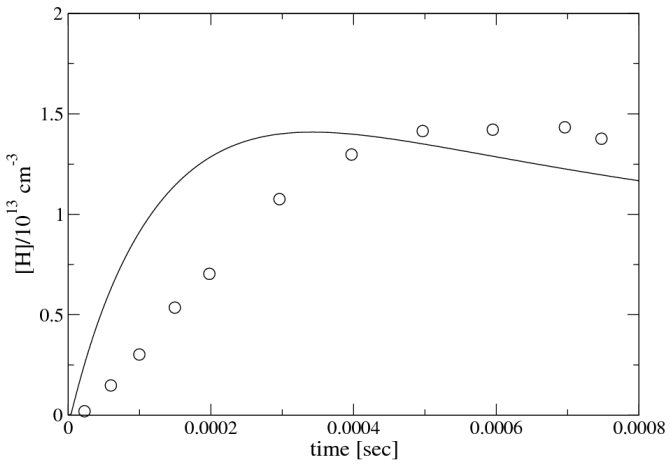


Figure 3.3 Hydrogen radical concentration against time for toluene thermal decomposition with an initial fuel concentration of 2.8 ppm, T = 1655 K and P = 1.89 bar. The solid line indicates the current computations and the circles indicate the experimental data from Braun-Unkhoff *et al.* [77].

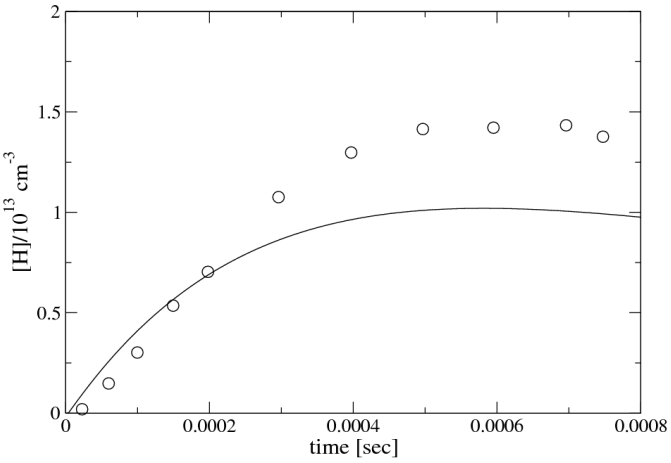


Figure 3.4 Hydrogen radical concentration against time for toluene thermal decomposition with an initial fuel concentration of 3.0 ppm, T = 1585 K and P = 1.93 bar. The solid line indicates the current computations and the circles indicate the experimental data from Braun-Unkhoff *et al.* [77].

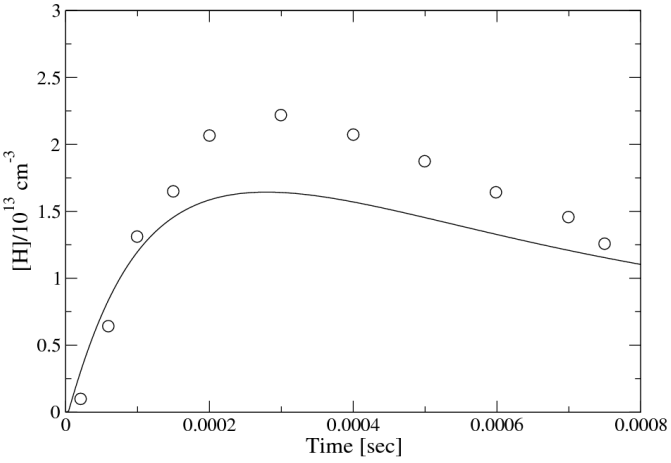


Figure 3.5 Hydrogen radical concentration against time for toluene thermal decomposition with an initial fuel concentration of 19.3 ppm, T = 1555 K and P = 1.92 bar. The solid line indicates the current computations and the circles indicate the experimental data from Braun-Unkhoff *et al.* [77].

A sensitivity analysis was also performed and the current model shows that the OH profile is sensitive to the chain branching reaction $O + H_2 \rightarrow OH + O$. The rate of Sun *et al.* [86], adopted from Baulch *et al.* [87], was tested for this reaction step and found to delay the onset of ignition by approximately 17% compared to the rate of Li *et al.* [88] adopted from Sutherland *et al.* [89]. A further analysis has been presented by Gkagkas and Lindstedt [90]. It was also shown that the reaction step is responsible for 12% of the OH radical production. In addition, the chain branching step $H + O_2 \rightarrow OH + O$ is responsible for 67% of the OH production and the rate has been studied extensively in the past (e.g. [91-93]). Reaction (2) also plays significant role in the OH evolution as shown in Fig. 3.7. The absence of this reaction step causes a delay in the OH ignition by around 20%.

$$C_5H_5 + C_2H_2 = C_7H_7 \qquad (2)$$

A further example of a OH concentration profile versus time is shown in Fig. 3.8 for a stoichimetric 250 ppm toluene mixture at T = 1648 K and P = 2.03 atm.

Ignition delay times were measured by Vasudevan *et al.* [70] in toluene/$O_2$/Ar mixtures for a temperature range 1510 – 1818 K with $\Phi = 1$ (0.1% toluene, 0.9% oxygen, 99% argon) and a pressure of 1 atm and defined the ignition delay time as the time needed for the OH radical concentration to reach 50% of the peak value by setting as zero the time of the arrival of the reflected shock. Ignition delay times were also measured for different fuel mole fractions varying from $2x10^{-4}$ – $2x10^{-2}$ with $\Phi = 1$, at a temperature of 1600 K and a pressure of 1 atm. Variations of the ignition delay times with temperature and fuel concentrations are presented in Figs. 3.9 – 3.10. As is evident in Fig. 3.9, the current toluene model agrees well with measurements at higher temperatures.

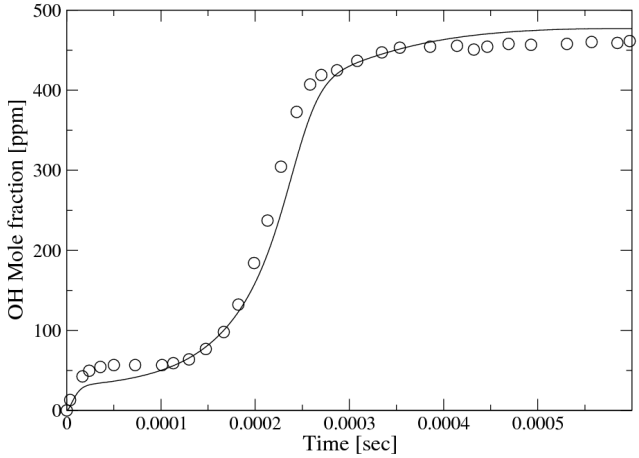


Figure 3.6 Time resolved OH radical concentrations obtained in Toluene/Oxygen/Argon mixtures in a shock tube with $\Phi = 1$ (0.1% toluene, 0.9% oxygen), T = 1689 K and P = 1.79 atm. The circles indicate the measurements from Vasudevan *et al.* [70] and the solid line indicates the scurrent simulation.

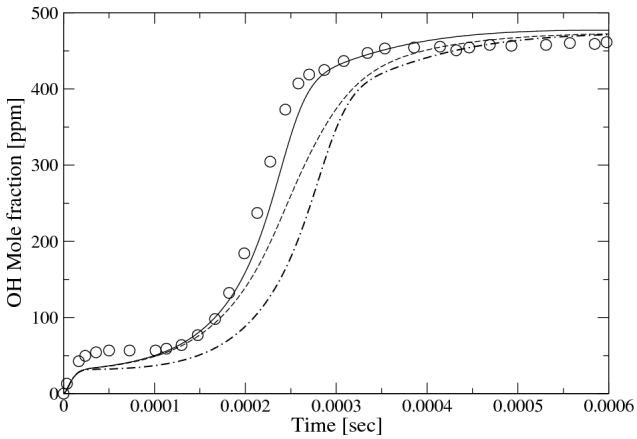


Figure 3.7 Sensitivity analysis of time resolved OH radical concentrations obtained in Toluene/Oxygen/Argon mixtures in shock tube with Φ = 1 (0.1% toluene, 0.9% oxygen), T = 1689 K and P = 1.79 atm. The circles indicate the measurements from Vasudevan *et al.* [70], the solid line indicates the current model, the dashed line indicates the current model with the rate of Sun *et al.* [86] for the reaction $O + H_2 \rightarrow OH + O$ and the dashed dotted line indicates the current model in the absence of the $C_5H_5 + C_2H_2 \rightarrow C_7H_7$ reaction.

The dependence of ignition delay times on fuel concentration is shown in Fig. 3.10. Ignition delay times were also measured by Burcat *et al.* [69] for toluene/oxygen/argon mixtures for a temperature range of 1379 – 1785 K, pressures of 1.96 – 2.81 atm for a stoichiometric mixture (0.497% $C_7H_8$, 4.48% $O_2$, 95.023% Ar). The comparison between the model and the experimental data is shown in Fig. 3.11.

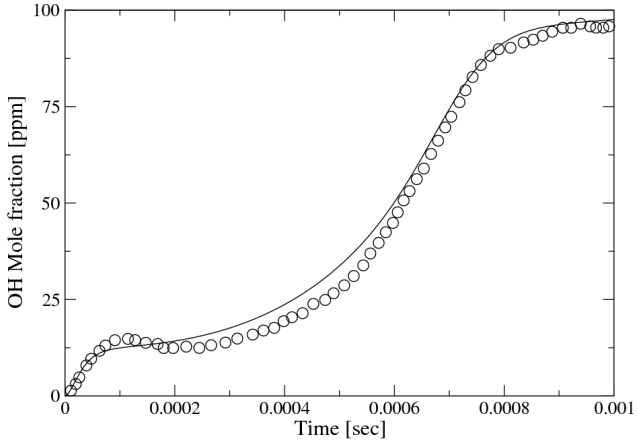


Figure 3.8 Time resolved *OH* radical concentrations obtained in Toluene/Oxygen/Argon mixtures in a shock tube with Φ = 1 (0.025% toluene, 0.225% oxygen), T = 1648 K and P = 2.03 atm. The circles indicate the measurements from Vasudevan *et al.* [70] and the solid line indicates the current simulation.

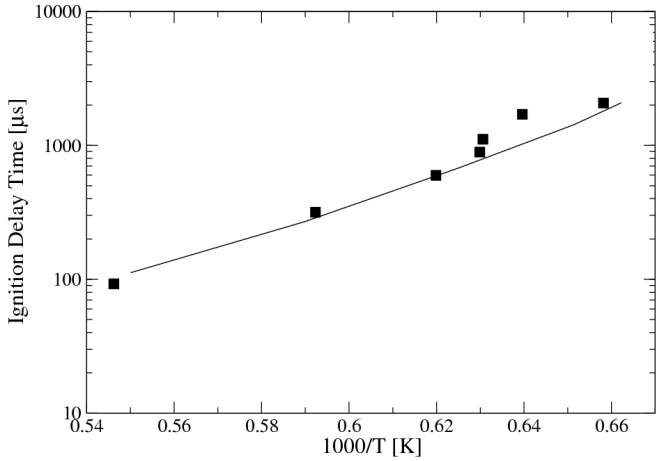


Figure 3.9 Ignition delay times of toluene with Φ = 1 (0.1% toluene, 0.9% oxygen, 99% argon) and P = 1 atm. Symbols indicate measurements from Vasudevan *et al.* [70] and the solid line indicates the current computations.

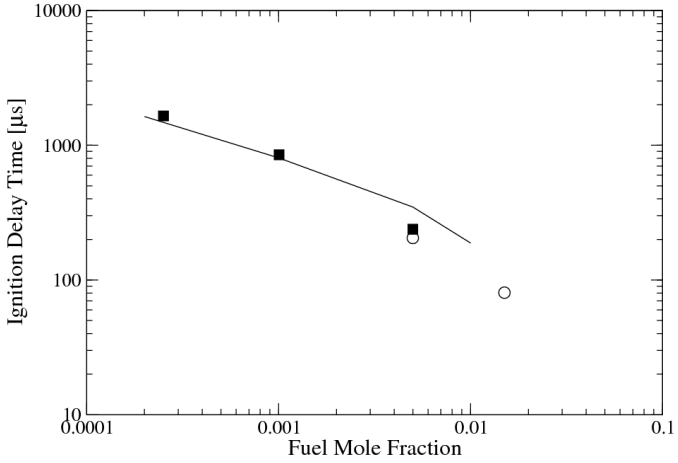


Figure 3.10 Ignition delay times for toluene mole fractions of $2x10^{-4}$ – $1x10^{-2}$ with Φ = 1 (toluene/oxygen/argon), T = 1600 K and P = 1 atm. The solid squares indicate the measurements from Vasudevan *et al.* [70], the open circles indicate experimental data from Burcat *et al.* [69] and the solid line indicates the current computations.

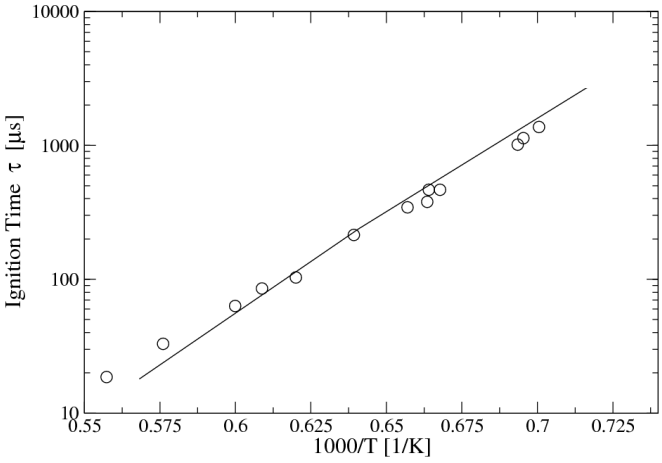


Figure 3.11 Ignition delay times for toluene obtained in a shock tube with Φ = 1 (0.497% $C_7H_8$, 4.48% $O_2$, 95.023% Ar) and P = 2.28 atm. The circles indicate experimental data from Burcat *et al.* [69] and the solid line indicates the current computations.

### 3.2 Path Analysis

A reaction rate analysis was performed for the toluene decomposition in shock tubes at the experimental conditions of Braun-Unkhoff *et al.* [77], as discussed above, and the major reaction pathways were determined. For the case of a toluene concentration of 2 ppm at 1515 K and 1.85 bar, the toluene decomposition is controlled by two major reaction channels. The C-H fission to the benzyl radical and atomic hydrogen (38) is responsible for 67% of the fuel decomposition. The reaction channel that proceeds via C-C scission to the formation of phenyl and methyl radical accounts for 27% of the toluene decomposition. The rates determined by Oehlschlaeger *et al.* [80] were applied to these channels.

The current findings highlight the dominance of reaction (38) in agreement with studies of Muller-Markgraf and Troe [75], Brouwer *et al.* [76], Rao and Skinner [74] and Hippler [78]. There is, however, a disagreement with Pamidimukkala *et al.* [73] who proposed reaction (39) as the main decomposition channel. As shown in the work by Oehlschlaeger *et al.* [80], the overall decomposition rate agrees with Braun-Unkhoff [77], Eng *et al.* [79] and Luther *et al.* [94] with a deviation of less than 30%. Recommendations of Pamidimukkala *et al.* [73] and Rao and Skinner [74] are significantly slower. The benzyl radical decomposes (90%) via reaction (2) leading to the cyclopentadienyl radical and acetylene.

$$C_5H_5 + C_2H_2 = C_7H_7 \qquad (2)$$

The cyclopentadienyl radical leads to the formation of the propargyl radical and acetylene (60%) or isomerizes to the linear form of $C_5H_5$(L) (38%) .

$$C_5H_5 = C_3H_3 + C_2H_2 \qquad (3)$$

$$C_5H_5 = C_5H_5(L) \qquad (8)$$

Both decomposition channels (3) and (8) were assigned rate constants computed from potential energy surfaces using variable transition state theory and Rice-Ramsperger-Kassel-Marcus/master equation approaches [15]. A faster rate of Kern *et al.* [36] was also tested but lead to overproduction of the hydrogen atom by 20%. The other main product of the toluene thermal decomposition, the phenyl radical, undergoes isomerization to the linear $C_6H_5$(B) or undergoes hydrogen fission reactions that follow a route from $C_6H_5 \rightarrow C_6H_4 \rightarrow C_6H_4L \rightarrow C_6H_3 \rightarrow C_6H_2$ and both channels lead to the formation of acetylene via 1,3-butadiyne. A schematic representation of the toluene thermal decomposition for 2.0 ppm of fuel at 1515 K and 1.85 bar is shown in Fig. 3.12. The temporal evolution of the hydrogen radical is controlled predominantly by reaction (38), which accounts for 92% of the production.

$$C_7H_8 = C_7H_7 + H \qquad (38)$$

The concentration of the hydrogen radical is also sensitive to reactions (40), (17), (18) and (41) which are responsible for 27%, 23%, 12% and 11% of the consumption respectively. The rates for reactions (40) and (41) were adopted from Oehlschlaeger *et al.* [80]. The rate for the hydrogen assisted hydrogen abstraction reaction (17) was adopted from Leung and Lindstedt [58]. The benzene formation reaction via hydrogen addition to the phenyl radical (18) was assigned a rate proposed by Baulch *et al.* [91].

| | | | | | |
|---|---|---|---|---|---|
| $C_7H_8$ | + H | = | $C_7H_7$ | + $H_2$ | (40) |
| $C_7H_8$ | + H | = | $C_6H_6$ | + $CH_3$ | (41) |
| $C_6H_5$ | + H | = | $C_6H_4$ | + $H_2$ | (17) |
| $C_6H_5$ | + H | = | $C_6H_6$ | | (18) |

The impact of reaction (40) on the hydrogen profile was also noted by Braun-Unkhoff *et al.* [77], who considered it in the context of a bringing agreement between their measured and computed hydrogen profiles. The rates proposed by Braun-Unkhoff *et al.* [77] and Baulch *et al.* [91] were tested for reaction (40) and caused an increase of the hydrogen concentration ~20% compared to the rate proposed by Oehlschlaeger *et al.* [80]

The reaction paths for toluene oxidation under shock tube conditions were analysed at the conditions of Vasudevan *et al.* [70], who measured the temporal evolution of the OH radical for a stoichiometric mixture of 0.1% toluene and 0.9% oxygen in argon mixture at 1689 K and 1.79 atm. The overall toluene decomposition is mainly controlled by four reactions as discussed above. These include the two main thermal decomposition pathways leading to the formation of benzyl (38) and the phenyl radical (39), which are jointly responsible for around 35% of the fuel consumption, and the two hydrogen assisted hydrogen abstraction reactions (40) and (41) leading to the formation of benzyl (29%) and phenyl radicals (10%).

According to the temporal evolution of the OH radical concentration, the fuel decomposition follows three stages. The first region where initiation reactions occur and the fuel is decomposed, the second region where ignition occurs due to chain branching reactions and the third region with zero net OH production. For the specific test case considered, the regions are separated for times up to 100 μs, 250 μs and 800 μs. Hence, the contribution of each decomposition step varies with time. Although reaction (38) plays a significant role in the overall fuel consumption, it is predicted that it is responsible for 20% in the first stage, it has no impact on the subsequent stages of the fuel oxidation process. Reaction (39) is responsible for 19%, 12% and 14% of the fuel decomposition over the three stages.

The contribution of reaction (40) to the fuel consumption increases over time from 27% in the first region to 45% in the second and third regions respectively. The reaction consumes the H radical and leads to the formation of the less reactive benzyl radical and molecular hydrogen. It must be noted that reactions that consume reactive radicals during fuel oxidation can inhibit ignition. Reaction (41) shows an increasing impact on the fuel consumption from 9% at the first stage to 15% up to the end of the fuel decomposition.

The benzyl radical produced from reactions (38) and (40), undergoes thermal dissociation that leads to the production of the cyclopentadienyl radical and acetylene via reaction (2) which accounts for 80% of the benzyl consumption.

$$C_5H_5 + C_2H_2 = C_7H_7 \quad (2)$$

Benzene is mostly produced (50%) via reaction (41) and consumed (38%) via reaction (25) for which a rate from Leung and Lindstedt [58] was adopted. A rate of Leung and Lindstedt was also assigned to reaction (22) which is responsible for 30% of the benzene consumption. The production of the phenoxy radical and the hydrogen atom via oxygen attack on benzene is responsible for 28% of the consumption of the latter with the rate adopted from DiNaro *et al.* [81].

$$C_7H_8 + H = C_6H_6 + CH_3 \quad (41)$$

$$C_6H_6 + OH = C_6H_5 + H_2O \quad (25)$$

$$C_6H_6 + H = C_6H_5 + H_2 \quad (22)$$

$$C_6H_6 + O = C_6H_5O + H \quad (23)$$

The phenyl radical is initially produced (75%) from the thermal decomposition of toluene via reaction (39). As most of the fuel is consumed, secondary reactions occur and the phenyl radical pool is produced via reactions (24, 22) that were assigned rates from Leung and Lindstedt [58]. The contribution of reaction (24) to the phenyl production remains the same up to 800 μs (47%), but reaction (22) is responsible for between 38% and 48% of the production.

$$C_7H_8 = C_6H_5 + CH_3 \quad (39)$$

$$C_6H_6 + OH = C_6H_5 + H_2O \quad (24)$$

$$C_6H_6 + H = C_6H_5 + H_2 \quad (22)$$

The consumption of the phenyl radical proceeds mainly (54%) via reaction (19) featuring molecular oxygen attack on the phenyl radical leading to the phenoxy radical and an oxygen atom. A rate from Frank *et al.* [95] was adopted for this step. In addition, a hydrogen atom is abstracted from the ring (18%) via hydrogen attack (17) that leads to the production of $C_6H_4$ and molecular hydrogen. The rate assigned to reaction (17) was

obtained from Leung and Lindstedt [58]. Approximately 12% of the phenyl radical consumption occurs via reaction (20), which involves molecular oxygen addition to the phenyl radical leading to the formation of the phenyl peroxy radical.

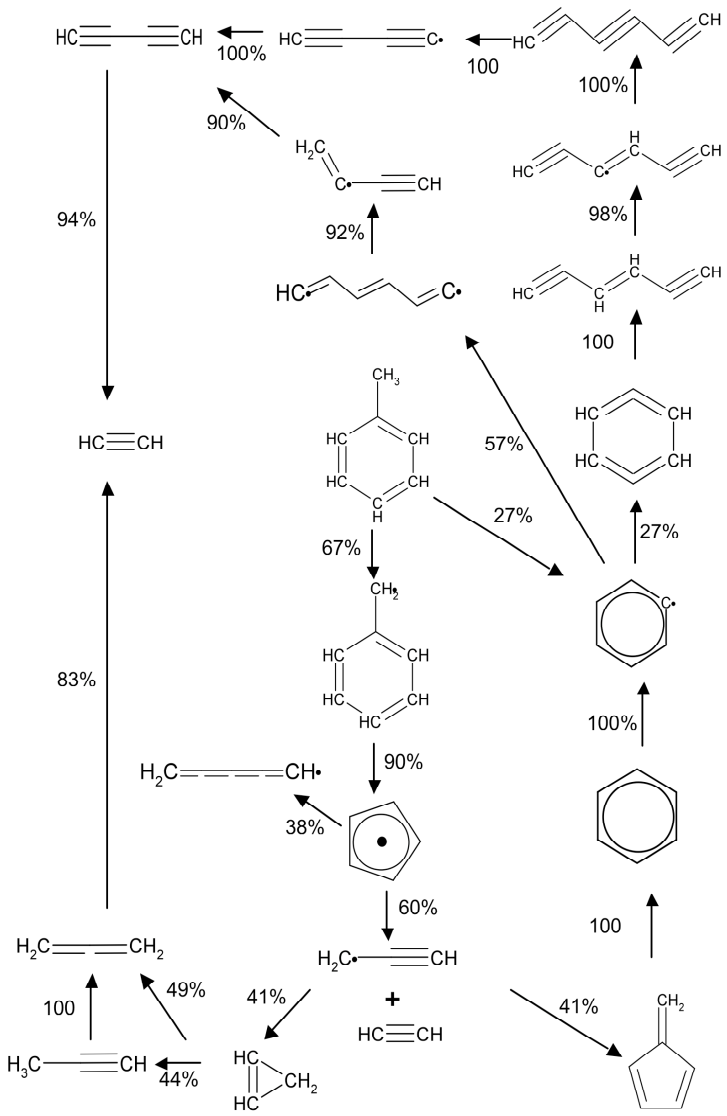


Figure 3.12 Predicted toluene thermal decomposition pathways corresponding to the study of Braun-Unkhoff *et al.* [77] with an initial fuel concentration of 2.0 ppm, T = 1515 K and P = 1.85 bar.

$C_6H_5 + O_2 = C_6H_5O + O$ (19)

$C_6H_5 + H = C_6H_4 + H_2$ (17)

$C_6H_5 + O_2 = C_6H_5OO$ (20)

The phenoxy radical is mainly produced (58%) from reaction (19) and leads (83%) to cyclopentadienyl and carbon monoxide (28) and with a fraction (15%) responsible for the formation of phenol (29). The rate for the carbon monoxide expulsion was adopted from Leung and Lindstedt [58] and the rate for the phenol formation from DiNaro *et al.* [81].

$C_6H_5O = C_5H_5 + CO$ (28)

$C_6H_5O + H = C_6H_5OH$ (29)

The consumption of $C_6H_4$ follows the reaction route $C_6H_4 \rightarrow C_6H_4L \rightarrow C_6H_3 \rightarrow C_6H_2 \rightarrow C_4H_2 \rightarrow C_4H_2O \rightarrow C_2H_2$ leading to acetylene. The phenylperoxy radical decays via two thermal pathways (31, 32) and leads to the formation of reactive radicals that are responsible for 68% and 22% of the consumption. Both decomposition steps were assigned the rates of DiNaro *et al.* [81]. The *p*-benzoquinone formed via (32) is decomposed to acetylene, carbon monoxide and formaldehyde following the global steps introduced by the latter authors.

$C_6H_5OO = C_6H_5O + O$ (31)

$C_6H_5OO = C_6H_4O_2 + H$ (32)

The cyclopentadienyl radical, which is produced via benzyl radical decomposition or via the phenyl radical degradation route, is decomposed via four main reaction pathways. Approximately 30% is thermally decomposed leading to the formation of acetylene and the propargyl radical and 29% reacts with the oxygen atom leading to carbon monoxide and $C_4H_5$(T). Moreover, 15% isomerizes to a linear structure and 13% recombines with hydrogen forming cyclopentadiene. Rates for reactions (3), (4) and (8) were calculated by Robinson [15] from potential energy surfaces determined using variable transition state theory and Rice-Ramsperger-Kassel-Marcus/master equation approaches. A rate from Kern *et al.* [36] was applied to the hydrogen recombination reaction (13).

$C_5H_5 = C_3H_3 + C_2H_2$ (3)

$C_5H_5 + O = C_4H_5(T) + CO$ (4)

$C_5H_5 = C_5H_5(L)$ (8)

$C_5H_6 = C_5H_5 + H$ (13)

Overall, the H atom profiles show generally good agreement with measurements under pyrolytic conditions. Under oxidation conditions and at high temperatures, the current toluene chemistry captures the temporal evolution of the OH radical in excellent agreement with the measurements. Ignition delay times for stoichiometric toluene mixtures were also computed and showed good agreement with the experimental data sets of Vasudevan *et al.* (2005) and Burcat *et al.* (1986).

The results outlined above are encouraging and suggest that the current reaction mechanism can be applied to other methyl substituted aromatic fuel compounds that form part of real and surrogate fuel formulations.

## 4.0 The Oxidation of n-Propylbenzene

Previous studies of the oxidation of n-alkyl benzenes have highlighted that after side chain removal, the fuels follow the same oxidation route as that of benzene. However, benzene itself can not represent more complex aromatic fuels that are present in commercial blends and n-propyl benzene is a potentially a good candidate representing the mono alkylated and mono cyclic aromatic component of fuels such as gasoline, diesel and kerosene [96]. The current work was focused on determining the side chain removal process and the steps that characterize it. Three routes were found: (i) Homolysis – direct cleavage of the side chain followed by the oxidation of the remaining radical, (ii) displacement of the alkyl side chain by a radical species and (iii) abstraction of a hydrogen atom from the alkyl group [97-100]. Due to the analogy between alkyl benzenes and alkanes regarding atomic hydrogen abstractions, relevant reactions in the n-propyl benzene chemistry were based on the chemistry of propane as appropriate. The current work also evaluates the relevance of this analogy in the context of the prediction of the combustion behaviour of n-propyl benzene.

The n-propyl benzene molecule has three primary, two secondary and two benzylic hydrogen atoms. According to the hydrogen carbon bonding rules, the benzylic bond is the weakest, as compared to the primary and secondary bonds, thus it is easier to abstract a hydrogen atom from the benzyl carbon atom. The benzylic bond strength is around 368 kJ/mol, the secondary 397 kJ/mol and the primary 410 kJ/mol. The benzylic C-H bond strength is less than at the other two sites due to the resonance of the resulting benzyl radical. The bond strengths thus suggest that the dominant abstraction reaction features the benzylic hydrogen atom [99, 100]. However, it is difficult for any other oxidation of the benzylic radical to occur as it is stereochemically hindered [101]. The active radical species are predominantly H, O and OH and the reactions may be written as below, where X = {X | H, O, OH}

$$C_6H_5\text{-}CH_2\text{-}CH_2\text{-}CH_3 + X \leftrightarrow C_6H_5\text{-}\dot{C}H\text{-}CH_2\text{-}CH_3 + XH \quad (4.1)$$

$$C_6H_5\text{-}\dot{C}H\text{-}CH_2\text{-}CH_3 \leftrightarrow C_6H_5\text{-}CH{=}CH_2 + CH_3 \quad (4.2)$$

The resulting benzylic radical will undergo a beta-scission to form styrene and the methyl radical (4.1) - (4.2). Hence, the early appearance of styrene shows that the above step is a significant fuel breakdown route. Styrene can be further decomposed to $C_6H_5C\dot{C}H$, benzene or react with oxygen leading to the formation of oxygenated species [99].

$$C_6H_5\text{-}CH{=}CH_2 + X \leftrightarrow C_6H_5\text{-}CH{=}CH + XH \quad (4.3)$$

$$C_6H_5\text{-}CH{=}CH \leftrightarrow C_6H_5\text{-}C{\equiv}CH + H \quad (4.4)$$

$$C_6H_5\text{-}CH{=}CH_2 + H \leftrightarrow C_6H_6 + CH{=}CH_2 \quad (4.5)$$

$$C_6H_5\text{-}CH{=}CH_2 + O \leftrightarrow C_6H_5\text{-}CH_2\text{-}CHO \quad (4.6)$$

$$C_6H_5\text{-}CH_2\text{-}CHO \leftrightarrow C_6H_5\text{-}CH_2 + HCO \quad (4.7)$$

The primary hydrogen abstraction is as follows:

$$C_6H_5\text{-}CH_2\text{-}CH_2\text{-}CH_3 + X \leftrightarrow C_6H_5\text{-}CH_2\text{-}CH_2\text{-}\dot{C}H_2 + XH \quad (4.8)$$

$$C_6H_5\text{-}CH_2\text{-}CH_2\text{-}\dot{C}H_2 \leftrightarrow C_6H_5\text{-}\dot{C}H_2 + CH_2{=}CH_2 \quad (4.9)$$

The resulting benzyl radical may lead to (i) toluene formation via hydrogen addition, (ii) benzaldehyde formation via oxygen addition or (iii) side chain alkyl radical addition. Ethylene appears in large quantities in experimental studies of n-propyl benzene oxidation showing that the primary hydrogen atom abstraction is a significant path in the fuel oxidation process [100]. Significant quantities of products from primary and benzylic hydrogen abstraction are measured and it is expected that secondary hydrogen abstractions occur due to the fact that the carbon bond strength is between the two other cases.

$$C_6H_5\text{-}CH_2\text{-}CH_2\text{-}CH_3 + X \leftrightarrow C_6H_5\text{-}CH_2\text{-}\dot{C}H\text{-}CH_3 \quad (4.10)$$

$$C_6H_5\text{-}CH_2\text{-}\dot{C}H\text{-}CH_3 \leftrightarrow C_6H_5\text{-}CH{=}CH\text{-}CH_3 + H \quad (4.11)$$

$$C_6H_5\text{-}CH_2\text{-}\dot{C}H\text{-}CH_3 \leftrightarrow C_6H_5 + CH_2{=}CH\text{-}CH_3 \quad (4.12)$$

$$C_6H_5\text{-}CH_2\text{-}\dot{C}H\text{-}CH_3 \leftrightarrow C_6H_5\text{-}C(\dot{C}H_2)\text{-}CH_3 \quad (4.13)$$

$$C_6H_5\text{-}C(\dot{C}H_2)\text{-}CH_3 \leftrightarrow C_6H_5\text{-}CH{=}CH_2 + CH_3 \quad (4.14)$$

Apart from the two products of reactions (4.11) - (4.12), isomerization (4.13) or phenyl shift (4.14) may also occur. Hydrogen shift from the benzylic to the secondary carbon atom is possible leading to the α-phenyl propyl radical and, following oxidation, to styrene. Instead of a hydrogen shift, it is also possible for the phenyl group to be transferred to the beta-carbon atom (4.14) [102]. The product of the phenyl shift (4.14) will lead to styrene production. The displacement of the propyl group by a radical species (e.g. a hydrogen atom) produces benzene and the propyl radical and the detection of propylene in the products provides evidence that the displacement reaction occurs.

$$C_6H_5\text{-}CH_2\text{-}CH_2\text{-}CH_3 + H \leftrightarrow C_6H_6 + C_3H_7 \quad (4.15)$$

The homolysis route involves carbon-carbon cleavage vi three possible routes.

$$C_6H_5\text{-}CH_2\text{-}CH_2\text{-}CH_3 \leftrightarrow C_6H_5 + \dot{C}H_2\text{-}CH_2\text{-}CH_3 \quad (4.16)$$

$$C_6H_5\text{-}CH_2\text{-}CH_2\text{-}CH_3 \leftrightarrow C_6H_5\text{-}\dot{C}H_2 + \dot{C}H_2\text{-}CH_3 \quad (4.17)$$

$$C_6H_5\text{-}CH_2\text{-}CH_2\text{-}CH_3 \leftrightarrow C_6H_5\text{-}CH_2\text{-}\dot{C}H_2 + CH_3 \quad (4.18)$$

The homolysis route is known to have large activation energies, hence it will only be an important path at high temperatures. The benzylic C-C bond is weaker than the other two in the chain and its breakage is expected to occur faster.

In this study, the oxidation steps of n-propyl benzene were analysed and the fuel breakdown was predicted for two different pressures and different stoichiometries. The reaction mechanism was derived from analogies with propane and toluene chemistries and validation was performed with data obtained in shock tubes and jet stirred reactors.

### 4.1 The Current Contribution

The updated n-propyl benzene reaction mechanism used here consists of 1683 reversible reactions involving 269 species. The thermochemical data were obtained from literature sources [56] and, when not available, were calculated with quantum mechanical methods using Gaussian-03 [15].

The oxidation of n-propyl benzene was studied under Jet Stirred Reactor (JSR) conditions at atmospheric pressure and predictions compared with measurements obtained by Dagaut *et al.* [96]. Three different stoichiometries ($\Phi$ = 0.5, 1.0 and 1.5) were analyzed for a temperature range of 900 – 1250 K (Table 4.1). Concentration profiles of all major species were computed at a mean residence time of $\tau$ = 70 ms and significant pathways for the fuel breakdown were identified. Comparisons between the simulations and experimental data sets from Dagaut *et al.* [96] are shown in Figs. 4.1 – 4.9.

| **Φ** | **P (atm)** | **T (K)** | **$X_{O2}$** | **$X_{C9H12}$** |
|---|---|---|---|---|
| 0.5 | 1.0 | 900-1200 | 0.024 | 0.001 |
| 1.0 | 1.0 | 950-1250 | 0.012 | 0.001 |
| 1.5 | 1.0 | 950-1250 | 0.008 | 0.001 |

Table 4.1 Experimental and modelling conditions for the oxidation of *n*-propyl benzene in a jet-stirred reactor at P = 1 atm. The species concentrations correspond to mole fractions

The major species measured by Dagaut *et al.* [96], apart from $O_2$, CO and $CO_2$, were ethyl benzene ($C_8H_{10}$), styrene ($C_8H_8$), toluene ($C_7H_8$), benzene ($C_6H_6$), acetylene ($C_2H_2$), ethylene ($C_2H_4$), methane ($CH_4$) and formaldehyde ($CH_2O$).

The fuel decay is reasonably well captured for all the three tested equivalence ratios and, as the stoichiometry increases, a better agreement between the model and the measurements is achieved for all the intermediate major species. The agreement between predictions and measurements suggests that the n-propyl benzene submechanism is adequate.

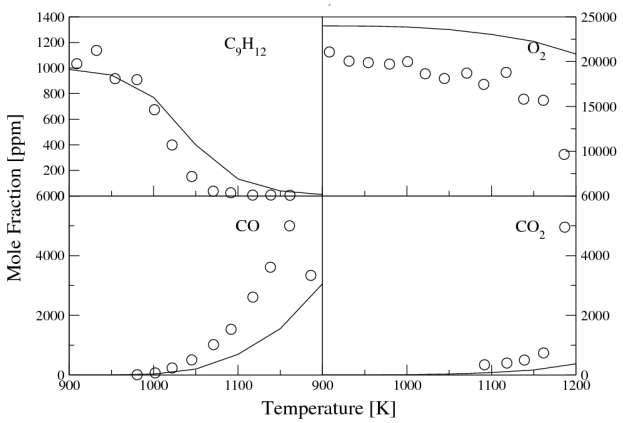


Figure 4.1 Concentration profiles of intermediate species during n-propyl benzene oxidation in a jet-stirred reactor with Φ = 0.5, P = 1 atm, T = 900 - 1200 K. The circles are measurements [96] and the solid line the current simulation.

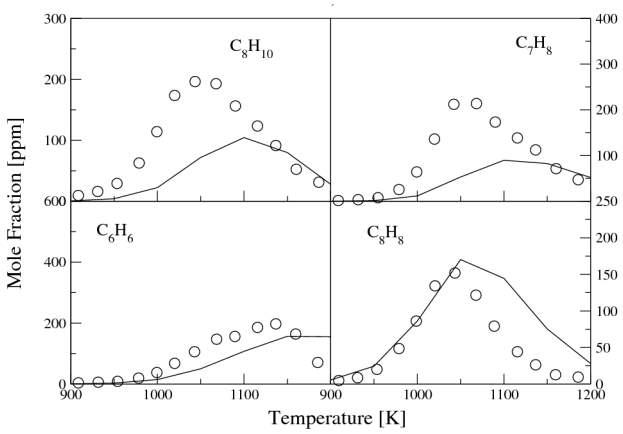


Figure 4.2 Concentration profiles of intermediate species during n-propyl benzene oxidation in a jet-stirred reactor with Φ = 0.5, P =1 atm, T = 900 - 1200 K. The circles are measurements [96] and the solid line the current simulation.

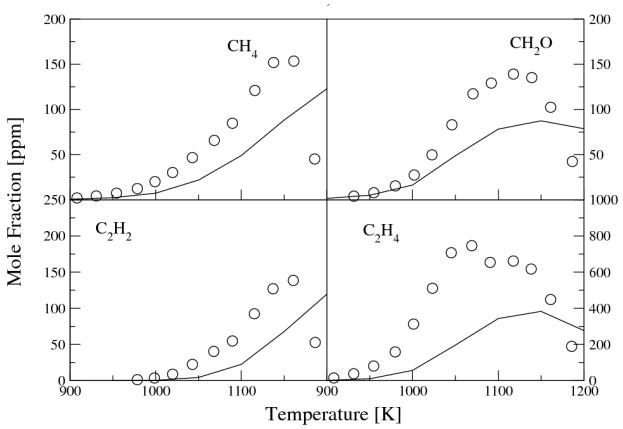


Figure 4.3 Concentration profiles of intermediate species during n-propyl benzene oxidation in a jet-stirred reactor with Φ = 0.5, P =1 atm, T = 900 - 1200 K. The circles are measurements [96] and the solid line the current simulation.

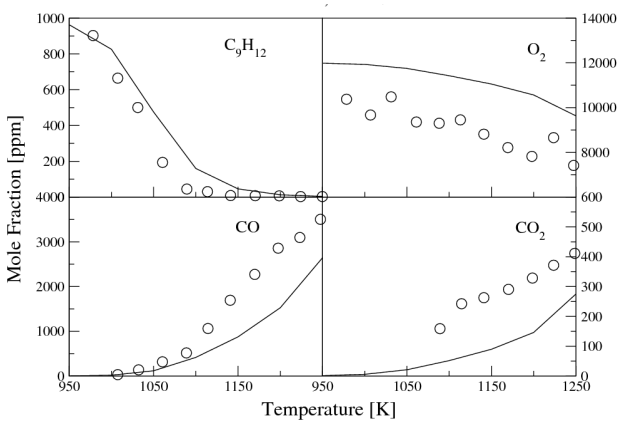


Figure 4.4 Concentration profiles of intermediate species during n-propyl benzene oxidation in a jet-stirred reactor with Φ = 1.0, P = 1 atm, T = 950 - 1250 K. The circles are measurements [96] and the solid line the current simulation.

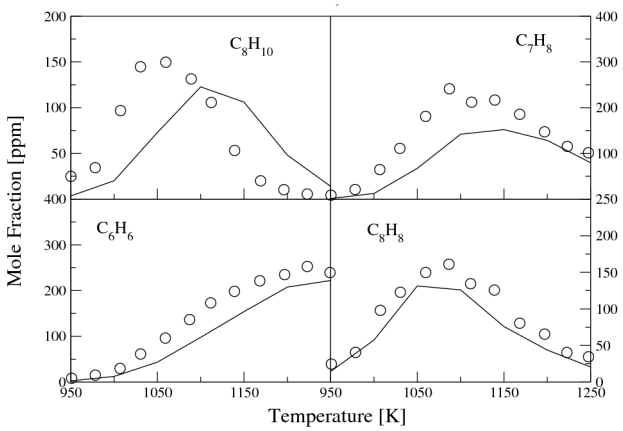


Figure 4.5 Concentration profiles of intermediate species during n-propyl benzene oxidation in a jet-stirred reactor with Φ = 1.0, P = 1 atm, T = 950 - 1250 K. The circles are measurements [96] and the solid line the current simulation.

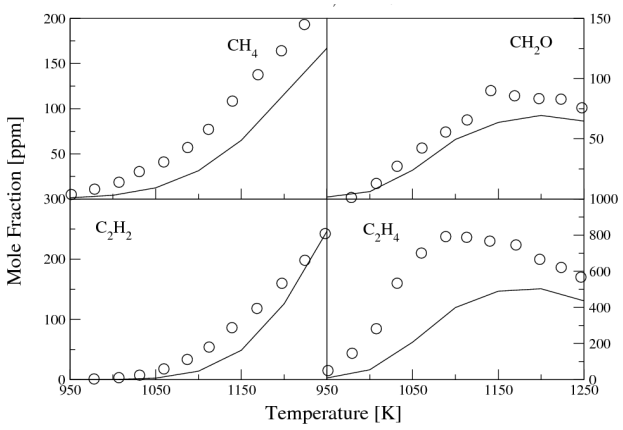


Figure 4.6 Concentration profiles of intermediate species during n-propyl benzene oxidation in a jet-stirred reactor with Φ = 1.0, P = 1 atm, T = 950 - 1250 K. The circles are measurements [96] and the solid line the current simulation.

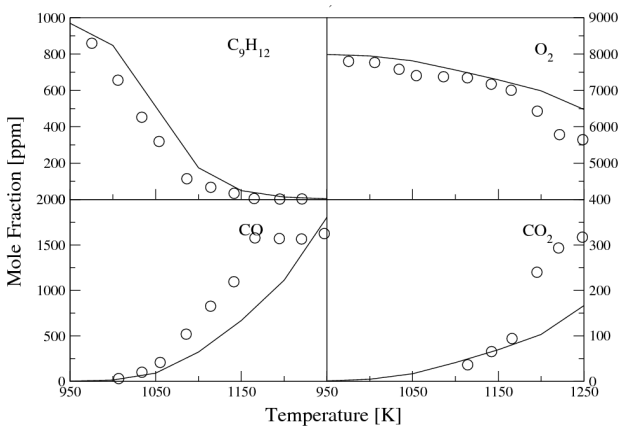


Figure 4.7 Concentration profiles of intermediate species during n-propyl benzene oxidation in a jet-stirred reactor with Φ = 1.5, P =1 atm, T = 950 - 1250 K. The circles are measurements [96] and the solid line the current simulation.

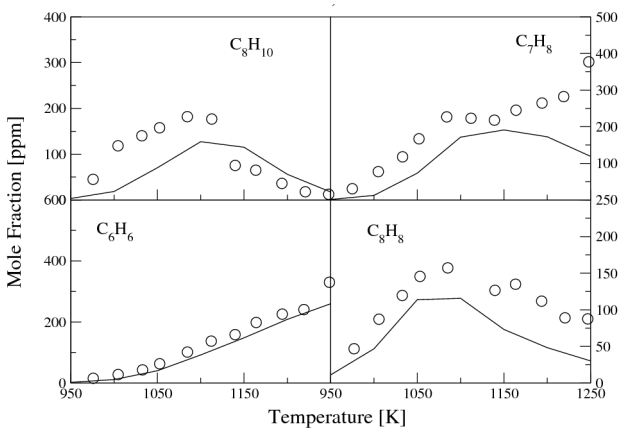


Figure 4.8 Concentration profiles of intermediate species during n-propyl benzene oxidation in a jet-stirred reactor with Φ = 1.5, P =1 atm, T = 950 - 1250 K. The circles are measurements [96] and the solid line the current simulation

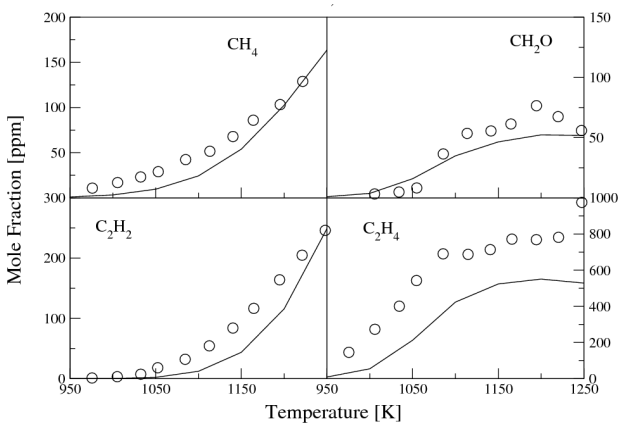


Figure 4.9 Concentration profiles of intermediate species during n-propyl benzene oxidation in a jet-stirred reactor with Φ = 1.5, P =1 atm, T = 950 - 1250 K. The circles are measurements [96] and the solid line the current simulation.

A reaction rate analysis was performed for a fuel rich mixture (Φ = 1.5) tested under oxidation conditions in jet-stirred reactor at a temperature of 1050 K and at atmospheric pressure. Computations show that the fuel decomposes predominantly (35%) by homolytic fission at the secondary carbon atom of the branch leading to the formation of benzyl and ethyl radicals. An additional 10% of the fuel is consumed via hydrogen abstraction through hydrogen atom attack on the 'benzylic' (primary) carbon atom leading to the 1-propyl benzyl radical (123). The kinetics of reaction (157) was estimated according to the approach of Dean [13]. The same approach was applied to the C-C homolytic steps that occur either at the primary or at the tertiary carbon atom to estimate their kinetics. The rate for reaction (123) was based on suggestions of Dagaut *et al.* [96]. Approximately 23% of the total fuel consumption leads to the formation of the 1-propyl benzyl radical via hydrogen atom abstraction with H, O and OH radicals. The primary homolytic reaction, which occurs via C-C scission leading to the phenyl and propyl radicals, corresponds to 8% of the total fuel consumption with a rate assigned based on the approach of Dean [13]. Approximately 16% of the total fuel concentration is decomposed via hydrogen abstraction reactions leading to the formation of the 2-propyl benzyl radical in comparison to 8% of the fuel that leads to the 3-propyl benzyl radical.

$C_9H_{12}$ = $C_7H_7$ + $C_2H_5$ (157)

$C_9H_{12}$ + H = $^1C_9H_{11}$ + $H_2$ (123)

The 1-propyl benzyl radical decomposes (100%) to styrene via methyl radical abstraction with a rate adopted by Dagaut *et al.* [96]. The step also constitutes the major styrene formation pathway. Once styrene was formed, five major routes were detected that contribute to its decay. Reaction (59) was assigned a rate proposed by Maurice [103] and contributes 21% to the consumption of styrene. The $C_8H_7$(P) recycles back to styrene (78%). The formation of the benzyl radical and CHO (61) constitutes the second major consumption pathway (18%) with a reaction rate suggested by Potter [60].

$C_8H_8$ + OH = $C_8H_7$(P) + $H_2O$ (59)

$C_8H_8$ + O = $C_7H_7$ + CHO (61)

Reactions (21), (16) and (62) make approximately equal contributions to the styrene consumption at 13, 12 and 10% respectively.

$C_6H_6$ + $C_2H_3$ = $C_8H_8$ + H (21)

$C_6H_5$ + $C_2H_4$ = $C_8H_8$ + H (16)

$C_8H_8$ + O = $C_6H_5$ + $CH_3CO$ (62)

The major product of the fuel decay, the benzyl radical, recombines with a hydrogen atom leading to the formation of toluene. The recombination step is the major toluene formation channel (90%) and was assigned a rate from Oehlschlaeger *et al.* [80]. Approximately 34% of the benzyl radical reacts with the methyl radical and forms ethyl benzene with the rate proposed by Lindstedt *et al.* [45]. The reaction step is the major ethyl benzene formation channel (97%). Moreover, 20% of the benzyl radical recombines leading to $C_{14}H_{14}$ with a reaction rate obtained from Oehlschlaeger et al. [80]. The major benzyl consumption steps are shown in Fig. 4.10 and the overall oxidation steps in Fig. 4.11.

Ethyl benzene is consumed via two major steps. The displacement of the ethyl branch via a hydrogen atom is responsible for 50% of the ethyl benzene consumption. The second major channel occurs via hydrogen atom abstraction to the formation of ethylbenzyl radical (34%), which essentially recycles back to ethyl benzene (95%).

$C_8H_{10} + H = C_6H_6 + C_2H_5$ (64)

$C_8H_{10} + H = C_8H_9 + H_2$ (63)

Benzene is partly consumed via oxygen atom addition and hydrogen abstraction (23) leading to $C_6H_5O$ (58%) with a rate adopted from DiNaro *et al.* [81] and (34%) to the phenyl radical via OH attack (25) with a rate of Leung *et al.* [58]. Oxygen addition to the phenyl radical leads to the production of $C_6H_5O$ (57%) and $C_6H_5OO$ (42%). The latter species are responsible for cyclopentadienyl radical production and contribute 70% and 25% respectively.

$C_6H_6 + O = C_6H_5O + H$ (23)

$C_6H_6 + OH = C_6H_5 + H_2O$ (25)

As mentioned above, the major fuel consumption pathway produces benzyl and ethyl radicals and also constitutes the major ethyl radical formation step (96%). The ethyl radical is consumed via hydrogen abstraction (95%) leading to the formation of ethylene (76%). Acetylene is also an important specie produced during propyl benzene oxidation. The main channel is via the thermal decomposition of the cyclopentadienyl radical (41%), which features an adjusted reaction rate based on that proposed by Kern *et al.* [36]. An additional 28% of the acetylene production occurs via methyl abstraction from the $C_3H_5(S)$ radical formed through the following reaction route $C_9H_{12} \leftrightarrow 2C_9H_{11} \leftrightarrow C_3H_6 \leftrightarrow C_3H_5(S) \leftrightarrow C_2H_2$.

Methane is formed via reaction routes directly linked to the fuel and involves hydrogen abstraction via methyl radical attack. The hydrogen abstraction reactions lead to the formation of $^1C_9H_{11}$ and $^3C_9H_{11}$ with each of these contributing 20% to the methane production. It must be noted that the methane production channel that produces $^2C_9H_{11}$ is

responsible for not more than 3% of the methane production. The rates assigned to the following reactions are based on the kinetics of propane suggested by Tsang [104].

$$C_9H_{12} + CH_3 = {}^1C_9H_{11} + CH_4 \quad (133)$$

$$C_9H_{12} + CH_3 = {}^3C_9H_{11} + CH_4 \quad (136)$$

$$C_9H_{12} + CH_3 = {}^2C_9H_{11} + CH_4 \quad (137)$$

The oxidation of n-propyl benzene was also studied under Jet Stirred Reactor (JSR) conditions at a pressure of 10 atm and validated using the measurements obtained by Dagaut *et al.* [96]. The stoichiometries tested were 0.5, 1.0, 1.5 and 2.0 for a temperature range of 900 – 1200 K at a residence time of $\tau$ = 0.5 sec. Comparisons between the simulations and experimental data sets from Dagaut *et al.* [96] are similar to those discussed above for atmospheric pressure and are hence omitted from the current report.

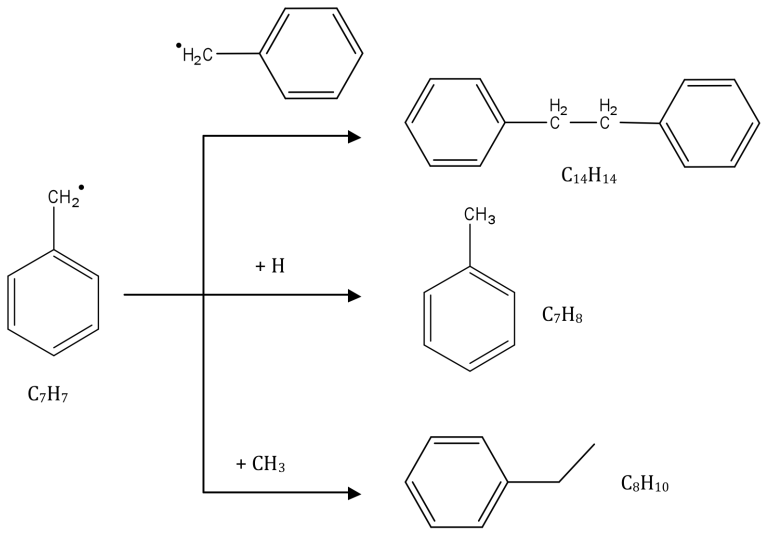


Figure 4.10 Benzyl radical consumption paths for $\Phi$ = 1.5, T = 1050 K and P = 1 atm in a jet-stirred reactor

Ignition delay times for n-propyl benzene were also computed and validated against measurements obtained by Eberius *et al.* [108] as shown in Fig. 4.12. The data were obtained in n-propyl benzene/$O_2$/Ar mixtures for a temperature range of 1400 – 1760 K, a pressure of 5 atm and stoichiometries from 0.8 – 1.142. The ignition delay time was defined by Eberius *et al.* [108] as the time needed for the CH-emission signal to reach its peak value. Low dilution conditions were responsible for difficulties in evaluating the measured data due to the change in density during the progress of reaction. Hence, a series of experiments for fuel/$O_2$ mixtures diluted in Argon were used. The set of conditions computed are shown in Table 4.2.

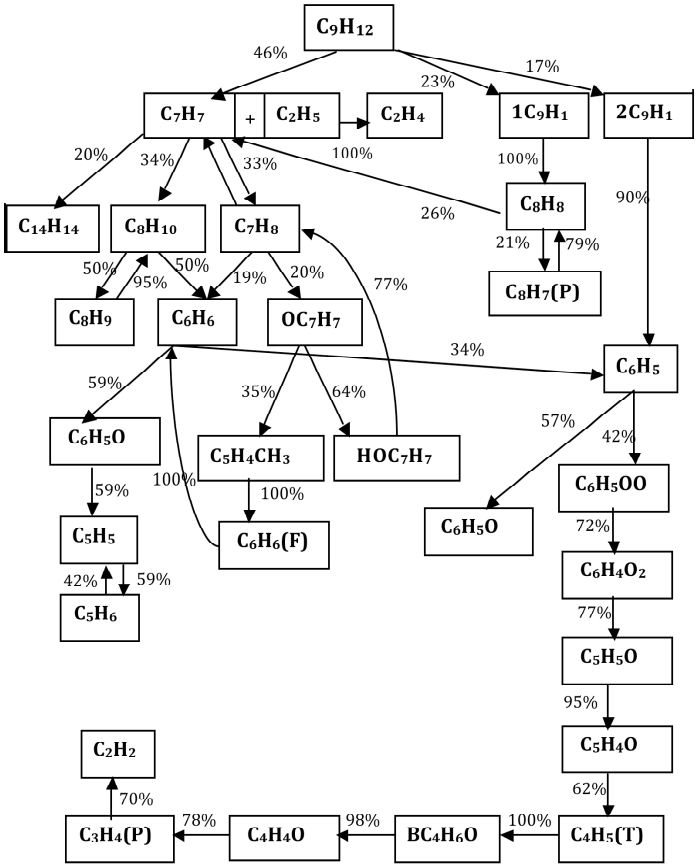


Figure 4.11. n-Propyl benzene oxidation pathways for Φ = 1.5, T = 1050 K and P = 1 atm in a jet stirred reactor

A comparison of experimental data with computaitons is shown in Fig. 4.12 and arguably the current n-propyl benzyl model provides satisfactory predictions of the ignition delay times at intermediate temperatures.

| | $[C_9H_{12}]$(ppm) | $[O_2]$ (ppm) | [Ar] (ppm) | Φ | P (atm) | T (K) |
|---|---|---|---|---|---|---|
| 1 | 537 | 8057 | 991406 | 0.800 | 5 | 1437 |
| 2 | 545 | 8057 | 991398 | 0.812 | 5 | 1416 |
| 3 | 537 | 8057 | 991406 | 0.800 | 5 | 1569 |
| 4 | 545 | 6289 | 993166 | 1.040 | 5 | 1468 |
| 5 | 544 | 6289 | 993167 | 1.038 | 5 | 1631 |
| 6 | 541 | 6289 | 993170 | 1.032 | 5 | 1549 |
| 7 | 598 | 6284 | 993118 | 1.142 | 5 | 1558 |
| 8 | 536 | 6284 | 993180 | 1.024 | 5 | 1555 |
| 9 | 542 | 6284 | 993174 | 1.035 | 5 | 1478 |
| 10 | 536 | 6284 | 993180 | 1.024 | 5 | 1759 |
| 11 | 538 | 6295 | 993167 | 1.026 | 5 | 1448 |
| 12 | 537 | 6295 | 993168 | 1.024 | 5 | 1606 |
| 13 | 553 | 6295 | 993152 | 1.054 | 5 | 1550 |

Table 4.2 Experimental and modelling conditions for *n*-propyl benzene ignition delay times in a shock tube

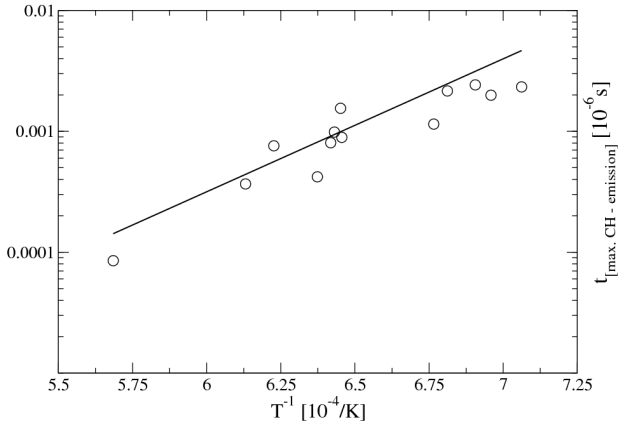


Figure 4.12 Ignition delay times of *n*-propyl benzene at P = 5 atm, 0.71 < Φ < 1.18. The circles are measurements [108] and the solid line the current simulation.

A reaction rate analysis was performed at 1448 K (Case 11, Table 4.2) and major reaction channels for the fuel breakdown were identified corresponding to Fig. 4.13. The fuel is solely decomposed via thermal breakdown to phenyl (46%) and benzyl (51%) radicals. The rates assigned to the thermal decomposition steps (156) and (157) were based on the approach of Dean [13].

$$C_9H_{12} = C_6H_5 + C_3H_7(N) \quad (156)$$

$$C_9H_{12} = C_7H_7 + C_2H_5 \quad (157)$$

The benzyl radical is predominantly (65%) consumed via hydrogen recombination to toluene. Under jet stirred reactor conditions the formation of toluene is responsible for 35% of the benzyl radical consumption. Most of the toluene (47%) recycles back to the benzyl radical via hydrogen abstraction reactions via H (40) and OH radical attack (43), while 14% produces benzene via C-C scission (41) and 12% is oxidized to $OC_7H_7$ (45). The rate assigned to reaction (40) was adopted from Oehlschlaeger *et al.* [80] and the second benzyl radical formation channel (43) used a rate proposed by Baulch *et al.* [91]. The rate proposed by Oehlschlaeger *et al.* [80] was used for reaction (41) while the toluene oxidation channel (45) was assigned a rate suggested by Hoffman *et al.* [109].

$$C_7H_8 + H = C_7H_7 + H_2 \quad (40)$$

$$C_7H_8 + OH = C_7H_7 + H_2O \quad (43)$$

$$C_7H_8 + H = C_6H_6 + CH_3 \quad (41)$$

$$C_7H_8 + O = OC_7H_7 + H \quad (45)$$

Most of the benzene is consumed via hydrogen abstraction with H (21%) and OH (42%) radicals leading to the phenyl radical. An additional 32% of benzene is oxidized to phenoxy via reaction with atomic oxygen. The phenyl radical constitutes the second major direct product from the fuel consumption. However, the production comes predominantly from

the decomposition of benzene. Once the phenyl radical is formed, 71% is oxidised to $C_6H_5O$ via (19) and 22% to $C_6H_5OO$ via (20) respectively.

$$C_6H_5 + O_2 = C_6H_5O + O \quad (19)$$

$$C_6H_5 + O_2 = C_6H_5OO \quad (20)$$

The phenoxy radical is further decomposed to cyclopentadienyl radical (80%), which subsequently is thermally decomposed (73%) to the propargyl radical and acetylene. Approximately 34% of $C_6H_5OO$, is converted to $C_6H_5O$ and the dominant consumption channel of $C_6H_5OO$ leads to $C_6H_4O_2$ formation. The latter goes through the sequence of reaction steps illustrated in Fig. 4.13 that lead to the formation of acetylene.

In summary, a detailed chemical mechanism for n-propyl benzene oxidation featuring 1683 reversible reactions and 269 species has been proposed and new reaction rates were evaluated and applied. The validation was performed via comparisons with ignition delay times and measured species concentrations obtained by Eberius *et al.* [108], Dagaut *et al.* [96] and Dagaut [105].

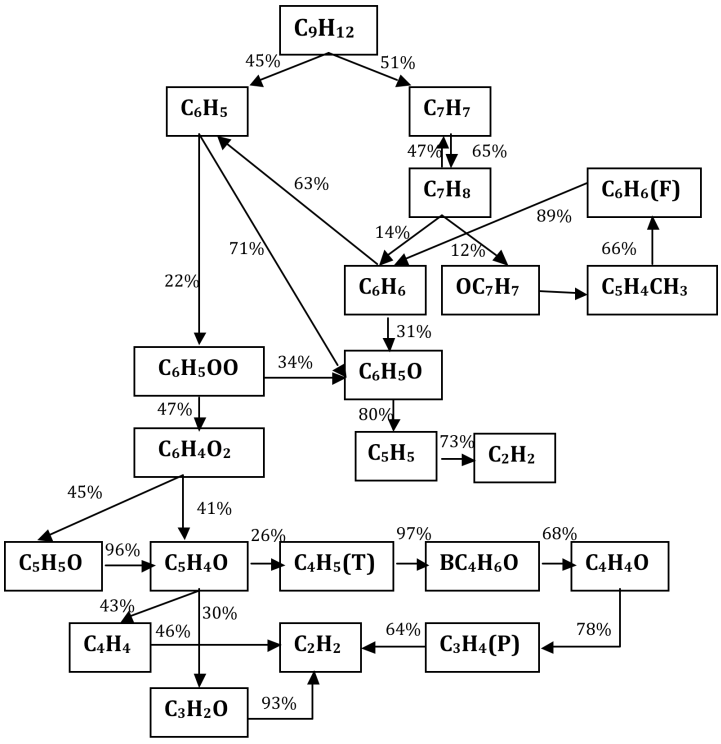


Figure 4.13 Reaction pathways for the oxidation of *n*-propyl benzene in a shock tube at T = 1448 K, Φ = 1.026 and P = 5.06 bar

The chemistry was partly developed based on chemical structure similarities with toluene and propane for reactions occurring at the n-propyl benzene branch. Extensive comparisons between computed results and the measurements for a pressure range of $1 \leq P\ (atm) \leq 10$,

temperatures of $900 \leq T\ (K) \leq 1250$ and for various stoichiometries between $0.5 \leq \Phi \leq 2.0$ illustrate the ability of the model to predict the oxidation of n-propyl benzene.

Important reaction paths were identified, including the generation of styrene. The significance of the thermal breakdown of the fuel at the primary and secondary carbon atom was also noted as small rate changes could lead to large discrepancies in the intermediate species concentrations. The dominant homolytic reaction step in both jet stirred reactors and shock tubes is predicted to lead to benzyl radical formation. The prediction and measurement of large early concentrations of specific species such as styrene, ethyl benzene or toluene is a clear indication that abstraction and homolytic reactions occur at the beginning of the fuel oxidation and promote the fuel decay.

The results presented here are encouraging and suggest that the current reaction class based approach can be applied also to other alkyl substituted aromatic fuel compounds that form part of real and surrogate fuel formulations. It must also be noted that as the chain increases in length, new categories of reaction steps are likely to occur such as radical isomerisations, cyclic transition states and group shifts along the chain that should be taken into account.

## 5.0 The Oxidation of Naphthalene and 1-Methyl Naphthalene

The formation and oxidation of polycyclic aromatic hydrocarbons is one of the central subjects of research in the area of pollutant emissions. Many studies in the literature have addressed the formation and growth of aromatic compounds that act as precursors to soot. The control and prediction of the combustion of aromatics is of direct importance to combustor life times as well as for both environmental and health reasons as PAHs are associated with tumorigenic effects. Hence, the ability to reproduce the chemical properties of aromatic hydrocarbon fuels is required.

The formation of benzene has received particular attention and has been subject to a number of studies [29, 58, 110-113]. Subsequent molecular growth mechanisms, specifically reaction routes that proceed via acetylene based addition to radicals, have been reported in the literature [29, 31, 114]. Marinov *et al.* [42] and Castaldi *et al.* [115] have suggested that naphthalene is produced by the recombination of two cyclopentadienyl radicals releasing two hydrogen atoms. The cyclopentadienyl recombination leading to naphthalene formation was also studied by Melius *et al.* [26] and Dean [116]. Moreover, Marinov *et al.* [117] and Richter *et al.* [118] highlighted the role of cyclopentadienyl radical in premixed flames. A more recent study of Lindstedt *et al.* [45] proposed a two-step mechanism involving the cyclopentadienyl route with energy barriers that are in accordance

with potential energy surfaces determined by Melius *et al.* [26]. The naphthalene formation and oxidation pathways are presented in this study and compared with plug flow reactor data obtained by Shaddix [119].

### 5.1 The Oxidation of Naphthalene

The reaction mechanism derived for naphthalene oxidation was based on reactions steps and reaction classes resulting from studies of the oxidation of benzene and cyclopentadiene with parameters adjusted according to molecular size and reactive site differences [54].

The studies by Lindstedt *et al.* [45], Maurice [103] and Potter [60] identified the importance of the linkages between aromatic $C_5$ and $C_6$ structures and the key role of the indene/indenyl system. In particular, the oxidation of indenyl was found to exert a strong influence on the overall oxidation kinetics of larger aromatic species such as naphthalene and 1-methyl naphthalene and on the subsequent product distribution of single ring aromatics. The studies identified possible reaction channels featuring molecular oxygen and provided preliminary fits for a limited temperature range (70, 71, 72). However, accurate estimates of the rates of reaction proved problematic [60]. In the current study, the aforementioned channels were considered along with $HO_2$ channels (68, 69) with DFT and composite quantum mechanical methods used to calculate the potential energy surfaces. Both RRKM/ME theory and VTST approaches were subseqently used to derive estimates of the rate constants [54].

$$C_9H_7 + O_2 = C_6H_5O + C_3H_2O \quad (71)$$

$$C_9H_7 + O_2 = C_7H_7 + CO + CO \quad (70)$$

$$C_9H_7 + O_2 = C_7H_6O + C_2HO \quad (72)$$

$$C_9H_7 + HO_2 = C_9H_7O + OH \quad (68)$$

$$C_9H_7 + HO_2 = C_9H_6O + H_2 \quad (69)$$

The full reaction mechanism consists of 1431 reversible reactions and 269 species and rate parameters for all reactions discussed in the current report are given in Appendix A.

The naphthalene mechanism was validated under plug flow reactor conditions and compared with measurements by Shaddix [119]. An offset of 32 ms in the temporal evolution of the experimental data was also reported [119]. Predictions of reactants and major species are presented Figs. 5.1 - 5.3. The measured naphthalene concentrations show scatter with the trend in reasonable agreement with computations. The fuel is decomposed via two major channels that involve H abstraction via the OH radical (49%) and O addition to the ring leading to the naphthoxy radical (44%). The rate assigned to reaction (78) was based on the reaction rate of the hydrogen atom abstraction from the benzene ring [58]. The

rate for reaction (77) is based on the proposal by DiNaro *et al.* [81] for the corresponding benzene reaction.

$C_{10}H_8 + OH = C_{10}H_7 + H_2O$ (78)

$C_{10}H_8 + O = C_{10}H_7O + H$ (77)

The naphthyl radical is further decomposed (67%) to naphthoxy via reaction (76) with the assigned rate based on the kinetics of benzene as proposed by Frank *et al.* [95].

$C_{10}H_7 + O_2 = C_{10}H_7O + O$ (76)

The naphthoxy radical decomposes thermally via one major pathway leading to the formation of the indenyl radical and CO. The rate assigned to reaction (80) was based on suggestions of Potter [60] and adjusted from benzene kinetics. The reaction is also the major (69%) indenyl radical production channel.

$C_{10}H_7O = C_9H_7 + CO$ (80)

The indenyl radical is consumed via three major pathways. Most (33%) recombines with the hydrogen atom to indene (65) with a reaction rate assigned based on suggestions of Potter [60]. The second route (19%) involves CO abstraction via oxygen attack leading to the formation of $C_8H_7$ (67). The rate assigned to this channel was based on suggestions of Maurice [103]. A further 17% of the indenyl concentration reacts with $HO_2$ forming the naphthoxy radical (68) with a rate proposed by Lindstedt *et al.* [54].

$C_9H_7 + H = C_9H_8$ (65)

$C_9H_7 + O = C_8H_7 + CO$ (67)

$C_9H_7 + HO_2 = C_9H_7O + OH$ (68)

Indene is formed via hydrogen addition to the indenyl radical. Once it is formed, it predominantly recycles back to the indenyl radical. The $C_8H_7$ radical decomposes (100%) to phenyl acetylene with a rate adopted from Wang and Frenklach [110].

$C_8H_7 = C_8H_6 + H$ (58)

Reaction (58) is also the major phenyl acetylene formation channel (75%). Phenyl acetylene is predominantly oxidised via the reaction routes shown below.

$C_8H_6 + O = C_6H_5 + C_2HO$ (54)

$C_8H_6 + OH = C_8H_5 + H_2O$ (52)

$C_8H_6 + O = C_8H_5O + H$ (53)

$C_8H_6 + O = C_6H_5O + C_2H$ (55)

$C_8H_6 + O = C_6H_5C_2O + H$ (51)

The major phenyl acetylene consumption channel (33%) occurs via oxygen attack and removes the side chain via C-C cleavage (54). The rate assigned to reaction (54) was adopted from suggestions of Lindstedt *et al.* [45]. The second major consumption channel (52) occurs via H abstraction by OH attack, which is responsible for 19% of $C_8H_6$ consumption. The reaction was assigned a rate recommended by Frenklach and Wang [110]. Reactions (53), (55) and (51) are responsible for 11%, 11% and 10% of the phenyl acetylene consumption respectively.

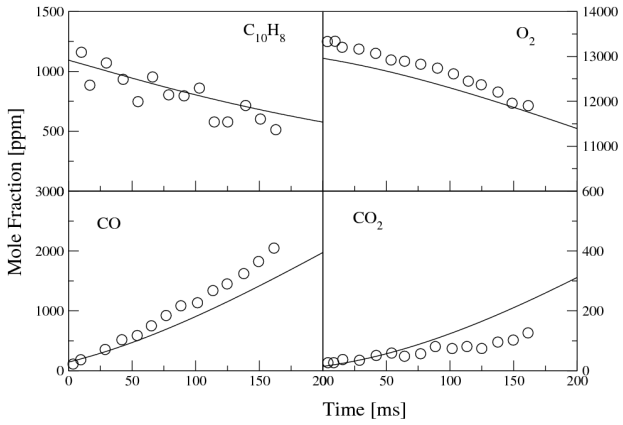


Figure 5.1 Concentration profiles of major species during naphthalene oxidation in a plug flow reactor for Φ = 1.1, T = 1197 and P = 1 atm. The solid lines indicate the current computations and the circles indicate the measurements [119].

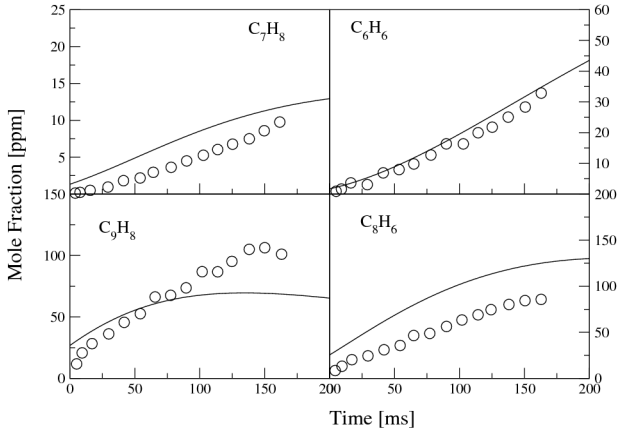


Figure 5.2 Concentration profiles of major species during naphthalene oxidation in a plug flow reactor for Φ = 1.1, T = 1197 and P = 1 atm. The solid lines indicate the current computations and the circles indicate the measurements [119].

Toluene is formed via the benzyl radical resulting from the oxidation of the indenyl radical via molecular oxygen attack (70). The rate assigned to reaction (70) was calculated through RRKM/ME and VTST approaches [54]. Approximately 20% of the benzyl radical is formed via $C_8H_8$ oxidation with OH (60) with the rate adopted from Maurice [103]. A further 11% of benzyl radical is formed via reaction (34) with a rate adopted from Colket *et al.* [59].

$C_9H_7 + O_2 = C_7H_7 + CO + CO$ (70)

$C_8H_8 + OH = C_7H_7 + CH_2O$ (60)

$C_7H_7 + C_2H_2 = C_9H_8 + H$ (34)

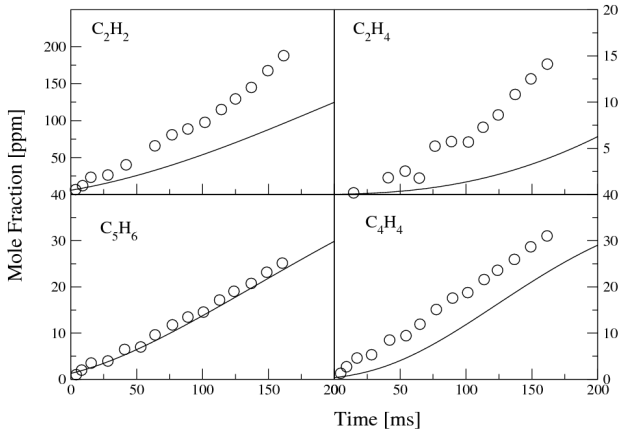


Figure 5.3 Concentration profiles of major species during naphthalene oxidation in a plug flow reactor for Φ = 1.1, T = 1197 and P = 1 atm. The solid lines indicate the current computations and the circles indicate the measurements [119].

Benzene is formed (32%) through hydrogen assisted isomerization (26) and (24%) from benzaldehyde via oxygen addition and $CO_2$ abstraction (47). Benzene is a precursor to the cyclopentadienyl radical from which cyclopentadiene is formed (92%). Benzene is consumed (47%) to the phenyl radical via H abstraction featuring OH radical attack and (40%) to the phenoxy radical via O addition and hydrogen abstraction. The phenyl radical predominantly (66%) leads to the phenoxy radical.

$C_6H_6(F) + M = C_6H_6 + M$ (26)

$C_7H_6O + O = C_6H_6 + CO_2$ (47)

The phenoxy radical is responsible (77%) for cyclopentadienyl radical production via CO expulsion (28) with a rate proposed by Leung and Lindstedt [58]. The cyclopentadienyl radical recombines with the H atom (92%) to the cyclopentadienyl radical (13) with a rate adopted from Kern *et al.* [36].

$C_6H_5O = C_5H_5 + CO$ (28)

$C_5H_6 = C_5H_5 + H$ (13)

Acetylene is also formed (44%) via the thermal breakdown of $C_5H_5$ that leads to $C_2H_2$ and $C_3H_3$. The rate used for reaction (3) was proposed by Kern *et al.* [36] and was reduced by a factor of 2 due to acetylene overproduction. The evolution of $C_2H_4$ is also affected by $C_5H_5$ via reaction channels that include $C_2H_2$ and $C_2H_2O$.

$C_5H_5 = C_2H_2 + C_3H_3$ (3)

Vinyl acetylene production is initially controlled by phenyl acetylene consumption via $C_8H_5O$, which thermally decomposes to $C_7H_5$ leading to $C_4H_4$ via $C_5H_4O$. A rate by Ristori *et al.* [120] was assigned to reaction (15), which is responsible for 94% of the $C_4H_4$ production.

$$C_5H_4O = C_4H_4 + CO \qquad (15)$$

Overall, the resulting mechanism shows comparativly good agreement when evaluated against the species profiles obtained from Shaddix [119].

The work shows that the naphthalene oxidation is controlled by two major channels that involve H abstraction via OH radical and O addition to the ring. Most of the oxidation process is assumed to follow a similar behaviour to the benzene chemistry. From the comparison between the computations and the measurements, is shown that the main oxidation channels are well represented and that the $C_9H_7 + O_2/HO_2$ reactions have an important role in determining the product distribution of single ring aromatics.

### 5.2 The Oxidation of 1-Methyl Naphthalene

Few studies on the combustion of polycyclic aromatic fuels have been reported in the literature and in the current work a mechanism for 1-methyl naphthalene was developed on the basis of reaction classes determined with toluene as a reference fuel. The choice is natural since 1-methyl naphthalene is the corresponding bicyclic analog.

Shaddix *et al.* [119, 121, 122] studied the oxidation of 1-methyl naphthalene in a plug flow reactor and obtained species profiles under atmospheric pressure conditions for a temperature range of 1165 – 1200 K and for equivalence ratios of 0.6, 1.0 and 1.6. The study arguably contains the first reported species profiles for the oxidation of a polycyclic hydrocarbon fuel. Based on the obtained profiles, a chemical mechanism for 1-methyl naphthalene was proposed. Elevated pressure (P = 13 atm) ignition delay times were measured by Pfahl *et al.* [123] under shock tube conditions for a temperature range of 840 – 1300 K. Pitsch [125] produced a reaction mechanism capable of reproducing the ignition delay times measured by Pfahl *et al.* [123] as well as ignition in the fuel lean mixture studied by Shaddix *et al.* [119, 121, 122]. A more recent study of the chemistry of 1-methyl naphthalene was performed by Mati *et al.* [124], who studied the oxidation under jet stirred reactior conditions for a temperature range of $800 < T < 1421$ K, a pressure range of $1 < P < 13$ atm and equivalence ratios of $0.5 < \Phi < 1.5$. Major species concentration profiles were obtained by on-line GC-MS, off-line GC-TCD-FID and GC-MS analyses and a kinetic model was proposed and validated. Important reactions pathways were identified in the above studies. Shaddix *et al.* [122] highlighted the fuel consumption paths that occur via i)

abstractions of the benzylic hydrogen atom by H/O radicals or molecular oxygen, ii) homolysis from C–H fission forming the 1-naphthyl methyl radical, iii) displacement of the methyl group by the hydrogen atom leading to the formation of naphthalene and iv) addition of an oxygen atom leading to the formation of 1-methyl-4-naphthol or 1-methyl naphthoxy radical.

The oxidation of 1-methyl naphthalene is here studied and compared against data from Mati *et al.* [124] and Shaddix [119]. The starting point is the detailed scheme for 1-methyl naphthalene derived by Potter [60] on the basis of the chemistry of toluene with modifications and updates applied as appropriate. The reaction pathways were analysed at conditions corresponding to the JSR experiments of Mati *et al.* [124] and plug flow reactor conditions of Shaddix [119] and Shaddix *et al.* [121, 122].

### 5.3 The Oxidation of 1-Methyl Naphthalene under JSR Conditions

The 1-methyl naphthalene mechanism was initially validated under jet-stirred reactor conditions using species data obtained by Mati *et al.* [124]. The measurements were aimed at clarifying the decomposition channels of the fuel. Three different stoichiometries were tested at atmospheric pressure over a temperature range of 1090–1450 K and at a fixed residence time (τ) of 0.1 s. The conditions are listed in Table 5.1 and examples of species profiles are shown in Figs. 5.4 – 5.15. The major species detected, besides CO and $CO_2$, were formaldehyde, methane, ethane, ethylene, acetylene, cyclopentadiene, benzene, toluene, styrene, indene and naphthalene.

| **Φ** | **P (atm)** | **T (K)** | **$X_{O2}$** | **$X_{C11H10}$** |
|---|---|---|---|---|
| 0.5 | 1.0 | 1097-1290 | 0.0270 | 0.001 |
| 1.0 | 1.0 | 1094-1400 | 0.0135 | 0.001 |
| 1.5 | 1.0 | 1147-1440 | 0.0090 | 0.001 |

Table 5.1 Experimental and modelling conditions for the oxidation of 1-methyl naphthalene in a jet-stirred reactor. The species concentrations correspond to mole fractions.

A reaction rate analysis was performed for a fuel lean mixture (Φ = 0.5) at a temperature of 1206 K at atmospheric pressure. The computations show that the major fuel decomposition pathways occur via hydrogen abstraction by OH attack and oxygen addition. The rates assigned to the reactions were adopted from Potter [60] and determined on the basis of the toluene chemistry. The OH attack on the methyl branch (86) is responsible for 31% of the fuel consumption, whereas the hydrogen abstraction from the ring (83) is responsible for 19%. The oxygen addition to the branch (88) accounts for 12% of the 1-methyl naphthalene consumption, whereas the oxygen addition to the ring (89) accounts for 23%.

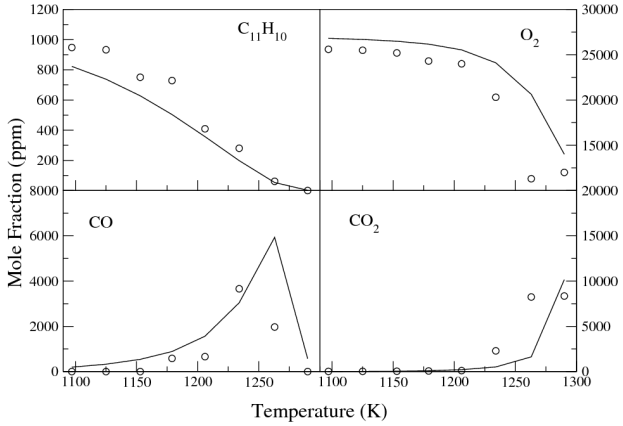


Figure 5.4 Concentration profiles of intermediate species during 1-methyl naphthalene oxidation in a jet-stirred reactor with Φ = 0.5, P = 1 atm and T = 1097 - 1290 K. Circles are experimental data [124] and the solid lines the current simulations.

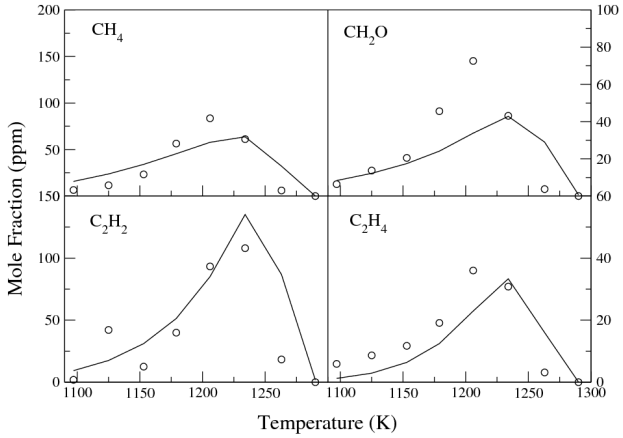


Figure 5.5 Concentration profiles of intermediate species during 1-methyl naphthalene oxidation in a jet-stirred reactor with Φ = 0.5, P = 1 atm and T = 1097 - 1290 K. Circles are experimental data [124] and the solid lines the current simulations.

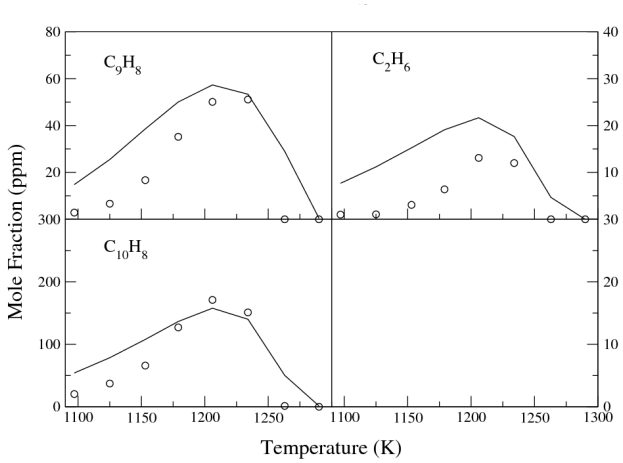


Figure 5.6 Concentration profiles of intermediate species during 1-methyl naphthalene oxidation in a jet-stirred reactor with Φ = 0.5, P = 1 atm and T = 1097 - 1290 K. Circles are experimental data [124] and the solid lines the current simulations.

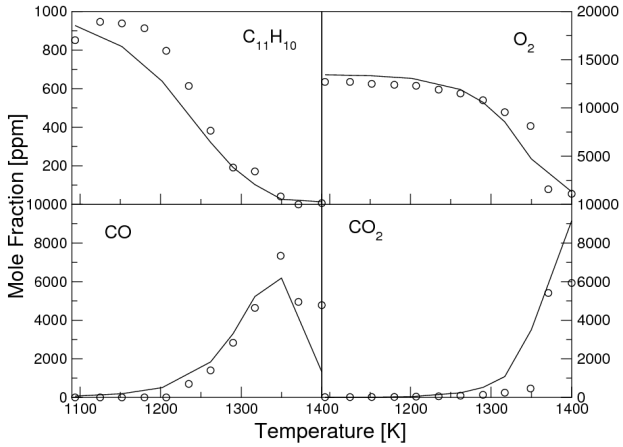


Figure 5.7 Concentration profiles of intermediate species during 1-methyl naphthalene oxidation in jet-stirred reactor. Φ =1.0, P = 1 atm and T = 1094 - 1400 K. Circles are experimental data [124] and the solid lines the current simulations.

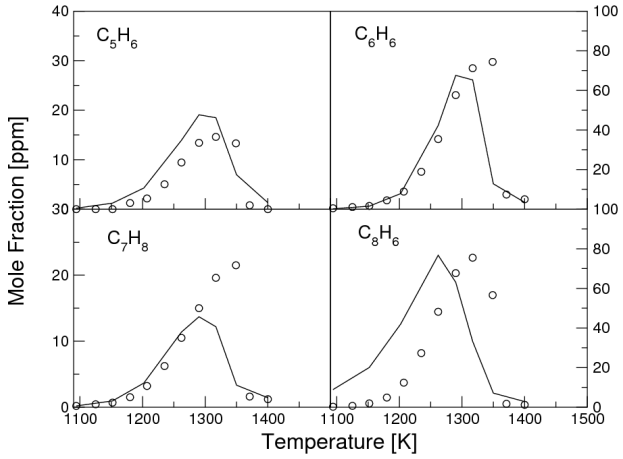


Figure 5.8 Concentration profiles of intermediate species during 1-methyl naphthalene oxidation in jet-stirred reactor. Φ =1.0, P = 1 atm and T = 1094 - 1400 K. Circles are experimental data [124] and the solid lines the current simulations.

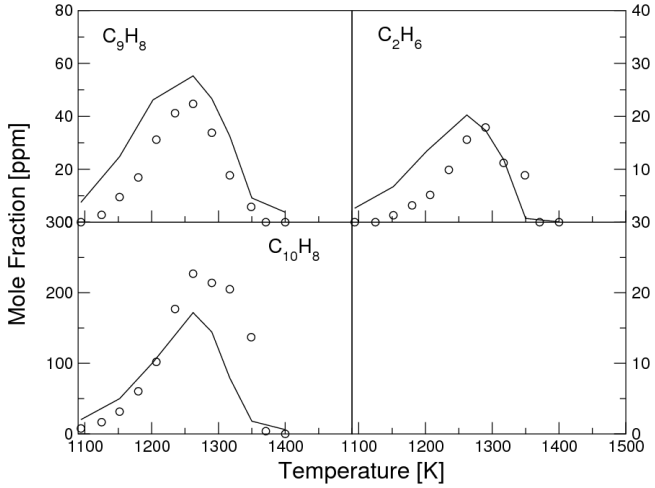


Figure 5.9 Concentration profiles of intermediate species during 1-methyl naphthalene oxidation in jet-stirred reactor. Φ =1.0, P = 1 atm and T = 1094 - 1400 K. Circles are experimental data [124] and the solid lines the current simulations.

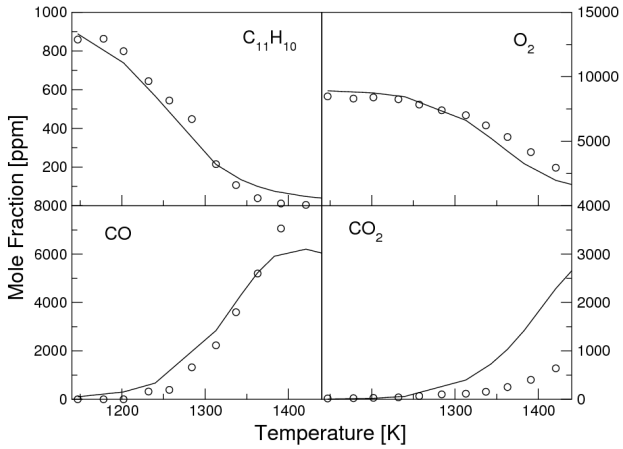


Figure 5.10 Concentration profiles of intermediate species during 1-methyl naphthalene oxidation in jet-stirred reactor. Φ = 1.5, P = 1 atm and T = 1147 - 1440 K. Circles are experimental data [124] and the solid lines the current simulations.

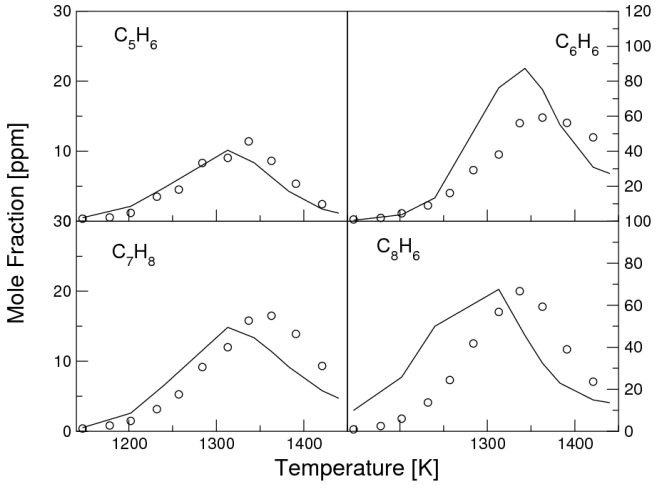


Figure 5.11 Concentration profiles of intermediate species during 1-methyl naphthalene oxidation in jet-stirred reactor. Φ = 1.5, P = 1 atm and T = 1147 - 1440 K. Circles are experimental data [124] and the solid lines the current simulations.

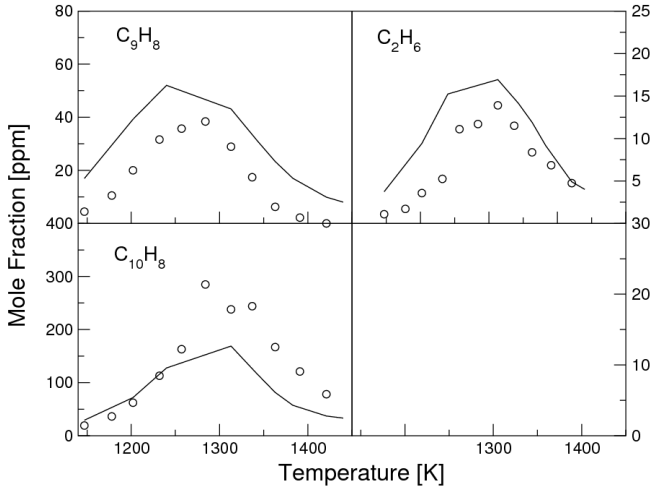


Figure 5.12 Concentration profiles of intermediate species during 1-methyl naphthalene oxidation in jet-stirred reactor. Φ = 1.5, P = 1 atm and T = 1147 - 1440 K. Circles are experimental data [124] and the solid lines the current simulations.

$C_{11}H_{10} + OH = C_{11}H_9 + H_2O$ (86)

$C_{11}H_{10} + OH = C_{11}H_9P + H_2O$ (83)

$C_{11}H_{10} + O = C_{11}H_9O + H$ (88)

$C_{11}H_{10} + O = OC_{11}H_9 + H$ (89)

The fuel is reformed from the 1-methylnaphthyl radical (82%) (-84). The reaction rate was adopted from Potter [60] and based on the toluene kinetics as proposed by Lindstedt and Maurice [67]. The formation from $HOC_{11}H_9$ also makes a contribution (17%) via OH replacement (87) with $HOC_{11}H_9$ also formed from the $OC_{11}H_9$ radical via H addition (92). The $OC_{11}H_9$ radical is formed from 1-methyl naphthalene by replacement of a hydrogen atom on the ring (89) with an oxygen atom (52%). The rate that stems from the kinetics of toluene proposed by Hoffman *et al*. [109] and from oxygen addition (32%) to the 1-methyl-4-naphthyl radical ($C_{11}H_9P$) via molecular oxygen attack (82) with a rate based on the toluene kinetics proposed by Lindstedt and Maurice [67]. The major 1-methyl naphthalene decomposition and formation pathways are shown in Figs. 5.13 – 5.14.

$C_{11}H_{10} = C_{11}H_9 + H$ (84)

$C_{11}H_{10} + OH = HOC_{11}H_9 + H$ (87)

$OC_{11}H_9 + H = HOC_{11}H_9$ (92)

$C_{11}H_{10} + O = OC_{11}H_9 + H$ (89)

$C_{11}H_9P + O_2 = OC_{11}H_9 + O$ (82)

Naphthalene is formed via thermal decomposition of the $C_{11}H_9O$ radical (91) (65%), which is formed from oxygen attack on 1-methyl naphthalene (88) (Fig. 5.15).

$C_{11}H_{10} + O = C_{11}H_9O + H$ (88)

$C_{11}H_9O = C_{10}H_8 + CHO$ (91)

Once naphthalene is formed, hydrogen abstraction via OH radical attack (78), leading to the formation of the naphthyl radical contributes 49% to consumption of the former. Moreover, 43% of the naphthalene forms naphthaldehyde (77) by oxygen addition and hydrogen abstraction. The naphthalene decomposition reactions were assigned rates based on the corresponding benzene channels. The naphthaldeyde thermally decomposes by CO abstraction leading to the formation of the indenyl radical and indene.

$C_{10}H_8 + O = C_{10}H_7O + H$ (77)

$C_{10}H_8 + OH = C_{10}H_7 + H_2O$ (78)

The formation of indene occurs (98%) from the indenyl radical. The indenyl radical is formed in a sequence of reaction steps initiated by the formation of the $OC_{11}H_9$ radical. The latter thermally decomposes via CO expulsion from the ring leading to the formation of

$C_9H_6CH_3$. The latter species recombines with a hydrogen atom leading to the formation of $C_9H_7CH_3$, which thermally decomposes to indenyl and methyl (50%). The rates of the last two steps were assigned from suggestions made by Laskin and Lifshitz [126]. In addition, the indenyl radical is formed by the thermal decomposition of naphthaldehyde (16%). A more direct link to the fuel is provided by (12%) the indenyl radical and acetylene formation from the 1-methylnaphthyl radical (81). The reverse reaction step was also tested with a rate relative to the benzyl radical formation channel proposed by Colket and Seery [62], but found to lead to excessive acetylene and indene concentrations. By contrast, the use of the 1-methyl naphthtyl radical thermal decomposition channel (81) with a rate relative to the benzyl radical thermal decomposition proposed by Braun-Unkhoff [77] leads to excellent agreement between computed and measured concentration profiles for both acetylene and indene.

$$C_{11}H_9 = C_9H_7 + C_2H_2 \qquad (81)$$

The oxidation of the indenyl radical by $HO_2$ leads to $C_9H_7O$ formation (68). Density Functional Theory and composite quantum mechanical methods were used to calculate the potential energy surfaces for the channel. Both RRKM/ME theory and VTST were subsequently used to derive an estimate of the rate constant [54]. The species is a precursor to phenyl acetylene ($C_8H_6$) formed through $C_8H_7$ decomposition. A rate proposed by Pitsch [125] was adopted for the CO expulsion from $C_9H_7O$ (75). The thermal decomposition of $C_8H_7$ is responsible for 71% of the phenyl acetylene formation (58) with a rate based on suggestions of Wang and Frenklach [110].

$$C_9H_7 + HO_2 = C_9H_7O + OH \qquad (68)$$

$$C_9H_7O = C_8H_7 + CO \qquad (75)$$

$$C_8H_7 = C_8H_6 + H \qquad (58)$$

Computations show that molecular oxygen attack (70) forms another important indenyl oxidation step responsible for 50% of the benzyl radical formation with the rate determined by Lindstedt *et al.* [54]. The benzyl radical leads to toluene via reaction (38) with the rate determined by Oehlschlaeger *et al.* [80].

$$C_9H_7 + O_2 = C_7H_7 + CO + CO \qquad (70)$$

$$C_7H_8 = C_7H_7 + H \qquad (38)$$

In addition to the fulvene reaction sequence, 25% of benzene is formed from benzaldehyde and a rate proposed by Potter [60] was used for reaction (47).

$$C_7H_6O + O = C_6H_6 + CO_2 \qquad (47)$$

Benzene is mostly formed (35%) from fulvene via isomerization (26) assigned a rate proposed by Marinov *et al.* [63]. Fulvene is produced (100%) by the methyl cyclo pentadienyl radical after thermal decomposition (27) and assigned a rate proposed by Lindstedt and Rizos [46].

$C_5H_4CH_3 = C_6H_6(F) + H$ (27)

$C_6H_6(F) + M = C_6H_6 + M$ (26)

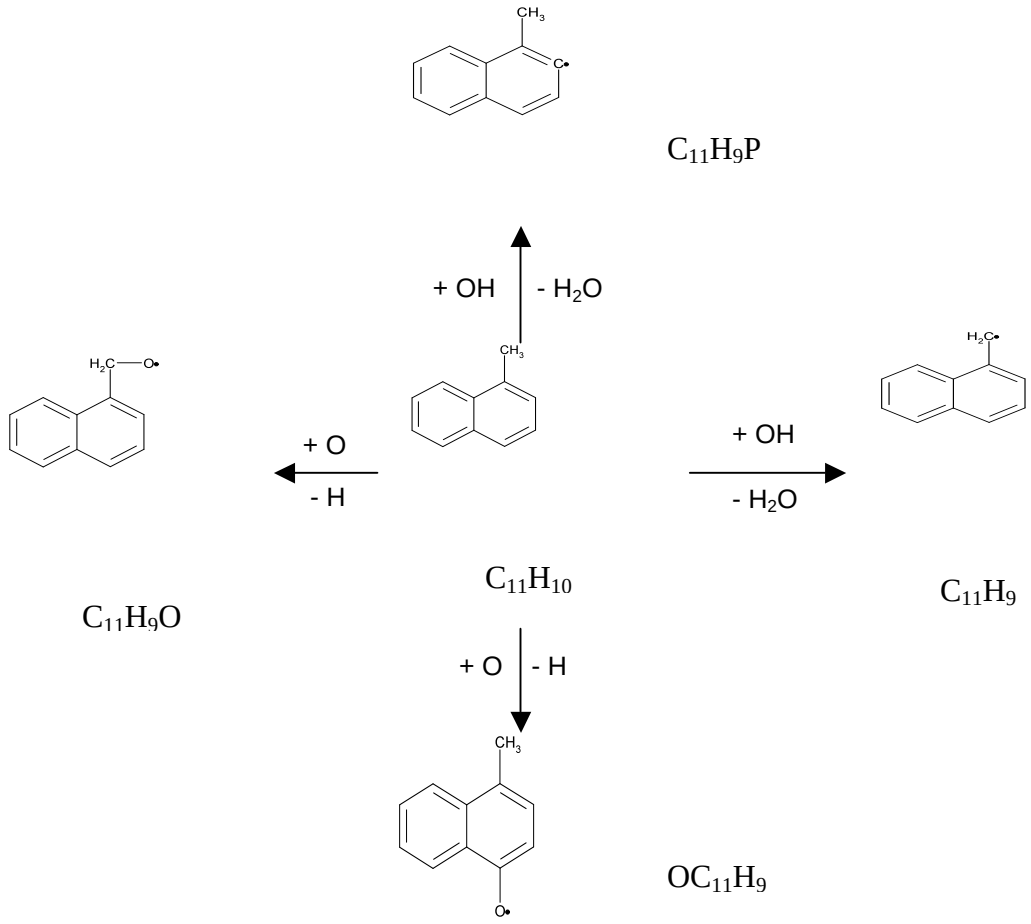


Figure 5.1 Major 1-methyl naphthalene decomposition pathways.

Benzene is consumed by reactions leading to phenyl (42%) and phenoxy (48%) radicals. The phenyl radical also predominantly (65%) leads to phenoxy which in turn leads to the formation of the cyclopentadienyl radical (80%) by CO expulsion. The cyclopentadienyl radical follows two major decomposition routes; 28% thermally decomposes to acetylene and the propargyl radical and 25% recombines with hydrogen leading to cyclopentadiene.

Cyclopentadiene is predominantly (90%) produced by the recombination of the cyclopentadienyl radical with atomic hydrogen. A rate proposed by Kern *et al.* [36] was applied to this channel. Cyclopentadiene then recycles back to cyclopentadienyl radical.

$$C_5H_6 = C_5H_5 + H \qquad (13)$$

Acetylene is formed via two major thermal decomposition channels. The dominant (39%) is the thermal decomposition of the 1-methyl naphthyl radical that forms acetylene and the indenyl radical (81) and acetylene is also formed (21%) via the thermal breakdown of cyclopentadienyl radical (3).

$$C_{11}H_9 = C_9H_7 + C_2H_2 \qquad (81)$$

$$C_5H_5 = C_3H_3 + C_2H_2 \qquad (3)$$

The rate of Kern *et al.* [36] was applied to reaction channel (3) but found to produce excessive acetylene concentrations, hence an adjustment was made by reducing the rate by 50%.

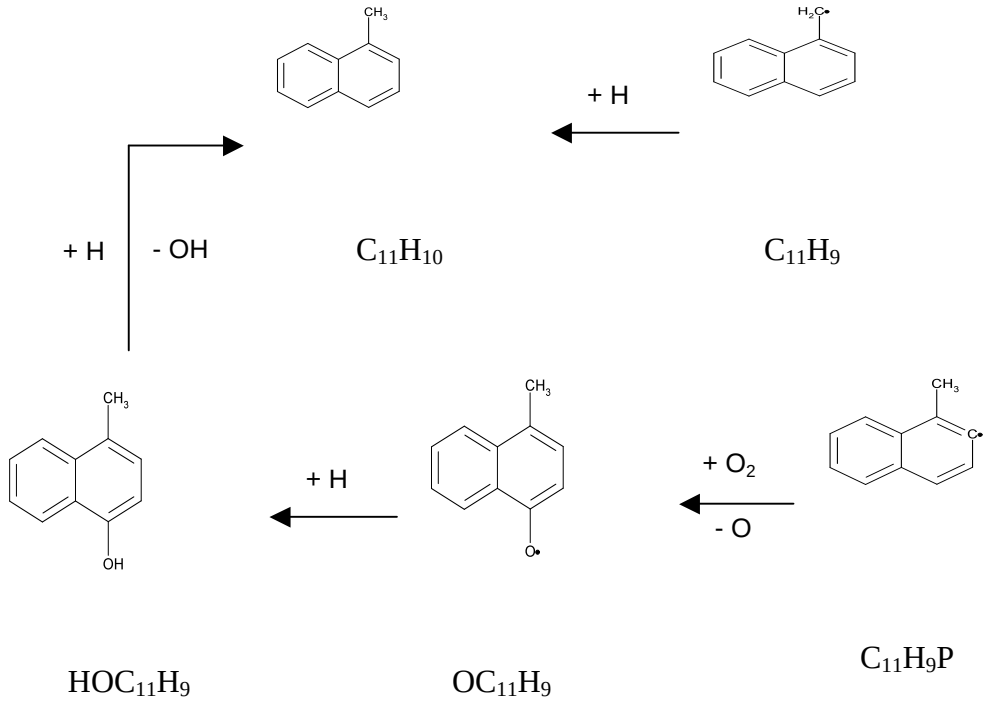


Figure 5.2 Major 1-methyl naphthalene formation pathways.

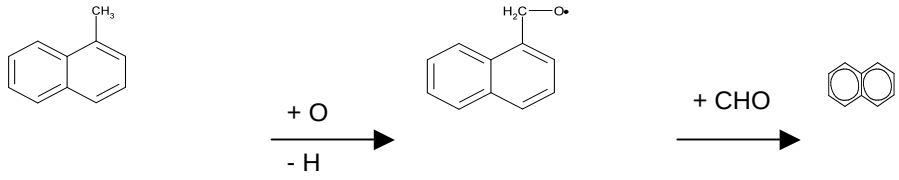


$C_{11}H_{10}$ $C_{11}H_9O$ $C_{10}H_8$

Figure 5.3 Naphthalene formation pathways

### 5.4 The Oxidation of 1-Methyl Naphthalene under TFR Conditions

Shaddix [119] performed gas-phase sampling to study the oxidation of 1-methyl naphthalene in the Princeton turbulent flow reactor and obtained concentration profiles for major species at atmospheric pressure and at a temperature of approximately 1170 K. Major fuel consumption routes and reaction classes were identified. Computations were performed corresponding to the experimental conditions for stoichiometric and fuel rich mixtures as shown in Table 5.2.

| **Φ** | **T (K)** | **P (atm)** | **[$O_2$] (ppm)** | **[$C_{11}H_{10}$] (ppm)** |
|---|---|---|---|---|
| 1.0 | 1169 | 1.0 | 14850 | 1100 |
| 1.5 | 1166 | 1.0 | 9900 | 1100 |
| 1.5 | 1198 | 1.0 | 9900 | 1100 |

Table 5.2 Experimental and modelling conditions for the oxidation of 1-methyl napthalene in a turbulent flow reactor.

Selected comparisons between computations and experimental data are shown in Figs. 5.16 – 5.19. The fuel profile is again well reproduced, suggesting that the 1-methyl naphthalene sub-mechanism is adequate. Moreover, naphthalene and indene, which are two of the major initial products of the fuel decomposition process, are very well reproduced for all the three test cases leading to good agreement between computations and measurements for subsequent products such as phenylacetylene, styrene and toluene.

The direct removal of the methyl group, either by replacement or via thermal decomposition, is a minor process contributing < 5% to the fuel breakdown. Once the 1-methylnaphthyl radical is formed, the proposed thermal decomposition channel leading to the indenyl radical and acetylene is important and affects the growth and evolution of major intermediate species such as indene, styrene, phenylacetylene, toluene, benzene, cyclopentadiene and acetylene.

In summary, the level of agreement obtained between the computed concentrations and measurements the naphthalene and indene implies that the accuracy of the fuel decay paths that involve oxygen addition and lead to the formation of $C_{11}H_9O$ and $OC_{11}H_9$ is adequate. The further decomposition of the oxygenated species leads to the formation of $C_{10}H_8$ and significant amounts of $C_9H_7$. The branching ratios between abstraction and addition pathways are also important for 1-methyl naphthalene combustion at intermediate temperatures and, again, the level of agreement obtained is encouraging. Furtermore, the distribution of the single-ring aromatics is also well reproduced.

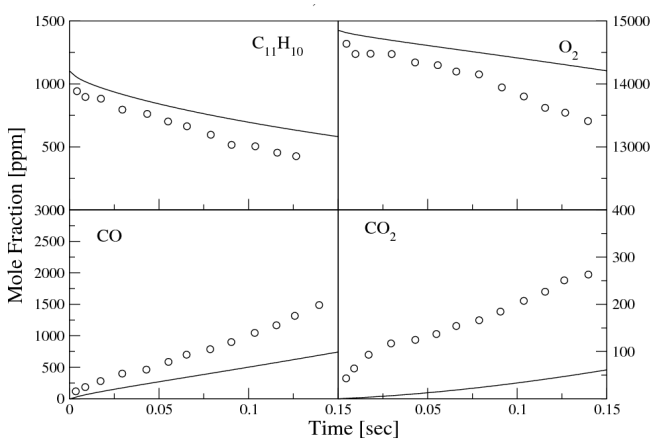


Figure 5.16 Concentration profiles of major species during 1-methyl naphthalene oxidation in a flow reactor (Φ = 1.0, P = 1 atm, T = 1169 K). Circles indicate measurements [119] and solid lines the current computations.

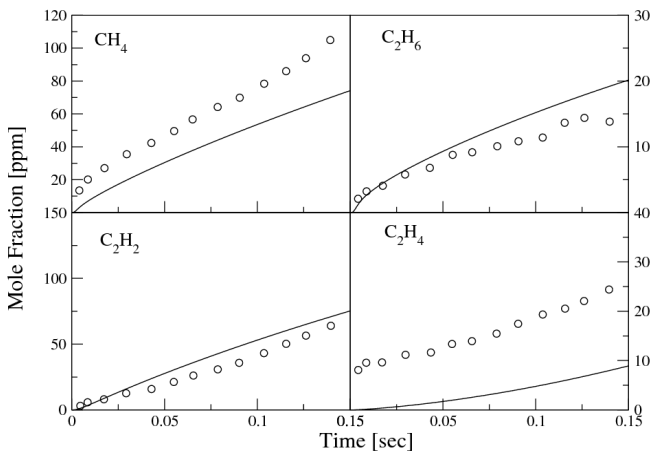


Figure 5.17 Concentration profiles of major species during 1-methyl naphthalene oxidation in a flow reactor (Φ = 1.0, P = 1 atm, T = 1169 K). Circles indicate measurements [119] and solid lines the current computations.

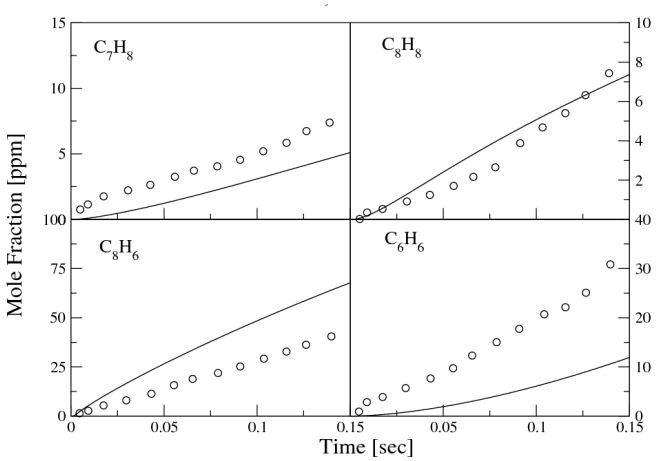


Figure 5.18 Concentration profiles of major species during 1-methyl naphthalene oxidation in a flow reactor (Φ = 1.0, P = 1 atm, T = 1169 K). Circles indicate measurements [119] and solid lines the current computations

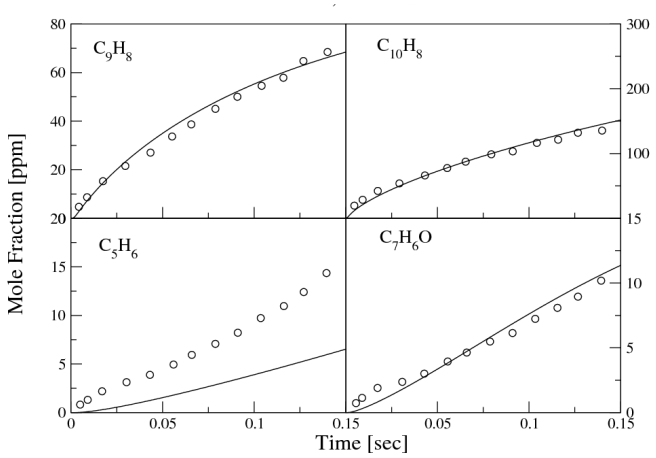


Figure 5.19 Concentration profiles of major species during 1-methyl naphthalene oxidation in a flow reactor (Φ = 1.0, P = 1 atm, T = 1169 K). Circles indicate measurements [119] and solid lines the current computations.

## 6.0 Conclusions

The main objective of the present work has been the development and validation of gas phase chemical kinetic mechanisms for aromatic components of aviation fuels and surrogates. A reaction class based approach was used for the generation of the chemical mechanisms and a broad range of reactors and conditions were considered. The mechanisms feature molecules up to $C_{11}$ that involve aliphatic compounds and sub-mechanisms for mono-substituted and polyaromatic hydrocarbons. The starting point for the work was the development and validation of a mechanism for cyclopentadiene, which constitutes a major intermediate component in the combustion of higher aromatics. The work was subsequently extended to toluene and n-propyl benzene and two-ringed aromatics such as naphthalene and 1-methyl naphthalene.

The oxidation of cyclopentadiene was studied under plug flow reactor conditions and concentration profiles were computed and compared with measurements of Butler [55]. Reaction rates for channels featuring O, $HO_2$ and OH were updated and validated. A variety of cases varying from stoichiometric to fuel rich were tested and reaction rate analyses performed for representative cases. The pyrolysis of cyclopentadiene was also studied for a variety of fuel concentrations. The detection of high concentrations of species such as naphthalene, toluene, benzene and acetylene suggest pathways leading to poly-aromatic hydrocarbons.

The combustion of toluene was further analysed under shock tube conditions. Pyrolytic and oxidation conditions corresponding to those obtained by Braun-Unkhoff *et al*. [77], Vasudevan *et al*. [70] and Burcat *et al*. [69] were included. Reaction rates were updated and new reaction pathways added to the starting mechanism. Hydrogen atom profiles were calculated under pyrolytic conditions and shown to capture the measured profiles of Braun-Unkhoff *et al.* [77] reasonably well. The implication is that the applied branching ratio of the toluene thermal decomposition to the benzyl radical or phenyl and methyl radicals is arguably correct.

Time resolved OH profile was also computed under shock tube conditions and compared against experimental data of Vasudevan *et al*. [70]. Reaction rate analyses were performed and important pathways identified. The results highlight the toluene thermal decomposition to the benzyl radical and phenyl and methyl radicals, as well as hydrogen assisted reactions leading to the production of the benzyl radical and benzene. The results suggest that the reaction class based approach can be applied to other methyl-substituted aromatic fuel components that form part of real and surrogate fuel formulations.

A reaction mechanism for n-propyl benzene was developed on the basis of the behaviour of benzene, toluene and propane. The mechanism was validated under jet-stirred reactor conditions for both low and high pressures for a wide range of stoichiometries and against ignition delay times. A reaction rate analysis highlighted the importance of the hydrogen abstraction reactions, which generate styrenes and promote the fuel consumption. The thermal breakdown of the n-propyl benzene chain at the primary and secondary sites is significant and small rate changes can cause big discrepancies in the intermediate species concentrations. Large early concentrations of styrene, ethyl benzene and toluene provide a clear indication that homolytic reactions occur and promote the fuel decay.

The work was expanded to two-ring aromatic compounds such as naphthalene and tested under plug flow reactor conditions at atmospheric pressure and compared to measurements

obtained by Shaddix [119]. Reaction rates for the $C_9H_7$ + $O_2$/$HO_2$ were obtained by Lindstedt *et al*. [54] and a reaction rate analysis performed showed that the channels play a significant role to the product distribution of single ring aromatics. It was also shown that hydrogen abstraction reaction via OH and oxygen addition to the ring constitute major fuel consumption pathways. However, due to limited availability of experimental data in the literature, only a single test case was analysed in this work. Hence, measurements of wider range of conditions are desirable for further refinements. However, the much more extensive work performed on the 1-methyl naphthalene system, outlined below, is complementary and adds further confidence in the modelling.

The 1-methyl naphthalene sub-mechanism was based on the toluene chemistry due to structural similarities. Reaction rates were updated and reaction steps added to the mechanism. Validation was performed under plug flow and jet stirred reactor conditions at atmospheric pressure for a variety of stoichiometries. Results were compared against measurements obtained by Shaddix and co-workers [119, 121] and Mati *et al.* [124]. A reaction rate analysis was performed for both plug flow and jet stirred reactor conditions and showed that the fuel decomposes via OH hydrogen abstraction from the chain and the ring and oxygen addition to both the chain and the ring. However, the attack on the chain side dominates the consumption of the fuel. The proposed thermal decomposition of the 1-methylnaphthyl radical to the indenyl radical and acetylene, was shown to constitute a major channel for the evolution of intermediate species. Moreover, the reaction sequence of $C_9H_7$ + $O_2$/$HO_2$ was again shown to be important for the distribution of single-ring aromatics. The good agreement between the computations and the measurements for the current 1-methyl naphthalene is encouraging.

Overall, the current work has resulted in a significantly improved understanding of key reaction pathways for both the oxidation and growth of aromatic species in combustion applications and opens up a route for further improvements in the predictions of not only global properties, such as ignition delay times, but also the speciation characteristics that are essential for the prediction of pollutant emissions.

## References

[1] J. P. Longwell, The Formation of Polycyclic Aromatic Hydrocarbons by Combustion, *Nineteenth Symposium (International) on Combustion* (1) 19 (1982), 1339-1350.

[2] W. J. Pitz, C. K. Westbrook, A. E. Lutz, R. J. Kee, S. M. Senkan and J. G. Seebold, Numerical Modeling Capabilities for the Simulation of toxic By-Products Formation in Combustion Processes, *Combust. Flame* 101 (1994), 383.

[3] J. B. Howard, J. P. Longwell, J. A. Marr, C. J. Pope, W. F. Busby, A. L. Lafleur and K. Taghizadeh, Effects of PAH Isomerizations on Mutagenicity of Combustion Products, *Combust. Flame* (3) 101 (1995), 262-270.

[4] D. R. Ballal, S. P. Heneghan, W. J. Schmoll, F. Tanakashi and M. D. Vangness, Combustion and Heat Transfer Studies utilising Advanced Diagnostics: Combustion Studies, (1992).

[5] T. Edwards, L. Q. Maurice, H. Lander and W. E. Harisson, Advances in Aviation Fuels: A Look Ahead via a Historical Perspective, *Fuel* 80 (2001), 747.

[6] P. Dagaut and M. Cathonnet, The Ignition, Oxidation and Combustion of Kerosene: A Review of Experimental and Kinetic Modeling, *Prog. Energy Combust. Sci.* (1) 32 (2006), 48-92.

[7] A. F. Sarofim, E. G. Eddings, S. Yan, A. Violi, S. Granata, T. Faravelli and E. Ranzi, Experimental Formulation and Kinetic Modeling for JP-8 Surrogate Mixtures, *Second Mediterranean Combustion Symposium, Sharm el Sheick, Egypt* (2002).

[8] R. P. Lindstedt, Modeling of the Chemical Complexities of Flames, *Symposium (International) on Combustion* (1) 27 (1998), 269-285.

[9] M. Bernabei, R. Reda, R. Galiero and G. Bocchinfuso, Determination of Total and Polycyclic Aromatic Hydrocarbons in Aviation Jet Fuel, *Journal of Chromatography A* (1-2) 985 (2003), 197-203.

[10] C. K. Westbrook and F. L. Dryer, Chemical Kinetic Modeling of Hydrocarbon Combustion, *Prog. Energy Combust. Sci.* (1) 10 (1984), 1-57.

[11] S. W. Benson, *Thermochemical Kinetics*, (John Wiley & Sons, INC, 1976).

[12] J. Troe, Towards a Quantitative Understanding of Elementary Combustion Reactions, *Twenty-Second Symposium (International) on Combustion, The Combustion Institute* (1) 22 (1989), 843-862.

[13] A. M. Dean, Predictions of Pressure and Temperature Effects upon Radical Addition and Recombination Reactions, *J. Phys. Chem.* 89 (1985), 4600-4608.

[14] A. Burcat and B. Ruscic, Third Millenium Ideal Gas and Condensed Phase Thermochemical Database for Combustion with Updates from Active Thermochemical Tables, (2005), ANL-05/20 and TAE 960 Technion-IIT, Aerospace Engineering and Argonne National Laboratory, Chemistry Division, September 2005.

[15] R. Robinson, Private Communication, (2009).

[16] J. A. Miller, R. J. Kee and C. K. Westbrook, Chemical Kinetics and Combustion Modeling, *Annu. Rev. Phys. Chem.* (1) 41 (1990), 345.

[17] W. P. Jones and R. P. Lindstedt, Global Reaction Schemes for Hydrocarbon Combustion, *Combust. Flame* (3) 73 (1988), 233-249.

[18] G. Dixon-Lewis, T. David, P. H. Gaskell, S. Fukutani, H. Jinno, J. A. Miller, R. J. Kee, M. D. Smooke, N. Peters, E. Effelsberg, J. Warnatz and F. Behrendt, Calculation of the Structure and Extinction Limit of a Methane-Air Counterflow Diffusion Flame in the Forward Stagnation Region of a Porous Cylinder, *Twentieth Symposium (International) on Combustion, The Combustion Institute* (1) 20 (1985), 1893-1904.

[19] R. J. Kee, J. A. Miller and T. H. Jefferson, A General purpose Problem-Independent Transortable Fortran Chemical Kinetics Code Package, (1980), Sandia National Laboratories Report SAND80-8003.

[20] J. Warnatz, J. Maas and R. W. Dibble, Combustion. Physical and Chemical Fundamentals, Modelling and Simulation, Experiments, Pollutant Formation, no. 3rd Edition (2001).

[21] S. Arrhenius, Uber die Reaktiosgeschwindigkeit bei der Inversion von Rohrzucker durch Sauren, *Z. Phys. Chem.* 4 (1889), 226.

[22] F. A. Lindemann, Discussion on "The radiation Theory of Chemical Action" *Trans. Faraday Soc.* 17 (1922), 599.

[23] M. J. Pilling and P. W. Seakins, *Reaction Kinetics*, (Oxford University Press Inc., New York, 1995).

[24] R. G. Butler and I. Glassman, Cyclopentadiene Combustion in a Plug Flow Reactor near 1150 K, *Proc. Combust. Inst.* In Press, Corrected Proof (2009).

[25] D. Wang, A. Violi, D. H. Kim and J. A. Mullholland, Formation of Naphthalene, Indene, and Benzene from Cyclopentadiene Pyrolysis: A DFT Study, *J. Phys. Chem. A* (14) 110 (2006), 4719-4725.

[26] C. F. Melius, M. E. Colvin, N. M. Marinov, W. J. Pit and S. M. Senkan, Reaction Mechanisms in Aromatic Hydrocarbon Formation Involving the C5H5 Cyclopentadienyl Moiety, *Twenty-Sixth Symposium (International) on Combustion, The Combustion Institute* (1) 26 (1996), 685-692.

[27] C. F. Melius, J. A. Miller and E. M. Evleth, Unimolecular Reaction Mechanisms Involving $C_3H_4$, $C_4H_4$, and $C_6H_6$ Hydrocarbon Species, *Twenty-Fourth Symposium (International) on Combustion, The Combustion Institute* (1) 24 (1992), 621-628.

[28] M. Frenklach, D. W. Clary, W. C. Gardiner Jr and S. E. Stein, Effect of Fuel Structure on Pathways to Soot, *Twenty-First Symposium (International) on Combustion* (1) 21 (1986), 1067-1076.

[29] M. Frenklach and J. Warnatz, Detailed Modeling of PAH Profiles in a Sooting Low-Pressure Acetylene Flame, *Combust. Sci. and Tech.* (4) 51 (1987), 265-283.

[30] M. Frenklach, D. W. Clary, T. Yuan, W. C. Gardiner and S. E. Stein, *Combust. Sci. and Tech.* (1) 50 (1986), 79-115.

[31] M. Frenklach, D. W. Clary, J. W. C. Gardiner and S. E. Stein, Detailed Kinetic Modeling of Soot Formation in Shock-Tube Pyrolysis of Acetylene, *Twentieth Symposium (International) on Combustion, The Combustion Institute* (1) 20 (1985), 887-901.

[32] A. Burcat and M. Dvinyaninov, Detailed Kinetics of Cyclopentadiene Decomposition Studied in a Shock Tube, *Int. J. Chem. Kinet.* (7) 29 (1997), 505-514.

[33] K. Roy, M. Braun-Unkhoff, P. Frank and T. Just, Kinetics of the Cyclopentadiene Decay and the Recombination of Cyclopentadienyl Radicals with H-Atoms: Enthalpy of Formation of the Cyclopentadienyl Radical, *Int. J. Chem. Kinet.* (3) 34 (2002), 209-222.

[34] K. Roy, C. Horn, P. Frank, V. G. Slutsky and T. Just, High-Temperature Investigations of the Pyrolysis of Cyclopentadiene, *Twenty-Seventh Symposium (International) on Combustion,The Combustion Institute* (1998), 329-336.

[35] M. B. Colket, The Pyrolysis of Cyclopentadiene, Eastern States Section Annual Meeting of the Combustion Institute, Orland, FL (1990).

[36] R. D. Kern, Q. Zhang, J. Yao, B. S. Jursic, R. S. Tranter, M. A. Greybill and J. H. Kiefer, Pyrolysis of Cyclopentadiene: Rates for Initial C-H Bond Fission and the Decomposition of c-$C_5H_5$, *Twenty-Seventh Symposium (International) on Combustion,The Combustion Institute* (1998), 143-150.

[37] X. Zhong and J. W. Bozzelli, Thermochemical and Kinetic Analysis of the H, OH, $HO_2$, O, and $O_2$ Association Reactions with Cyclopentadienyl Radical, *The Journal of Physical Chemistry A* (20) 102 (1998), 3537-3555.

[38] A. B. Lovell, K. Brezinsky and I. Glassman, Benzene Oxidation Perturbed by $NO_2$ Addition, *Twenty-Second Symposium (International) on Combustion, The Combustion Institute* (1) 22 (1989), 1063-1074.

[39] J. L. Emdee, K. Brezinsky and I. Glassman, A Kinetic Model for the Oxidation of Toluene near 1200 K, *J. Phys. Chem.* 96 (1992), 2151-2161.

[40] L. V. Moskaleva and M. C. Lin, Computational Study of the Kinetics and Mechanisms for the Reaction of H atoms with c-$C_5H_6$, *Proc. Combust. Inst* (1) 29 (2002), 1319-1327.

[41] G. B. Bacskay and J. C. Mackie, The Pyrolysis of Cyclopentadiene: Quantum Chemical and Kinetic Modelling Studies of the Acetylene Plus Propyne/Allene Decomposition Channels, *Phys. Chem. Chem. Phys.* 3 (2001), 2467-2473.

[42] N. M. Marinov, W. J. Pitz, C. K. Westbrook, M. J. Castaldi and S. M. Senkan, Modelling of Aromatic and Polycyclic Aromatic Hydrocarbon Formation in Premixed Methane and Ethane Flames, *Combust. Sci. and Tech.* 116-117 (1996), 211-287.

[43] V. V. Kislov and A. M. Mebel, The Formation of Naphthalene, Azulene, and Fulvalene from Cyclic $C_5$ Species in Combustion:An Ab Initio/RRKM Study of 9-H-Fulvalenyl ($C_5H_5$-$C_5H_4$) Radical Rearrangements, *J. Phys. Chem. A* (38) 111 (2007), 9532-9543.

[44] M. Lu and J. A. Mulholland, Aromatic Hydrocarbon Growth from Indene, *Chemosphere* (5-7) 42 (2001), 625-633.

[45] R. P. Lindstedt, L. Q. Maurice and M. Meyer, Thermodynamic and Kinetic Issues in the Formation and Oxidation of Aromatic Species, *Faraday Discuss.* 119 (2001), 409-432.

[46] R. P. Lindstedt and K. A. Rizos, The Formation and Oxidation of Aromatics in Cyclopentene and Methyl-Cyclopentadiene Mixtures, *Proc. Combust. Inst.* 29 (2002), 2291-2298.

[47] C. S. McEnally and L. Pfefferle, The Use of Carbon-13-Labeled Fuel Dopants For Identifying Napthalene Formation Pathways in Non-Premixed Flames, *Proc. Combust. Inst.* 28 (2000), 2569-2576.

[48] J. A. Mulholland, M. Lu and D.-H. Kim, Pyrolytic Growth of Polycyclic Aromatic Hydrocarbons by Cyclopentadienyl Moieties, *Twenty-Eighth Symposium (International) on Combustion, The Combustion Institute* (2) 28 (2000), 2593-2599.

[49] A. D'Anna and A. Violi, A Kinetic Model for the Formation of Aromatic Hydrocarbons in Premixed Laminar Flames, *Twenty-Seventh Symposium (International) on Combustion,The Combustion Institute* (1) 27 (1998), 425-433.

[50] A. Violi, A. F. Sarofim and T. N. Truong, Quantum Mechanical Study of Molecular Weight Growth Process by Combination of Aromatic Molecules, *Combust. Flame* (1-2) 126 (2001), 1506-1515.

[51] A. Violi, A. F. Sarofim and T. N. Truong, Mechanistic Pathways to Explain H/C Ratio of Soot Precursors, *Combust. Sci. and Tech.* (11) 174 (2002), 205 - 222.

[52] V. V. Kislov and A. M. Mebel, An Ab Initio G3-Type/Statistical Theory Study of the Formation of Indene in Combustion Flames. II. The Pathways Originating from Reactions of Cyclic $C_5$ Species Cyclopentadiene and Cyclopentadienyl Radicals, *J. Phys. Chem. A* (4) 112 (2008), 700-716.

[53] L. V. Moskaleva, A. M. Mebel and M. C. Lin, The $CH_3$+$C_5H_5$ Reaction: A Potential Source of Benzene at High Temperatures, *Twenty-Sixth Symposium (International) on Combustion* (1) 26 (1996), 521-526.

[54] R. P. Lindstedt, V. Markaki and R. Robinson, Oxidation of Two-Ringed Aromatic Species as Models for Soot Surface Reactions, *Proc. of Anacapri Workshop on Fine Carbon Based Particles* (2009), 483-506.

[55] R. G. Butler, Combustion Chemistry of 1-3 Cyclopentadiene, In *Department of Chemistry*, (Princeton University, PhD Thesis, 2001).

[56] A. Burcat and B. Ruscic, Third Millennium Ideal Gas and Condensed Phase Thermochemical Database for Combustion with Updates from Active Thermochemical Tables, (Techion-IIT, Aerospace Engineering and Argonne National Laboratory, 2005).

[57] K. A. Rizos, Detailed Chemical Kinetic Modelling of Homogeneous Systems, (2003).

[58] K. M. Leung and R. P. Lindstedt, Detailed Kinetic Modelling of $C_1$-$C_2$ Alkane Diffusion Flames, *Combust. Flame* 102 (1995), 129-160.

[59] M. B. Colket, R. J. Hall and M. D. Smooke, Mechanistic Models of Soot Formation, In *Final Report on AFOSR Contract*, (F49620-91-C-0056, 1994).

[60] M. L. Potter, Detailed Chemical Kinetic Modelling of Propulsion Fuels, (Imperial College London, 2003).

[61] M. Frenklach and H. Wang, Detailed Mechanism and Modelling of Soot Particle Formation in Soot Formation in Combustion: Mechanisms and models, (Springer-Verlag, first edition, 1994).

[62] M. B. Colket and D. J. Seery, Reaction Mechanisms for Toluene Pyrolysis, *Twenty-Fifth Symposium (International) on Combustion* (1) 25 (1994), 883-891.

[63] N. M. Marinov, M. J. Castaldi, C. F. Melius and W. Tsang, Aromatic and Polycyclic Aromatic Hydrocarbon Formation in a Premixed Propane Flame, *Combust. Sci. and Tech.* (1) 128 (1997), 295 - 342.

[64] H. Richter, O. A. Mazyar, R. Sumathi, W. H. Green, J. B. Howard and J. W. Bozzelli, Detailed Kinetic Study of the Growth of Small Polycyclic Aromatic Hydrocarbons. 1. 1-Naphthyl + Ethyne, *J. Phys. Chem. A* 105 (2001), 1561-1573.

[65] S. D. Klotz, K. Brezinsky and I. Glassman, Modeling the Combustion of Toluene-Butane Blends, *Twenty-Seventh Symposium (International) on Combustion,The Combustion Institute* (1) 27 (1998), 337-344.

[66] P. Dagaut, G. Pengloan and A. Ristori, Oxidation, Ignition and Combustion of Toluene: Experimental and Detailed Chemical and Kinetic Modelling., *Phys. Chem. Chem. Phys.* 4 (2002), 1846-1854.

[67] R. P. Lindstedt and L. Q. Maurice, Detailed Kinetic Modelling of Toluene Combustion, *Combust. Sci. and Tech.* 120 (1996), 119.

[68] R. Sivaramakrishnan, R. S. Tranter and K. Brezinsky, A high pressure model for the oxidation of toluene, *Proc. Combust. Inst* 30 (2005), 1165-1173.

[69] A. Burcat, C. Snyder and T. Brabbs, Ignition Delay Times of Benzene and Toluene With Oxygen in Argon Mixtures., In *Technical Memorandum 87312*, (NASA, 1986).

[70] V. Vasudevan, D. F. Davidson and R. K. Hanson, Shock tube measurements of toluene ignition times and OH concentration time histories, *Proc. Combust. Inst* 30 (2005), 1155–1163.

[71] D. F. Davidson, B. M. Gauthier and R. K. Hanson, Shock tube ignition measurements of iso-octane/air and toluene/air at high pressures, *Proc. Combust. Inst* 30 (2005), 1175-1182.

[72] W. J. Pitz, R. Seiser, J. W. Bozzelli, I. Da Costa, R. Fournet, F. Billaud, F. Battin-Leclerc, K. Seshadri and C. K. Westbrook, Chemical Kinetic Characterization of Combustion of Toluene, (Lawrence Livermore National Laboratory, 2001).

[73] K. M. Pamidimukkala, R. D. Kern, M. R. Patel, H. C. Wei and J. H. Kiefer, High-Temperature Pyrolysis of Toluene, *J. Phys. Chem.* 91 (1987), 2148-2154.

[74] V. S. Rao and G. B. Skinner, Formation of H and D Atoms in the Pyrolysis of Toluene-d, and ToIuene-α,α,α-d3 behind Shock Waves, *J. Phys. Chem.* 93 (1989), 1864-1869.

[75] W. Muller-Markgraf and J. Troe, Thermal Decompositlon of Ethylbenzene, Styrene, and Bromophenylethane: UV Absorption Study in Shock Waves, *J. Phys. Chem.* 92 (1988), 4914-4922.

[76] L. D. Brouwer, W. Muller-Markgraf and J. Troe, Thermal Decomposition of Toluene: A comparison of Thermal and Laser-Photochemical Activation Experiments, *J. Phys. Chem.* 92 (1988), 4905.

[77] M. Braun-Unkhoff, P. Frank and T. Just, A Shock Tube Study on the Thermal Decomposition of Toluene and of the Phenyl Radical at High Temperatures, *Twenty-Second Symposium (International) on Combustion, The Combustion Institute* (1) 22 (1989), 1053-1061.

[78] H. Hippler and J. Troe, Thermodynamic Properties of Benzyl Radicals: Enthalpy of Formation from Toluene, Benzyl Iodide, and Dibenzyl Dissociation Equilibria, *J. Phys. Chem.* 94 (1990), 3803-3806.

[79] R. A. Eng, A. Gebert, E. Goos, H. Hippler and C. Kachiani, Incubation Times, Fall-Off and Branching Ratios in the Thermal Decomposition of Toluene: Experiments and Theory, *Phys. Chem. Chem. Phys.* 4 (2002), 3989-3996.

[80] M. A. Oehlschlaeger, D. F. Davidson and R. K. Hanson, Thermal decomposition of toluene: Overall rate and branching ratio, *Proc. Combust. Inst* (1) 31 (2007), 211-219.

[81] J. L. DiNaro, J. B. Howard, W. H. Green, J. W. Tester and J. W. Bozzelli, Elementary Reaction Mechanism for Benzene Oxidation in Supercritical Water, *J. Phys. Chem. A* 104 (2000), 10576-10586.

[82] T. B. Hunter, T. A. Litzinger, H. Wang and M. Frenklach, Ethane Oxidation at Elevated Pressures in the Intermediate Temperature Regime: Experiments and Modelling, *Combust. Flame* 104 (1996), 505-523.

[83] R. Zellner and F. Ewig, Computational Study of the $CH_3 + O_2$ Chain Branching Reaction, *J. Phys. Chem.* 92 (1988), 2971-2974.

[84] S. P. Walch, Characterization of the Potential Energy Surface for $CH_3 + O_2$ = Products, *Chem. Phys. Lett.* (1) 215 (1993), 81-86.

[85] P. Q. Clothier, D. Shen and H. O. Pritchard, Stimulation of Diesel-Fuel Ignition by Benzyl Radicals, *Combust. Flame* 101 (1995), 383-386.

[86] H. Sun, S. I. Yang, G. Jomaas and C. K. Law, High-Pressure Laminar Flame Speeds and Kinetic Modelling of Carbon Monoxide / Hydrogen Combustion, *Proc. Combust. Inst.* 31 (2007), 439-446.

[87] D. L. Baulch, C. T. Bowman, C. J. Cobos, R. A. Cox, T. Just, J. A. Kerr, M. J. Pilling, D. Stocker, J. Troe, W. Tsang, R. W. Walker and J. Warnatzota, Evaluated Kinetic Data for Combustion Modelling: Supplement II, *J. Phys. Chem. Ref. Data* (3) 34 (2005), 757-1397.

[88] J. Li, Z. Zhao, A. Kazakov and F. L. Dryer, An Updated Comprehensive Kinetic Model of Hydrogen Combustion, *Int. J. Chem. Kinet.* (10) 36 (2004), 566-575.

[89] J. W. Sutherland, J. V. Michael, A. N. Pirraglia, F. L. Nesbitt and R. B. Klemm, Rate Constant for the Reaction of O(3P) with $H_2$ by the Flash Photolysis-Shock Tube and Flash Photolysis-Resonance Fluorescence Techniques; 504 K < T < 2495 K, *Proc. Combust. Inst.* 21 (1986), 929-941.

[90] K. Gkagkas and R. P. Lindstedt, The Impact of Reduced Chemistry on Auto-gnition of $H_2$ in turbulent flows *Combust. Theor. Model.* (2009), In Press.

[91] D. L. Baulch, C. J. Cobos, R. A. Cox, C. Esser, P. Frank, T. Just, J. A. Kerr, M. J. Pilling, J. Troe, R. W. Walker and J. Warnatz, Evaluated Kinetic Data for Combustion Modelling, *J. Phys. Chem. Ref. Data* (3) 21 (1992), 411-734.

[92] C.-L. Yu, M. Frenklach, D. A. Masten, R. K. Hanson and C. T. Bowman, Reexamination of Shock-Tube Measurements of the Rate Coefficient of $H + O_2$ .fwdarw. OH + O, *The Journal of Physical Chemistry* (17) 98 (1994), 4770-4771.

[93] W. J. Pitz, R. Seiser, J. W. Bozzelli, D. C. I., R. Fournet, F. Billaud, F. Battin-Leclerc, K. Seshadri and C. K. Westbrook, *Second Joint Meeting, US Sections of the Combustion Institute* Paper 253 (2001).

[94] K. Luther, J. Troe and K. M. Weitzel, Carbon-Carbon and Carbon-Hydrogen Bond Splits of Laser-Excited Aromatic Molecules. 2. In Situ Measurements of Branching Ratios, *J. Phys. Chem.* (16) 94 (1990), 6316-6320.

[95] P. Frank, J. Herzler, T. Just and C. Wahl, High-Temperature Reactions of Phenyl Oxidation, *Twenty-Fifth Symposium (International) on Combustion, The Combustion Institute* (1) 25 (1994), 833-840.

[96] P. Dagaut, A. Ristori, A. E. Bakali and M. Cathonnet, Experimental and Kinetic Modelling Study of the Oxidations of n-Propylbenzene, *Fuel* 81 (2002), 173-184.

[97] K. Brezinsky, G. T. Linteris, T. A. Litzinger and I. Glassman, High Temperature Oxidation of n-Alkyl Benzenes, *Twenty-first Symposium (International) on Combustion,The Combustion Institute* (1) 21 (1986), 833-840.

[98] T. A. Litzinger, K. Brezinsky and I. Glassman, Gas-Phase Oxidation of Isopropylbenzene at High Temperature, *J. Phys. Chem.* (3) 90 (1986), 508-513.

[99] T. A. Litzinger, K. Brezinsky and I. Glassman, The Oxidation of Ethylbenzene Near 1060 K, *Combust. Flame* (1-2) 63 (1986), 251-267.

[100] T. A. Litzinger, K. Brezinsky and I. Glassman, Reactions of N-Propylbenzene During Gas Phase Oxidation, *Combust. Sci. and Tech.* (1) 50 (1986), 117-133.

[101] A. Roubaud, R. Minetti and L. R. Sochet, Oxidation and Combustion of Low Alkylbenzenes at High Pressure: Comparative Reactivity and Auto-ignition, *Combust. Flame* (3) 121 (2000), 535-541.

[102] F. H. Seubold, The Rearrangement of the Neophyl Radical, *J.A.C.S.* (10) 75 (1953), 2532-2533.

[103] L. Q. Maurice, Detailed Chemical Kinetic Models for Aviation Fuels, PhD Thesis, Imperial College, London (1996).

[104] W. Tsang, Chemical Kinetic Data Base for Combustion Chemistry. Part 3. Propane, *J. Phys. Chem. Ref. Data* 17 (1988), 887-951.

[105] P. Dagaut, Computational Fluid Dynamics for Combustion. Final Report on Chemical Delay Measurements., (2001).

[106] C. Ellis, M. S. Scott and R. W. Walker, Addition of Toluene and Ethylbenzene to Mixtures of $H_2$ and $O_2$ at 772 K: Part 2: Formation of Products and Determination of Kinetic Data for H+ additive and for other Elementary Reactions Involved, *Combust. Flame* (3) 132 (2003), 291-304.

[107] D. Robaugh, W. Tsang, A. Fahr and S. E. Stein, Ethylbenzene Pyrolysis: Benzyl C-C or C-H Bond Homolysis, *Ber. Bunsenges. Phys. Chemistry* 90 (1986), 77.

[108] H. Eberius, P. Frank and C. Wahl, Computational Fluid Dynamics For Combustion, (DLR Institute for Combustion Technology, Stuttgart, 2001).

[109] A. Hoffman, M. Klatt and H. G. Wagner, An Investigation of the Reaction Between O(3) and Toluene at High Temperatures, *Z. Phys. Chem ( Neue Folge)* 168 (1990).

[110] H. Wang and M. Frenklach, A Detailed Kinetic Modelling Study of Aromatics Formation in Laminar Premixed Acetylene and Ethylene Flames, *Combust. Flame* 110 (1997), 173-221.

[111] J. A. Miller and C. F. Melius, Kinetic and Thermodynamic Issues in the Formation of Aromatic Compounds in Flames of Aliphatic Fuels, *Combust. Flame* (1) 91 (1992), 21-39.

[112] P. Dagaut and M. Cathonnet, A Comparative Study of the Kinetics of Benzene Formation from Unsaturated $C_2$ to $C_4$ Hydrocarbons, *Combust. Flame* (4) 113 (1998), 620-623.

[113] H. Richter and J. B. Howard, Formation of Polycyclic Aromatic Hydrocarbons and their Growth to Soot - A Review of Chemical Reaction Pathways, *Prog. Energy Combust. Sci.* 26 (2000), 565.

[114] F. C. Stehling, J. D. Frazee and R. C. Anderson, Carbon Formation from Acetylene, *Sixth Symposium (International) on Combustion, The Combustion Institute* (1) 6 (1957), 247-254.

[115] M. J. Castaldi, N. M. Marinov, C. F. Melius, J. Huang, S. M. Senkan, W. J. Pit and C. K. Westbrook, Experimental and Modeling Investigation of Aromatic and Polycyclic Aromatic Hydrocarbon Formation in a Premixed Ethylene Flame, *Twenty-Sixth Symposium (International) on Combustion, The Combustion Institute* (1) 26 (1996), 693-702.

[116] A. M. Dean, Detailed Kinetic Modelling of Autocatalysis in Methane Pyrolysis, *J. Phys. Chem.* 94 (1990), 1432-1439.

[117] N. M. Marinov, W. J. Pitz, C. K. Westbrook, A. M. Vincitore, M. J. Castaldi, S. M. Senkan and C. F. Melius, Aromatic and Polycyclic Aromatic Hydrocarbon Formation in a Laminar Premixed n-Butane Flame, *Combust. Flame* 114 (1998), 192-213.

[118] H. Richter, W. J. Grieco and J. B. Howard, Formation Mechanism of Polycyclic Aromatic Hydrocarbons and Fullerenes in Premixed Benzene Flames, *Combust. Flame* 119 (1999), 1-22.

[119] C. R. Shaddix, An Experimental Study of the High Temperature Oxidation of 1-Methylnapthalene, (Princeton University, USA, 1993).

[120] A. Ristori, P. Dagaut, A. E. Bakali, G. Pengloan and M. Cathonnet, Benzene Oxidation: Experimental Results in a JDR and Comprehensive Kinetic Modelling in JSR, Shock-Tube and Flame, *Combust. Sci. and Tech.* 167 (2001), 223-256.

[121] C. R. Shaddix, K. Brezinsky and I. Glassman, Oxidation of 1-Methylnaphthalene, *Twenty-Fourth Symposium (International) on Combustion, The Combustion Institute* (1) 24 (1992), 683-690.

[122] C. R. Shaddix, K. Brezinsky and I. Glassman, Analysis of Fuel Decay Routes in the High-Temperature Oxidation of 1-Methylnaphthalene, *Combust. Flame* (1-2) 108 (1997), 139-157.

[123] U. Pfahl, K. Fieweger and G. Adomeit, Self-Ignition of Diesel-Relevant Hydrocarbon-air Mixtures Under Engine Conditions, *Twenty-Sixth Symposium (International) on Combustion, The Combustion Institute* (1996), 781-789.

[124] K. Mati, A. Ristori, G. Pengloan and P. Dagaut, Oxidation of 1-Methylnaphthalene at 1–13 atm: Experimental Study in a JSR and Detailed Chemical Kinetic Modelling, *Combust. Sci. and Tech.* 179 (2007), 1261-1285.

[125] H. Pitsch, Detailed Kinetic Reaction Mechanism For Ignition and Oxidation of α-Methylnapthalene, *Twenty-Sixth Symposium (International) on Combustion, The Combustion Institute* (1996), 721-728.

[126] A. Laskin and A. Lifshitz, Thermal Decomposition of Indene. Experimental Results and Kinetic Modelling, *Twenty-Seventh Symposium (International) on Combustion,The Combustion Institute* (1998), 313-320.

[127] R. Atkinson, D. L. Baulch, R. A. Cox, R. F. Hampson, J. A. Kerr, M. J. Rossi and J. Troe, Evaluated Kinetic and Photochemical and Heterogeneous Data for Atmospheric Chemistry: Supplement V - IUPAC Subcommittee on Gas Kinetic Data Evaluation for Atmospheric Chemistry, *J. Phys. Chem. Ref. Data* (3) 26 (1997), 521.

[128] R. P. Lindstedt and G. Skevis, A Study of Acetylene Chemistry in Flames, *Combust. Sci. and Tech.* (1) 125 (1997), 73 - 137.

[129] A. J. Dean, D. F. Davidson and R. K. Hanson, A Shock Tube Study of Reactions of Carbon Atoms with Hydrogen and Oxygen Using Excimer Photolysis of $C_3O_2$ and Carbon Atom Atomic Resonance Absorption Spectroscopy, *J. Phys. Chem.* (1) 95 (1991), 183-191.

[130] M. W. Slack, Kinetics and Thermodynamics of the CN Molecule. III. Shock Tube Measurement of CN Dissociation Rates, *J. Chem. Phys.* (1) 64 (1976), 228.

[131] R. P. Lindstedt and G. Skevis, Molecular Growth and Oxygenated Species Formation in Laminar Flames, *Proc. Combust. Inst.* 28 (2000), 1801-1807.

[132] T. Bohland and F. Temps, Direct Determination of the Rate Constant for the Reaction $CH_2$ + H = CH + $H_2$, *Ber. Bunsenges. Phys. Chem.* 88 (1984), 459.

[133] J. Peeters, W. Boullart and K. Devriendt, CH(a4.SIGMA.- and/or X2.PI.) Formation in the Reaction Between Ketenyl Radicals and Oxygen Atoms. Determination of the CH-yield between 405 and 960 K, *J. Phys. Chem.* (11) 99 (1995), 3583-3591.

[134] C. Dombrowsky and H. G. Wagner, Investigation of the $CH_2$(T) + $O_2$ Reaction in Shock Waves, *Ber. Bunsenges. Phys. Chem.* 96 (1992), 1048.

[135] D. L. Baulch, C. J. Cobos, R. A. Cox, P. Frank, G. Hayman, T. Just, J. A. Kerr, T. Murrells, M. J. Pilling, J. Troe, R. W. Walker and J. Warnatz, Evaluated Kinetic Data for Combustion Modelling Supplement I, *J. Phys. Chem. Ref. Data* (6) 23 (1994), 847-1033.

[136] C.-L. Yu, C. Wang and M. Frenklach, Chemical Kinetics of Methyl Oxidation by Molecular Oxygen, *J. Phys. Chem.* 99 (1995), 14377-14387.

[137] R. l. Quiceno, J. PÈrez-RamÌrez, J. r. Warnatz and O. Deutschmann, Modeling the High-Temperature Catalytic Partial Oxidation of Methane over Platinum Gauze: Detailed Gas-Phase and Surface Chemistries Coupled with 3D Flow Field Simulations, *Appl. Catal. A-Gen* (2) 303 (2006), 166-176.

[138] M. J. Rabinowitz, J. W. Sutherland, P. M. Patterson and R. B. Klemm, Direct Rate Constant Measurements OF H + $CH_4$ = $CH_3$ + $H_2$ at 897-1729 K, Using the Flash Photolysis-Shock Tube Technique, *J. Phys. Chem.* (2) 95 (1991), 674-681.

[139] C. C. Hsu, A. M. Mebel and M. C. Lin, Ab Initio Molecular Orbital Study of the HCO+O Reaction: Direct versus Indirect Abstraction Channels, *J. Chem. Phys.* (6) 105 (1996), 2346-2352.

[140] Y. Hidaka, T. Oki, H. Kawano and T. Higashihara, Thermal Decomposition of Methanol in Shock Waves, *J. Phys. Chem.* (20) 93 (1989), 7134-7139.

[141] T. J. Held and F. L. Dryer, An Experimental and Computational Study of Methanol Oxidation in the Intermediate-and High-Temperature Regimes, *Twenty-Fifth Symposium (International) on Combustion* (1) 25 (1994), 901-908.

[142] W. Tsang and V. Mokrushin, Mechanism and Rate Constants for 1,3-Butadiene Decomposition, *Twenty-Eighth Symposium (International) on Combustion, The Combustion Institute* (2) 28 (2000), 1717-1723.

[143] I. A. B. Reid, C. Robinson and D. B. Smith, Spontaneous Ignition of Methane: Measurement and Chemical Model, *Twentieth Symposium (International) on Combustion, The Combustion Institute* (1) 20 (1985), 1833-1843.

[144] P. D. Lightfoot, R. A. Cox, J. N. Crowley, M. Destriau, G. D. Hayman, M. E. Jenkin, G. K. Moortgat and F. Zabel, Organic Peroxy Radicals: Kinetics, Spectroscopy and Tropospheric Chemistry, *Atmos. Environ. Part A* (10) 26 (1992), 1805-1961.

[145] W. Tsang and R. F. Hampson, Chemical Kinetic Data Base for Combustion Chemistry. Part I, Methane and Related Compounds, *J. Phys. Chem. Ref. Data* 15 (1986).

[146] A. R. Fairbairn, The Dissociation of Carbon Monoxide, *Proc. R. Soc. London A* 312 (1969), 207.

[147] S. L. Baughcum and R. C. Oldenborg, Measurement of the $C_2$(a3πu) and $C_2$(x1Σg+) Disappearence Rates with O2 from 298-1300K, *The Chemistry of Combustion, ACS Symp. Ser(Ed. T.M. Sloane)* 249 (1984), 257.

[148] A. Laskin and H. Wang, On Initiation Reactions of Acetylene Oxidation in Shock Tubes A Quantum Mechanical and Kinetic Modelling Study, *Chem. Phys. Lett.* 303 (1999), 43-49.

[149] B. Eiteneer and M. Frenklach, Experimental and Modeling Study of Shock-Tube Oxidation of Acetylene, *Int. J. Chem. Kinet.* (9) 35 (2003), 391-414.

[150] A. M. Dean and P. R. Westmoreland, Bimolecular QRRK Analysis of Methyl Radical Reactions, *Int. J. Chem. Kinet.* (3) 19 (1987), 207-228.

[151] S. G. Davis, C. K. Law and H. Wang, Propene Pyrolysis and Oxidation Kinetics in a Flow Reactor and Laminar Flames, *Combust. Flame* (375-399) 119 (1999), 375.

[152] H. Wang and M. Frenklach, Calculations of Rate Coefficients for the Chemically Activated Reactions of Acetylene with Vinylic and Aromatic Radicals, *J. Phys. Chem.* 98 (1994), 11465-11489.

[153] R. P. Duran, V. T. Amorebieta and A. J. Colussi, Is the Homogeneous Thermal Dimerization of Acetylene a Free-Radical Chain Reaction? Kinetic and Thermochemical Analysis, *J. Phys. Chem.* (3) 92 (1988), 636-640.

[154] V. D. Knyazev, A. Bencsura, S. I. Stoliarov and I. R. Slagle, Kinetics of the $C_2H_3 + H_2 = H + C_2H_4$ and $CH_3 + H_2 = H + CH_4$ Reactions, *J. Phys. Chem.* (27) 100 (1996), 11346-11354.

[155] T. B. Hunters, T. A. Litzinger, H. Wang and M. Frenklach, Ethane Oxidation at Elevated Pressures in the Intermediate Temperature Regime: Experiments and Modelling, *Combust. Flame* 104 (1996), 505-523.

[156] Y. Hidaka, T. Nishimori, K. Sato, Y. Henmi, R. Okuda and K. Inami, Shock-Tube and Modelling Study of Ethylene Pyrolysis and Oxidation, *Combust. Flame* 117 (1999), 755–776.

[157] M. Frenklach, H. Wang and M. J. Rabinowitz, Optimization and Analysis of Large Chemical Kinetic Mechanisms Using the Solution Mapping Method-Combustion of Methane, *Prog. Energy Combust. Sci.* (1) 18 (1992), 47-73.

[158] H.-H. Carstensen, C. V. Naik and A. M. Dean, Detailed Modelling of the Reaction of $C_2H_5 + O_2$, *J. Phys. Chem. A* 109 (2005), 2264-2281.

[159] E. V. Shafir, I. R. Slagle and V. D. Knyazev, Kinetics of the Self-Reaction of $C_2H_5$ Radicals, *J. Phys. Chem. A* (35) 107 (2003), 6804-6813.

[160] S. J. Klippenstein, J. A. Miller and L. B. Harding, Resolving the Mystery of Prompt $CO_2$: The HCCO + $O_2$ Reaction, *Proc. Combust. Inst* 29 (2002), 1209–1217.

[161] Y. Hidaka, K. Kimura and H. Kawano, High-Temperature Pyrolysis of Ketene in Shock Waves, *Combust. Flame* (1) 99 (1994), 18-28.

[162] J. Warnatz, *Combustion Chemistry*, (Springer-Verlag, 1984).

[163] C. E. Canosa-Mas, H. M. Frey and R. Walsh, Studies of Methylene Chemistry by Pulsed Laser-Induced Decomposition of ketene, *J. Chem. Soc. Faraday Trans 2* (561) 80 (1984).

[164] P. R. Westmoreland, A. M. Dean, J. B. Howard and J. P. Longwell, Forming Benzene in Flames by Chemically Activated Isomerization, *J. Phys. Chem.* (25) 93 (1989), 8171-8180.

[165] P. Dagaut, M. Cathonnet and J.-C. Boettner, A Kinetic Modeling Study of Propene Oxidation in JSR and Flame, *Combust. Sci. and Tech.* (4) 83 (1992), 167 - 185.

[166] C. Horn, K. Roy, P. Frank and T. Just, Shock-Tube Study on the High Temperature Pyrolysis of Phenol, *Twenty-Seventh Symposium (International) on Combustion,The Combustion Institute* (1998), 321-328.

[167] W. Tsang, Chemical Kinetic Data Base for Combustion Chemistry Part V. Propene, *J. Phys. Chem. Ref. Data* (2) 20 (1991), 221-273.

[168] P. Dagaut and M. Cathonnet, Isobutene Oxidation and Ignition: Experimental and Detailed Kinetic Modeling Study, *Combust. Sci. and Tech.* (1) 137 (1988), 237 - 275.

[169] W. J. Pitz, C. K. Westbrook, W. M. Proscia and F. L. Dryer, A comprehensive Chemical Kinetic Reaction Mechanism for the Oxidation of n-Butane, *Twentieth Symposium (International) on Combustion, The Combustion Institute* (1) 20 (1985), 831-843.

[170] Y. Hidaka, T. Nakamura, H. Tanaka, A. Jinno and H. Kawano, Shock Tube and Modelling Study of Propene Pyrolysis, *Int. J. Chem. Kinet.* (9) 24 (1992), 761-780.

[171] R. D. Wilk, N. P. Cernansky, W. J. Pitz and C. K. Westbrook, Propene Oxidation at Low and Intermediate Temperatures: A Detailed Chemical Kinetic Study, *Combust. Flame* (2) 77 (1989), 145-170.

[172] A. Bencsura, V. D. Knyazev, S.-B. Xing, I. R. Slagle and D. Gutman, Kinetics of the Thermal Decomposition of theN-Propyl Radical, *Twenty-Fourth Symposium (International) on Combustion, The Combustion Institute* (1) 24 (1992), 629-635.

[173] D. L. Baulch, C. J. Cobos, R. A. Cox, P. Frank, G. Hayman, T. Just, J. A. Kerr, T. Murrells, M. J. Pilling, J. Troe, R. W. Walker and J. Warnatz, Summary Table of Evaluated Kinetic Data for Combustion Modeling: Supplement 1, *Combust. Flame* (1-2) 98 (1994), 59-79.

[174] S. W. Benson, The Kinetics and Thermochemistry of Chemical Oxidation with Application to Combustion and Flames, *Prog. Energy Combust. Sci.* (2) 7 (1981), 125-134.

[175] R. D. Wilk, N. P. Cernansky and R. S. Cohen, The Oxidation of Propane at Low and Transition Temperatures, *Combust. Sci. and Tech.* 49 (1986), 41-78.

[176] K. H. Homann, Reaktionen des Butadiins ii. Die Reaction mit Sauerstoffatomen., *Ber. Bunsenges. Phys. Chem.* 79 (1975), 536.

[177] A. Laskin, H. Wang and C. K. Law, Detailed Kinetic Modeling of 1,3-Butadiene Oxidation at High Temperatures, *Int. J. Chem. Kinet.* (10) 32 (2000), 589-614.

[178] R. D. Kern, H. J. Singh and C. H. Wu, Thermal Decomposition of 1,2 Butadiene, *Int. J. Chem. Kinet.* (9) 20 (1988), 731-747.

[179] J. A. Cole, J. D. Bittner, J. P. Longwell and J. B. Howard, Formation Mechanisms of Aromatic Compounds in Aliphatic Flames, *Combust. Flame* (1) 56 (1984), 51-70.

[180] Y. Hidaka, T. Higashihara, N. Ninomiya, H. Oshita and H. Kawano, Thermal Isomerization and Decomposition of 2-Butyne in Shock Waves, *J. Phys. Chem.* (42) 97 (1993), 10977-10983.

[181] P. Dagaut and M. Cathonnet, The Oxidation of 1,3-Butadiene: Experimental Results and Kinetic Modeling, *Combust. Sci. and Tech.* (1) 140 (1998), 225 - 257.

[182] A. Chakir, M. Cathonnet, J. C. Boettner and F. Gaillard, Kinetic Study of N-Butane oxidation, *Combust. Sci. and Tech.* (4) 65 (1989), 207 - 230.

[183] W. Tsang, Pyrolysis of 2,4-Dimethylhexene-l and the Stability of Isobutenyl Radicals, *Int. J. Chem. Kinet.* (6) 5 (1973), 929-946.

[184] J. Gang, M. J. Pilling and S. H. Robertson, Asymmetric Internal Rotation: Application to the 2-$C_4H_9CH_3$+$C_3H_6$ Reaction, *J. Chem. Soc. Faraday Trans.* 93 (1997), 1481-1491.

[185] R. R. Baker, R. R. Baldwin, A. R. Fuller and R. W. Walker, Addition of n-$C_4H_{10}$ and $C_4H_8$ to Slowly Reacting Mixtures of Hydrogen and Oxygen at 480°C, *Faraday Discuss.* 71 (1975), 736-755.

[186] J. A. Kerr and A. F. Trotman-Dickenson, The Reactions of Alkyl Radicals. Part III. n-Butyl Radicals from the Photolysis of n-Valeraldehyde, *J. Chem. Soc.* (1960).

[187] W. Tsang, Chemical Kinetic Data Base for Combustion Chemistry Part 4. Isobutane, *J. Phys. Chem. Ref. Data* (1) 19 (1990), 1-68.

[188] W. J. Pitz and C. K. Westbrook, Chemical Kinetics of the High Pressure Oxidation of n-Butane and its Relation to Engine Knock, *Combust. Flame* (1-2) 63 (1986), 113-133.

[189] S. Kojima, Detailed Modeling of n-Butane Autoignition Chemistry, *Combust. Flame* (1) 99 (1994), 87-136.

[190] A. C. Lloyd, Evaluated and Estimated Kinetic Data for Phase Reactions of the Hydroperoxyl Radical, *Int. J. Chem. Kinet.* (2) 6 (1974), 169-228.

[191] M. U. Alzueta, P. Glarborg and K. Dam-Johansen, Experimental and Kinetic Modelling Study of the Oxidation of Benzene, *Int. J. Chem. Kinet.* (8) 32 (2000), 498-522.

[192] J. S. Gaffney, R. Atkinson and J. N. Pitts, Temperature Dependence of the Relative Rate Constants for the Reaction of O(3P) Atoms with Selected Olefins, Monoterpenes and Unsaturated Aldehydes, *J. Am. Chem. Soc.* 97 (1975), 6481.

[193] A. Fahr and S. E. Stein, Reactions of Vinyl and Phenyl Radicals with Ethyne, Ethene and Benzene *Twenty-Second Symposium (International) on Combustion, The Combustion Institute* 22 (1989), 1023.

[194] E. Ikeda, R. S. Tranter, J. H. Kiefer, R. D. Kern, H. J. Singh and Q. Zhang, The Pyrolysis of Methylcyclopentadiene: Isomerization and Formation of Aromatics, *Proc. Combust. Inst* 28 (2000), 1725-1732.

[195] H. Richter and J. B. Howard, Formation and Consumption of Single-Ring Aromatic Hydrocarbons and Their Precursors in Premixed Acetylene, Ethylene and Benzene Flames, *Phys. Chem. Chem. Phys.* 4 (2002), 2038-2055.

[196] M. Braun-Unkhoff, P. Frank and T. Just, High Temperature Reactions of Benzyl Radicals, *Ber. Bunsenges. Phys. Chem.* 94 (1990), 1417.

[197] H. Hippler, C. Reihs and J. Troe, Shock Tube UV Absorption Study of the Oxidation of Benzyl Radicals, *Twenty-Third Symposium (International) on Combustion, The Combustion Institute* (1) 23 (1991), 37-43.

[198] A. Fahr and S. E. Stein, Gas-Phase Reactions of Phenyl Radicals with Aromatic Molecules, *J. Phys. Chem.* (17) 92 (1988), 4951-4955.

[199] M. A. Grela and A. J. Colussi, Kinetics and Mechanism of the Thermal Decomposition of Unsaturated Aldehydes: Benzaldehyde, 2-Butenal, and 2-Furaldehyde, *J. Phys. Chem.* (3) 90 (1986), 434-437.

[200] Y. Z. He, W. G. Mallard and W. Tsang, Kinetics of Hydrogen and Hydroxyl Radical Attack on Phenol at High Temperatures, *J. Phys. Chem.* 92 (1988), 2196-2201.

[201] R. K. Solly and S. W. Benson, Kinetics of the Gas-Phase Unimolecular Decomposition of the Benzoyl Radical, *J. Am. Chem. Soc.* (9) 93 (1971), 2127-2131.

[202] R. Buth, K. Hoyermann and G. Rohde, Mechanisms and Rates of Benzoyl Reactions: The Reactions $C_6H_5CHO+Cl$, $C_6H_5CO+O$ and $C_6H_5CO+H$, *Twenty-Fourth Symposium (International) on Combustion, The Combustion Institute* (1) 24 (1992), 669-674.

[203] I. W. C. E. Arends, R. Louw and P. Mulder, Kinetic Study of the Thermolysis of Anisole in a Hydrogen Atmosphere, *J. Phys. Chem.* 97 (1993), 7914-7925.

[204] M. Koch, F. Temps and A. F. Wagner, Kinetics of the Reactions of $CH_2$(a-1A1) with $CH_3C_2H$, HCN, $CO_2$, $N_2O$ and COS, *Ber. Bunsenges. Phys. Chem.* 94 (1990), 645.

[205] R. A. Perry, R. Atkinson and J. N. Pitts, Kinetics and Mechanism of the Gas Phase Reaction of Hydroxyl Radicals with Methoxybenzene and o-Cresol over the Temperature Range 299-435 K, *J. Phys. Chem.* (17) 81 (1977), 1607-1611.

[206] M. F. R. Mulcahy, B. G. Tucker, D. J. Williams and J. R. Wilmshurst, Reactions of Free Radicals with Aromatic Compounds in the Gaseous Phase, *Aust. J. Chem.* 20 (1967), 1155-1171.

[207] M. Eichholtz, A. Schneider, D. V. Stucken, J. T. Vollmer and H. G. Wagner, The Reactions of Phenylacetylene With O(3) in the Gas Phase, *Twenty-Fifth Symposium (International) on Combustion,The Combustion Institute* (1994), 859.

[208] C. K. Westbrook, J. r. Warnatz and W. J. Pitz, A Detailed Chemical Kinetic Reaction Mechanism for the Oxidation of Iso-Octane and n-Heptane over an Extended Temperature Range and its Application to Analysis of Engine Knock, *Twenty-Second Symposium (International) on Combustion, The Combustion Institute* (1) 22 (1989), 893-901.

[209] W. Tsang, Thermal Decomposition of Cyclopentane and Related Compounds, *Int. J. Chem. Kinet.* (6) 10 (1978), 599-617.

[210] A. Chakir, M. Bellimam, J. C. Boettner and M. Cathonnet, Kinetic Study of n-Heptane Oxidation, *Int. J. Chem. Kinet.* (4) 24 (1992), 385-410.

[211] W. Tsang and J. A. Walker, Hydrogen-Atom Attack on 1-Phenylpropene at High Temperatures, *Twenty-Fifth Symposium (International) on Combustion, The Combustion Institute* (1) 25 (1994), 867-874.

[212] N. Cohen, Are Reaction Rate Coefficients Additive? Revised Transition State Theory Calculations for OH + Alkane Reactions, *Int. J. Chem. Kinet.* (5) 23 (1991), 397-417.

[213] L. V. Gurvich, I. V. Veyts and C. B. Alcock, Thermodynamic Properties of Individual Substances, In *4th Ed.*, (Begel House, New York, 1996).

[214] R. O. Foelsche, J. M. Keen and W. C. Solomon, A Non-Equilibrium Computational Method for Predicting Fuel Rich Gas Generator Performance and Exhaust Properties Volume II: Reaction Kinetics and Computational Results, (University of Illinois, 1993).

[215] A. Burcat and B. J. McBride, Ideal Gas Thermodynamic Data for Combustion and Air Pollution Use, (TAE697, 1994).

[216] A. Burcat, R. C. Farmer, R. L. Espinoza and R. A. Matula, Comparative Ignition Delay Times For Selected Ring-Structured Hydrocarbons, *Combust. Flame* 36 (1979), 313-316.

[217] B. R. Stanmore, J. F. Brilhac and P. Gilot, The Oxidation of Soot: A Review of Experiments, Mechanisms and Models, *Carbon* (15) 39 (2001), 2247-2268.

# Appendix A

## 3.3 Reaction Mechanisms

The detailed chemical reaction mechanism that was developed and utilized in the present work is shown in Table A.1. Reaction rates are expressed in the form:

$$k = AT^n \exp(-E_a / RT) \qquad \text{(A.1)}$$

where A = frequency factor, $(\text{kmol/m}^3)^{(1-m)}/\text{s}$, m is the order of the reaction

n = temperature dependence exponent

$E_\alpha$ = activation energy, kJ/mole

R = ideal gas constant, 8.314 kJ/K/kmol

T = temperature, K

Unimolecular and recombination reactions generally exhibit complex pressure dependence. Troe [12] proposed a generalised expression for the fall-off behaviour of such reactions:

$$k = \frac{k_o k_\infty [M]}{k_o [M] + k_\infty} F \qquad \text{(A.2)}$$

where $k_\infty$ is the high pressure limit rate constant, $k_o$ is the low pressure limit, [M] is the concentration of the third body collision partner and F is the broadening factor which is defined as :

$$\log F = \frac{\log F_c}{1 + \left\{\log\left(k_o [M] / k_\infty\right) / N\right\}^2} \qquad \text{(A.3)}$$

where $N = 0.75 - 1.27 \log F_c$ (A.4)

and Fc is a temperature dependent parameter specifically defined for a particular reaction. The reaction mechanism follows.

**TABLE A.1**
**Rate parametyers for elementary reactions discussed in the current report**
**(units are kmol, $m^3$, s, K and kJ/mol)**

| No | Reaction | A | n | Ea | Ref |
|---|---|---|---|---|---|
| 1 | $C_5H_5 + CH_3 = C_5H_4CH_3 + H$ | 2.0000E+10 | 0.00 | 26.00 | [46] |
| 2 | $C_5H_5 + C_2H_2 = C_7H_7$ | 3.7200E+08 | 0.00 | 34.72 | [81] |
| 3 | $C_5H_5 = C_3H_3 + C_2H_2$ | 3.1500E+13 | 0.075 | 260.66 | Adj.[36] |
| 4 | $C_5H_5 + O = C_4H_5(T) + CO$ | 2.1260E+53 | -12.56 | 89.96 | [15] |
| 5 | $C_5H_5 + HO_2 = C_5H_5O + OH$ | 6.2480E+62 | -16.16 | 82.82 | [15] |
| 6 | $C_5H_5 + C_5H_5 = C_{10}H_9F + H$ | 2.0000E+10 | 0.00 | 34.00 | [45] |
| 7 | $C_5H_5 + HO_2 = C_5H_4O + H_2O$ | 6.2480E+62 | -16.16 | 82.82 | [15] |
| 8 | $C_5H_5 = C_5H_5(L)$ | 1.0740E+38 | -7.49 | 307.55 | [15] |
| 9 | $C_5H_6 + H = C_5H_5 + H_2$ | 3.4970E+04 | 18.56 | 18.74 | [15] |
| 10 | $C_5H_6 + O = C_5H_5 + OH$ | 1.8100E+10 | 0.00 | 12.87 | [58] |
| 11 | $C_5H_6 + OH = C_5H_5 + H_2O$ | 1.1430E+06 | 1.18 | -1.87 | [57] |
| 12 | $C_5H_6 + C_5H_5 = C_9H_8 + CH_3$ | 3.0000E+13 | 0.00 | 177.10 | [25] |
| 13 | $C_5H_6 = C_5H_5 + H$ [15] | 1.0000E+19 | -0.65 | 368.19 | [36] |
| 14 | $C_5H_7 = C_5H_6 + H$ | 3.1600E+15 | 0.00 | 185.40 | [46] |
| 15 | $C_5H_4O = C_4H_4 + CO$ | 2.5000E+11 | 0.00 | 221.90 | Adj. [120] |
| 16 | $C_6H_5 + C_2H_4 = C_8H_8 + H$ | 2.5100E+09 | 0.00 | 25.93 | [193] |
| 17 | $C_6H_5 + H = C_6H_4 + H_2$ | 1.5000E+11 | 0.00 | 0.00 | [58] |
| 18 | $C_6H_5 + H = C_6H_6$ | 7.8300E+10 | 0.00 | 0.00 | [91] |
| 19 | $C_6H_5 + O_2 = C_6H_5O + O$ | 2.6000E+10 | 0.00 | 25.61 | [95] |
| 20 | $C_6H_5 + O_2 = C_6H_5OO$ | 3.0800E+09 | -0.15 | 0.66 | [60] |
| 21 | $C_6H_6 + C_2H_3 = C_8H_8 + H$ | 7.4900E+08 | 0.00 | 26.77 | [45] |
| 22 | $C_6H_6 + H = C_6H_5 + H_2$ | 2.5000E+11 | 0.00 | 66.94 | [58] |
| 23 | $C_6H_6 + O = C_6H_5O + H$ | 2.4000E+10 | 0.00 | 19.53 | [81] |
| 24 | $C_6H_6 + O = C_6H_5 + OH$ | 2.0000E+10 | 0.00 | 61.52 | [58] |
| 25 | $C_6H_6 + OH = C_6H_5 + H_2O$ | 1.6300E+05 | 1.42 | 6.10 | [58] |
| 26 | $C_6H_6(F) + M = C_6H_6 + M$ | 3.0000E+09 | 0.500 | 8.37 | [63] |
| 27 | $C_5H_4CH_3 = C_6H_6(F) + H$ | 1.0000E+14 | 0.00 | 217.00 | [46] |
| 28 | $C_6H_5O = C_5H_5 + CO$ | 4.5000E+11 | 0.00 | 126.68 | [58] |
| 29 | $C_6H_5O + H = C_6H_5OH$ | 2.5000E+11 | 0.00 | 0.00 | [81] |
| 30 | $C_6H_4O_2 + O = C_6H_3O_2 + OH$ | 1.4000E+10 | 0.00 | 61.55 | [81] |
| 31 | $C_6H_5OO = C_6H_5O + O$ | 4.2700E+15 | -0.70 | 138.27 | [81] |

| No | Reaction | A | n | Ea | Ref |
|---|---|---|---|---|---|
| 32 | $C_6H_5OO = C_6H_4O_2 + H$ | 4.0000E+08 | 0.00 | 0.00 | [81] |
| 33 | $C_7H_7 + O = C_7H_6O + H$ | 3.5000E+10 | 0.00 | 0.00 | [197] |
| 34 | $C_7H_7 + C_2H_2 = C_9H_8 + H$ | 1.0000E+09 | 0.00 | 20.92 | [59] |
| 35 | $C_7H_7 + O_2 = C_7H_7O + O$ | 8.6400E+10 | 0.00 | 131.36 | [60] |
| 36 | $C_7H_7 + O_2 = C_7H_7OO$ [6] | $k_\infty =$<br>$k_0 =$ | 1.3400E+06<br>5.3100E+19 | 1.10<br>-3.30 | 0.00<br>0.00 | [60] |
| 37 | $C_7H_7 = C_7H_6 + H$ | 8.2000E+14 | 0.00 | 337.52 | [80] |
| 38 | $C_7H_8 = C_7H_7 + H$ | 2.0900E+15 | 0.00 | 366.14 | [80] |
| 39 | $C_7H_8 = C_6H_5 + CH_3$ | 2.6600E+16 | 0.00 | 409.52 | [80] |
| 40 | $C_7H_8 + H = C_7H_7 + H_2$ | 1.2600E+12 | 0.00 | 61.99 | [80] |
| 41 | $C_7H_8 + H = C_6H_6 + CH_3$ | 5.7800E+10 | 0.00 | 33.84 | [80] |
| 42 | $C_7H_8 + H = C_7H_7P + H_2$ | 2.5000E+11 | 0.00 | 66.94 | [57] |
| 43 | $C_7H_8 + OH = C_7H_7 + H_2O$ | 5.1900E+06 | 1.00 | 3.65 | [91] |
| 44 | $C_7H_8 + CH_3 = CH_4 + C_7H_7$ | 3.1600E+09 | 0.00 | 0.00 | [80] |
| 45 | $C_7H_8 + O = OC_7H_7 + H$ | 3.1000E+10 | 0.00 | 16.62 | [109] |
| 46 | $C_7H_8 + O = C_7H_7 + OH$ | 6.3000E+08 | 0.00 | 0.00 | [109] |
| 47 | $C_7H_6O + O = C_6H_6 + CO_2$ | 2.0000E+10 | 0.00 | 0.00 | [60] |
| 48 | $C_7H_7OH + C_6H_5 = C_7H_6O + C_6H_6 + H$ | 1.4000E+09 | 0.00 | 18.41 | [39] |
| 49 | $C_7H_7OO = C_7H_6O + OH$ | 1.0000E+10 | 0.00 | 121.00 | [103] |
| 50 | $C_7H_7OO = C_7H_7O + O$ | 7.8300E+16 | 0.00 | 244.78 | Est.(31) |
| 51 | $C_8H_6 + O = C_6H_5C_2O + H$ | 2.1900E+03 | 2.09 | 6.53 | [60] |
| 52 | $C_8H_6 + OH = C_8H_5 + H_2O$ | 2.1000E+10 | 0.00 | 19.10 | [61] |
| 53 | $C_8H_6 + O = C_8H_5O + H$ | 2.4000E+10 | 0.00 | 19.53 | [60] |
| 54 | $C_8H_6 + O = C_6H_5 + C_2HO$ | 6.5100E+03 | 2.09 | 6.54 | [45] |
| 55 | $C_8H_6 + O = C_6H_5O + C_2H$ | 2.2000E+10 | 0.00 | 18.95 | est. |
| 56 | $C_8H_7 + OH = C_6H_5 + CH_3CO$ | 3.0000E+10 | 0.00 | 0.00 | [103] |
| 57 | $C_8H_7 + O = C_6H_5 + C_2H_2O$ | 3.0000E+10 | 0.00 | 0.00 | [103] |
| 58 | $C_8H_7 = C_8H_6 + H$ | 1.3000E+41 | -8.65 | 46.10 | [110] |
| 59 | $C_8H_8 + OH = C_8H_7(P) + H_2O$ | 2.1000E+10 | 0.00 | 19.10 | [103] |
| 60 | $C_8H_8 + OH = C_7H_7 + CH_2O$ | 3.0000E+10 | 0.00 | 0.00 | [103] |
| 61 | $C_8H_8 + O = C_7H_7 + CHO$ | 4.2020E+03 | 1.88 | 0.76 | [57] |
| 62 | $C_8H_8 + O = C_6H_5 + CH_3CO$ | 2.5000E+03 | 1.88 | 0.76 | [60] |
| 63 | $C_8H_{10} + H = C_8H_9 + H_2$ | 1.2600E-01 | 3.44 | 13.05 | [103] |
| 64 | $C_8H_{10} + H = C_6H_6 + C_2H_5$ | 1.2000E+10 | 0.00 | 21.33 | [107] |
| 65 | $C_9H_7 + H = C_9H_8$ | 2.0000E+11 | 0.00 | 0.00 | [60] |
| 66 | $C_9H_7 + O = C_8H_7(P) + CO$ | 4.5000E+10 | 0.00 | 0.00 | [60] |

| No | Reaction | A | n | Ea | Ref |
|---|---|---|---|---|---|
| 67 | $C_9H_7 + O = C_8H_7 + CO$ | 1.0000E+11 | 0.00 | 0.00 | [103] |
| 68 | $C_9H_7 + HO_2 = C_9H_7O + OH$ | 8.5770E+65 | -16.69 | 101.78 | [54] |
| 69 | $C_9H_7 + HO_2 = C_9H_6O + H_2O$ | 1.9600E+30 | -6.14 | 228.50 | [54] |
| 70 | $C_9H_7 + O_2 = C_7H_7 + CO + CO$ | 1.7420E+09 | 0.31 | 123.10 | [54] |
| 71 | $C_9H_7 + O_2 = C_6H_5O + C_3H_2O$ | 1.8760E+10 | -0.05 | 124.68 | [54] |
| 72 | $C_9H_7 + O_2 = C_7H_6O + C_2HO$ | 1.7420E+09 | 0.31 | 123.10 | [54] |
| 73 | $C_9H_8 + H = C_9H_7 + H_2$ | 2.1120E+10 | 0.00 | 9.45 | [60] |
| 74 | $C_9H_8 + OH = C_9H_7 + H_2O$ | 8.6230E+05 | 1.18 | -1.87 | [60] |
| 75 | $C_9H_7O = C_8H_7 + CO$ | 2.0000E+14 | 0.00 | 155.00 | [125] |
| 76 | $C_{10}H_7 + O_2 = C_{10}H_7O + O$ | 2.1500E+10 | 0.00 | 25.61 | [60] |
| 77 | $C_{10}H_8 + O = C_{10}H_7O + H$ | 2.5000E+10 | 0.00 | 19.54 | [60] |
| 78 | $C_{10}H_8 + OH = C_{10}H_7 + H_2O$ | 1.7000E+05 | 1.42 | 6.07 | [60] |
| 79 | $C_{10}H_9F = C_{10}H_8 + H$ | 3.0000E+13 | 0.00 | 197.00 | [103] |
| 80 | $C_{10}H_7O = C_9H_7 + CO$ | 1.8000E+11 | 0.00 | 183.68 | [60] |
| 81 | $C_{11}H_9 = C_9H_7 + C_2H_2$ | 8.0000E+09 | 0.00 | 186.60 | Adj.[77] |
| 82 | $C_{11}H_9P + O_2 = OC_{11}H_9 + O$ | 1.9575E+10 | 0.00 | 25.61 | [60] |
| 83 | $C_{11}H_{10} + OH = C_{11}H_9P + H_2O$ | 1.7000E+05 | 1.42 | 6.07 | [60] |
| 84 | $C_{11}H_{10} = C_{11}H_9 + H$ | 4.4800E+15 | 0.00 | 381.30 | [60] |
| 85 | $C_{11}H_{10} + O_2 = C_{11}H_9 + HO_2$ | 1.2670E+09 | 0.00 | 166.28 | [60] |
| 86 | $C_{11}H_{10} + OH = C_{11}H_9 + H_2O$ | 4.1520E+06 | 1.00 | 3.66 | [60] |
| 87 | $C_{11}H_{10} + OH = HOC_{11}H_9 + H$ | 1.8320E+09 | 0.00 | -1.49 | [60] |
| 88 | $C_{11}H_{10} + O = C_{11}H_9O + H$ | 1.2420E+10 | 0.00 | 16.62 | [60] |
| 89 | $C_{11}H_{10} + O = OC_{11}H_9 + H$ | 2.4000E+10 | 0.00 | 16.54 | [60] |
| 90 | $C_{11}H_8O + O = C_{10}H_8 + CO_2$ | 1.6000E+10 | 0.00 | 0.00 | [60] |
| 91 | $C_{11}H_9O = C_{10}H_8 + CHO$ | 4.0000E+12 | 0.00 | 79.00 | [60] |
| 92 | $OC_{11}H_9 + H = HOC_{11}H_9$ | 2.0000E+11 | 0.00 | 0.00 | [60] |

**TABLE A.2**
**Sub-mechanism for n-propyl benzene oxidation**
**(units are kmol, $m^3$, s, K and kJ/mol)**

| No | Reaction | A | n | Ea | Ref |
|---|---|---|---|---|---|
| 93 | $^1C_9H_{10}$ + H = $C_6H_5$ + $C_3H_6$ | 1.0000E+10 | 0.00 | 44.57 | [211] |
| 94 | $^1C_9H_{10}$ + H = $C_8H_8$ + $CH_3$ | 3.9800E+10 | 0.00 | 9.97 | [211] |
| 95 | $^1C_9H_{10}$ + H = $C_6H_6$ + $C_3H_5$(S) | 1.5848E+11 | 0.00 | 52.35 | [211] |
| 96 | $^1C_9H_{10}$ + H = $C_9H_9$(T) + $H_2$ | 1.5848E+11 | 0.00 | 46.53 | [211] |
| 97 | $^1C_9H_{10}$ + O = $C_7H_6O$ + $C_2H_4$ | 5.2300E+04 | 1.57 | -2.63 | [60] |
| 98 | $^1C_9H_{10}$ + $O_2$ = $C_9H_9$(T) + $HO_2$ | 2.0000E+10 | 0.00 | 184.10 | [60] |
| 99 | $^1C_9H_{10}$ + $O_2$ = $C_7H_6O$ + $CH_3CHO$ | 1.0000E+10 | 0.00 | 0.00 | [60] |
| 100 | $^1C_9H_{10}$ + $HO_2$ = $C_7H_6O$ + $C_2H_4$ + OH | 1.0000E+09 | 0.00 | 0.00 | [60] |
| 101 | $^1C_9H_{10}$ + OH = $C_7H_6O$ + $C_2H_5$ | 1.0000E+10 | 0.00 | 0.00 | [60] |
| 102 | $^2C_9H_{10}$ + H = $^3C_9H_{11}$ | 7.2300E+09 | 0.00 | 12.14 | [60] |
| 103 | $^2C_9H_{10}$ + H = $C_6H_5$ + $C_3H_6$ | 1.0000E+11 | 0.00 | 44.57 | [60] |
| 104 | $^2C_9H_{10}$ + H = $C_7H_7$ + $C_2H_4$ | 2.6000E+05 | 1.50 | 8.36 | Present Work |
| 105 | $^2C_9H_{10}$ + H = $C_6H_6$ + $C_3H_5$(S) | 1.5848E+11 | 0.00 | 52.35 | [60] |
| 106 | $^2C_9H_{10}$ + O = $C_8H_8$ + $CH_2O$ | 5.2300E+04 | 1.57 | 2.63 | [60] |
| 107 | $^1C_9H_{11}$ = $^1C_9H_{10}$ + H | 6.3000E+13 | 0.00 | 154.39 | [60] |
| 108 | $^1C_9H_{11}$ = $C_7H_7$ + $C_2H_4$ | 2.0000E+10 | 0.00 | 123.50 | [60] |
| 109 | $^2C_9H_{11}$ = $^2C_9H_{10}$ + H | 3.1500E+13 | 0.00 | 154.39 | [60] |
| 110 | $^2C_9H_{11}$ = $C_8H_8$ + $CH_3$ | 2.0000E+10 | 0.00 | 123.43 | [60] |
| 111 | $^2C_9H_{11}$ = $^1C_9H_{10}$ + H | 3.1500E+13 | 0.00 | 154.39 | [60] |
| 112 | $^2C_9H_{11}$ = $C_6H_6$ + $C_3H_5$(S) | 4.0000E+13 | 0.00 | 197.75 | [60] |
| 113 | $^2C_9H_{11}$ = $C_6H_6$ + $C_3H_5$(A) | 0.00 | 0.00 | 0.00 | [60] |
| 114 | $^3C_9H_{11}$ + $HO_2$ = $C_8H_{10}$ + CHO + OH | 2.5000E+09 | 0.00 | 0.00 | [60] |
| 115 | $^3C_9H_{11}$ + $HO_2$ = $C_8H_9$ + $CH_2O$ + OH | 2.5000E+09 | 0.00 | 0.00 | [60] |
| 116 | $^3C_9H_{11}$ = $C_8H_8$ + $CH_3$ | 2.0000E+13 | 0.00 | 113.10 | [60] |
| 117 | $^1C_9H_{11}$ = $C_8H_8$ + $CH_3$ | 1.0000E+14 | 0.00 | 145.81 | [96] |
| 118 | $^1C_9H_{11}$ + O = $C_7H_6O$ + $C_2H_5$ | 1.6000E+10 | 0.00 | 0.00 | [96] |
| 119 | $^1C_9H_{11}$ + OH = $C_7H_6O$ + $C_2H_6$ | 1.6000E+10 | 0.00 | 0.00 | [96] |
| 120 | $^2C_9H_{11}$ + OH = $C_7H_8$ + $CH_3CHO$ | 2.0000E+10 | 0.00 | 16.73 | [96] |
| 121 | $^2C_9H_{11}$ = $C_6H_5$ + $C_3H_6$ | 1.0000E+14 | 0.00 | 145.60 | [96] |
| 122 | $^3C_9H_{11}$ = $C_7H_7$ + $C_2H_4$ | 1.2300E+13 | -0.10 | 126.37 | Present Work |
| 123 | $C_9H_{12}$ + H = $^1C_9H_{11}$ + $H_2$ | 1.0100E+01 | 2.90 | 8.07 | [96] |
| 124 | $C_9H_{12}$ + O = $^1C_9H_{11}$ + OH | 4.7700E+01 | 2.70 | 4.62 | Adj.[104] |

| No | Reaction | A | n | Ea | Ref |
|---|---|---|---|---|---|
| 125 | $C_9H_{12}$ + OH = $^1C_9H_{11}$ + $H_2O$ | 7.0800E+03 | 1.90 | -4.84 | [96] |
| 126 | $C_9H_{12}$ + H = $^2C_9H_{11}$ + $H_2$ | 1.0100E+01 | 2.90 | 12.26 | [96] |
| 127 | $C_9H_{12}$ + O = $^2C_9H_{11}$ + OH | 4.7700E+01 | 2.70 | 8.81 | Adj.[104] |
| 128 | $C_9H_{12}$ + OH = $^2C_9H_{11}$ + $H_2O$ | 4.7865E+03 | 1.40 | 3.56 | [60] |
| 129 | $C_9H_{12}$ + H = $^3C_9H_{11}$ + $H_2$ | 1.3300E+03 | 2.50 | 28.26 | [96] |
| 130 | $C_9H_{12}$ + O = $^3C_9H_{11}$ + OH | 1.9300E+02 | 2.70 | 15.54 | [96] |
| 131 | $C_9H_{12}$ + OH = $^3C_9H_{11}$ + $H_2O$ | 3.1600E+04 | 1.80 | 3.90 | Adj.[212] |
| 132 | $C_9H_{12}$ + $HO_2$ = $^1C_9H_{11}$ + $H_2O_2$ | 9.6400E+00 | 2.60 | 54.01 | [96] |
| 133 | $C_9H_{12}$ + $CH_3$ = $^1C_9H_{11}$ + $CH_4$ | 1.5000E-03 | 3.46 | 22.90 | Adj.[104] |
| 134 | $C_9H_{12}$ + $HO_2$ = $^2C_9H_{11}$ + $H_2O_2$ | 9.6400E+00 | 2.60 | 58.20 | Adj.[104] |
| 135 | $C_9H_{12}$ + $HO_2$ = $^3C_9H_{11}$ + $H_2O_2$ | 4.7600E+01 | 2.50 | 69.01 | Adj.[104] |
| 136 | $C_9H_{12}$ + $CH_3$ = $^3C_9H_{11}$ + $CH_4$ | 9.0300E-04 | 3.65 | 29.90 | Adj.[104] |
| 137 | $C_9H_{12}$ + $CH_3$ = $^2C_9H_{11}$ + $CH_4$ | 1.5055E-03 | 3.46 | 22.90 | Adj.[104] |
| 138 | $C_9H_{12}$ + $C_2H_5$ = $^1C_9H_{11}$ + $C_2H_6$ | 1.2100E-03 | 3.46 | 31.26 | Adj.[104] |
| 139 | $C_9H_{12}$ + $C_2H_5$ = $^2C_9H_{11}$ + $C_2H_6$ | 1.2100E-03 | 3.46 | 31.26 | Adj.[104] |
| 140 | $C_9H_{12}$ + $C_2H_5$ = $^3C_9H_{11}$ + $C_2H_6$ | 9.0400E-04 | 3.65 | 38.24 | Adj.[104] |
| 141 | $C_9H_{12}$ + $C_2H_3$ = $^1C_9H_{11}$ + $C_2H_4$ | 1.0000E+00 | 3.10 | 36.94 | Adj.[104] |
| 142 | $C_9H_{12}$ + $C_2H_3$ = $^2C_9H_{11}$ + $C_2H_4$ | 1.0000E+00 | 3.10 | 36.94 | Adj.[104] |
| 143 | $C_9H_{12}$ + $C_2H_3$ = $^3C_9H_{11}$ + $C_2H_4$ | 6.0000E-01 | 3.30 | 43.94 | Adj.[104] |
| 144 | $C_9H_{12}$ + $C_3H_5$(A) = $^1C_9H_{11}$ + $C_3H_6$ | 7.9400E+08 | 0.00 | 67.82 | [96] |
| 145 | $C_9H_{12}$ + $C_3H_5$(A) = $^2C_9H_{11}$ + $C_3H_6$ | 7.9400E+08 | 0.00 | 67.78 | [96] |
| 146 | $C_9H_{12}$ + $C_3H_5$(A) = $^3C_9H_{11}$ + $C_3H_6$ | 7.9400E+08 | 0.00 | 85.77 | [96] |
| 147 | $C_9H_{12}$ + $C_6H_5$ = $^1C_9H_{11}$ + $C_6H_6$ | 7.9400E+08 | 0.00 | 67.78 | [96] |
| 148 | $C_9H_{12}$ + $C_6H_5$ = $^2C_9H_{11}$ + $C_6H_6$ | 7.9400E+08 | 0.00 | 67.68 | [96] |
| 149 | $C_9H_{12}$ + $C_6H_5$ = $^3C_9H_{11}$ + $C_6H_6$ | 7.9400E+08 | 0.00 | 85.77 | [96] |
| 150 | $C_9H_{12}$ + $C_7H_7$ = $^1C_9H_{11}$ + $C_7H_8$ | 7.9400E+08 | 0.00 | 67.78 | [96] |
| 151 | $C_9H_{12}$ + $C_7H_7$ = $^2C_9H_{11}$ + $C_7H_8$ | 7.9400E+08 | 0.00 | 67.68 | [96] |
| 152 | $C_9H_{12}$ + $C_7H_7$ = $^3C_9H_{11}$ + $C_7H_8$ | 7.9400E+08 | 0.00 | 85.84 | [96] |
| 153 | $C_9H_{12}$ + $O_2$ = $^1C_9H_{11}$ + $HO_2$ | 4.0000E+10 | 0.00 | 149.78 | [96] |
| 154 | $C_9H_{12}$ + $O_2$ = $^2C_9H_{11}$ + $HO_2$ | 4.0000E+10 | 0.00 | 207.10 | [96] |
| 155 | $C_9H_{12}$ + $O_2$ = $^3C_9H_{11}$ + $HO_2$ | 4.0000E+10 | 0.00 | 211.71 | [96] |
| 156 | $C_9H_{12}$ = $C_6H_5$ + $C_3H_7$(N) | 1.0000E+16 | 0.00 | 305.43 | Adj.[13] |
| 157 | $C_9H_{12}$ = $C_7H_7$ + $C_2H_5$ | 1.0000E+16 | 0.00 | 305.43 | Adj.[13] |
| 158 | $C_9H_{12}$ = $C_8H_9$ + $CH_3$ | 8.0000E+16 | 0.00 | 353.13 | Adj.[13] |
| 159 | $C_9H_{12}$ + H = $C_3H_7$(N) + $C_6H_6$ | 5.7800E+10 | 0.00 | 33.84 | Adj.[80] |

| No | Reaction | A | n | Ea | Ref |
|---|---|---|---|---|---|
| 160 | $C_9H_{12} = {}^3C_9H_{11} + H$ | 8.0000E+15 | 0.00 | 419.27 | [96] |
| 161 | $C_9H_{12} = {}^2C_9H_{11} + H$ | 8.0000E+15 | 0.00 | 414.00 | [96] |
| 162 | $C_9H_{12} = {}^1C_9H_{11} + H$ | 8.0000E+15 | 0.00 | 360.70 | [96] |
| 163 | $C_9H_{12} + C_3H_5(T) = {}^1C_9H_{11} + C_3H_6$ | 7.9400E+08 | 0.00 | 67.78 | [96] |
| 164 | $C_9H_{12} + C_3H_5(S) = {}^1C_9H_{11} + C_3H_6$ | 7.9400E+08 | 0.00 | 67.78 | [96] |
| 165 | $C_9H_{12} + C_3H_5(T) = {}^2C_9H_{11} + C_3H_6$ | 7.9400E+08 | 0.00 | 67.78 | [96] |
| 166 | $C_9H_{12} + C_3H_5(S) = {}^2C_9H_{11} + C_3H_6$ | 7.9400E+08 | 0.00 | 67.78 | [96] |
| 167 | $C_9H_{12} + C_3H_5(T) = {}^3C_9H_{11} + C_3H_6$ | 7.9400E+08 | 0.00 | 85.77 | [96] |
| 168 | $C_9H_{12} + C_3H_5(S) = {}^3C_9H_{11} + C_3H_6$ | 7.9400E+08 | 0.00 | 85.77 | [96] |

**Enhanced Collision Efficiencies**

Unless otherwise specified all collision efficiencies are set equal to 1.